THE ZEBRAFISH PLASMA MEMBRANE CA^{2+} PUMP ATP2B1A ACTS IN THE DEVELOPMENT OF MECHANORECEPTORS AND EARLY BONE CALCIFICATION

WILLIAM GO TECK WAH

(BSc (Merit), NUS)

A THESIS SUBMITTED FOR THE DEGREE OF PHILOSOPHY

INSTITUTE OF MOLECULAR AND CELL BIOLOGY

DEPARTMENT OF BIOCHEMISTRY

NATIONAL UNIVERSITY OF SINGAPORE

2011

ACKNOWLEDGEMENTS

I would like to express my heartfelt gratitude to my supervisor, Assoc. Prof. Vladimir Korzh, for his inspiration, advice, guidance and patience throughout all these years. I am also grateful to Prof. Hong Wanjin for being my liaison project supervisor to NUS, Dr Yang Xiaohang and Dr Sinnakaruppan Mathavan for serving as my thesis advisory committee and providing valuable input during the course of this work.

I acknowledge with gratitude the following scientists for their generous contributions: Dr. Dmitri Bessarab for first started me out on my journey on researching *atp2b1a* and taught me the basic but necessary skills on *in situ* hybridization, Dr Igor Kondrichin and Dr Cathleen Teh for generating all these beautiful GFP and later, Killer Red enhancer trap lines, Dr Steven Fong for showing me how to perform blastomere microinjection and hanging drop cultures and Dr Garcia-Lecea Marta for showing me the ropes of confocal imaging.

The past and present members of the Korzh lab deserve special thanks. They include, Drs Svetlana Korzh, Yang Shulan, Poon Kar Lai, Li Zhen, Cecilia Lanny Winata, Nguyen Thi Thu Hang, Shi Xianke, Ying Ao and Ms Shen Hongyuan. Their constructive criticisms during lab meetings and willingness to share resources and ideas have created a truly supportive lab environment. I am grateful to Mr Sek Junyan, Melvin Sin Wai Loong and Ms Loh Siau Lin for providing technical support. Dr You May-Su deserves special mention for her excellent management of the Zebrafish Facility and her capable team (Mr Ix Wee, Mohd Azrin, Benjamin Tan, Vincent Foo, Mohd Agus, Alex Tok, Ms Oh Sock Ying, Neo Sui Hoon, Madam Leong Ah Yan and Lok Foon Ying) – without their hard work; no fish research would have been possible in IMCB. Also I express my gratitude to the IMCB Sequencing Facility, Central Imaging Facility and Equipment Maintenance department for their professional technical support.

I would like to express my utmost gratitude to my parents and siblings for their constant warmth and encouragement. I want to thank especially my dear wife and our little baby Jodi, for being the cornerstone of my life and have provided me with much inspiration and emotional support throughout this journey. Their presence have helped me realized the purpose and significance of all these effort. And I thank all of them from the bottom of my heart.

Table of Contents

ACKNOWLEDGEMENTS 2
SUMMARY 8
List of Tables 9
List of Figures 10
List of Abbreviations 13
Publications 14

CHAPTER 1 15
Introduction 15
1.1 Outline of this thesis 16
1.2 Zebrafish and Enhancer Trap Transgenics 16
1.3 Research Objectives 18
1.4 Plasma Membrane Ca^{2+} ATPase 21
1.5 Mechanosensory Hair Cells 22
1.6 The Ultimobranchial body 27

CHAPTER 2 32
Materials and Methods 32
2.1 DNA Applications 33
2.1.1 Long-term Storage of Bacteria 34
2.1.2 Competent Cell Preparation 34
2.1.3 Transformation of Bacterial Competent Cells 35
2.1.4 Polymerase Chain Reaction (PCR) 35
2.1.5 Cloning of PCR Products 36
2.1.6 Restriction Enzyme Digestion 37
2.1.7 Agarose Gel Electrophoresis 38
2.1.8 DNA Gel Purification 39
2.1.9 Small-scale Purification of Plasmid DNA 39
2.1.10 Midi-Scale Purification of Plasmid DNA 40

2.2 RNA Procedures 41
2.2.1 Isolation of total RNA from Zebrafish Embryos 41
2.2.2 One-step RT-PCR 42
2.2.3 First-strand cDNA Synthesis 43
2.2.4 Long-range PCR 43
2.2.5 Messenger RNA Synthesis for Rescue Experiments 44
2.2.6 Quantitative Real-time PCR 45
2.3 Zebrafish 46
2.3.1 Fish Maintenance 46
2.3.2 Stages of Embryonic Development 47
2.3.3 Microinjection into Blastula Stage Zebrafish Embryos 47
2.3.4 Design of Antisense Morpholinos 48
2.3.5 Embryo Anesthesia 49
2.3.6 Behavioral Assay 49
2.3.7 16-cell Blastomeres Injection 50
2.4 Functional Assays 51
2.4.1 Pharmacological Treatment 51
2.4.2 Acid-free Dual Staining of Bones and Cartilage 51
2.4.3 Vital Dye Staining on Live Embryos 52
2.4.4 Bone Mineralization Assay 53
2.4.5 Live Ca^{2+} Imaging 54
2.4.6 Birefringency of somite 55
2.4.7 Hanging Drop Culture 56
2.5 *In situ* Hybridization 56
2.5.1 Antisense Probe Synthesis 56
2.5.2 RNA Probe Clean Up 57
2.5.3 Fixation of Staged Embryos 58
2.5.4 Proteinase K (PK) Treatment 58
2.5.5 Pre-hybridization 59
2.5.6 Hybridization 59
2.5.7 Preparation of Pre-adsorbed Anti-DIG Antibody 60

2.5.8 Incubation with Pre-absorbed Antibodies 60
2.5.9 DIG and Fast Red Staining 61
2.5.10 Two Color *In situ* Hybridization 61
2.6 Cryostat Sectioning 62
2.6.1 Mounting Specimen for Cryostat Sectioning 62
2.6.2 Freezing and Collecting Sectioned Specimens 63
2.7 Protein Applications 63
2.7.1 Immunohistochemical Staining 63
2.7.2 Cell Proliferation Assay (BrdU assay) 65
2.8 Microscopy 66
2.8.1 Embryo Mounting and Imaging Using Upright Light Microscope 66
2.8.2 Multi-channels Viewing and Confocal Microscopy 66

CHAPTER 3 68
Results 68
3.1 *atp2b1a* in Mechanosensory Hair Cells 69
3.1.1 Cloning and expression analysis of *atp2b1a* 69
3.1.2 *atp2b1a* functions in the context of lateral line development 72
3.1.3 Atp2b1a regulates dynamics of Ca^{2+} in developing and mature hair cells 77
3.1.4 Formations of kinocilium was affected in *atp2b1a* morphants 81
3.1.5 Late phenotypes of *atp2b1a* morphants 84
3.1.6 *atp2b1a* expression is downstream of and regulated by *atoh1a* 86
3.1.7 *atp2b1a* and cell proliferation in neuromasts 91
3.1.8 *atp2b1a* expression is induced during hair cell regeneration 93
3.2 *atp2b1a* in Ultimobranchial Body (UB) 96
3.2.1: *atp2b1a* is expressed in UB of the developing zebrafish 96
3.2.2 Close 3D contact of UB and pharyngeal teeth 98
3.2.3 UB cells provide Ca2+ for developing pharyngeal teeth 99
3.2.4 During early differentiation of UB cells *ascl1* acts upstream of *atp2b1a* 102
3.2.5 *atp2b1a* knockdown caused a defect in calcification of bones 106

3.2.6 *atp2b1a* knockdown affects expression of genes expressed in UB and pharyngeal dentition 112

3.3 Other Expression Domains of *atp2b1a* 116

3.3.1 *atp2b1a* can be regulated by Delta-Notch signaling and is required for the normal development of optic tectum and sensory patches 116

3.3.2 *atp2b1a* is required for muscle development 119

3.3.3 Early function of *atp2b1a* is required for normal cell adhesion 122

3.3.4 *atp2b1a* has roles in heart valves' function 125

3.3.5 *atp2b1a* is expressed in statoacoustic ganglion 127

CHAPTER 4 129

Discussion 129

4.1 *atp2b1a* in mechanosensory hair cells 130

4.2 *atp2b1a* in Ultimobranchial body (UB) 135

CHAPTER 5 140

Conclusions 140

REFERENCES 144

SUMMARY

Tol2 enhancer-trap transgenic line SqET4 is widely used for studies of development and disease of mechanosensory hair cells. We showed that it represents Tg:*atp2b1a*-EGFP. This provided a possibility to study a function of Atp2b1a/PMCA1. Combining the morpholino mediated-knockdown and small molecule inhibition, I showed that deficiency of Atp2b1a results in auditory and vestibular defects due to defects of Ca^{2+} export by mechanosensory hair cells. Acting downstream of the transcriptional regulator Atoh1a, Atp2b1a plays a crucial role in division of terminally determined mechanosensory hair cells progenitors. Serendipitously, another domain of GFP/Atp2b1a expression was identified in the ultimobranchial bodies (UB) of SqET4. In mammals UB gives rise to the calcitonin-producing cells of the thyroid gland. Since in zebrafish UB remains a separate organ, SqET4 provided a useful tool to study the anatomy and function of developing UB. In particular, a connection between UB and pharyngeal dentition and function of Atp2b1a during bones calcification was demonstrated.

List of Tables

Table 1: Vectors and commercial competent cells used in this study. 33

Table 2: Bacteria selection. 33

Table 3: Bacterial culture media. 33

Table 4: Ligation reaction set-up. 37

Table 5: Restriction digestion set-up. 38

Table 6: Primers used in RT-PCR. 43

Table 7: Components of *in vitro* mRNA synthesis. 44

Table 8: Primers used for quantitative real-time PCR analysis. 46

Table 9: A list of morpholinos used in this study. 49

Table 10: Vital dyes used and their working dilution. 53

Table 11: A list of molecular markers used in this study. 57

Table 12: Permeabilization of zebrafish embryos and larvae by Proteinase K (PK). 59

Table 13: Primary and secondary antibodies used. 65

Table 14: Reduction of number of neuromasts caused by *atp2b1a* knockdown is dosage-dependent. 77

Table 15: Neuromast and hair cells count in embryos of SqET4 transgenics after *atp2b1a* knockdown, mRNA rescue and PMCA inhibitor (5(6)-Carboxyeosin) treatment. 81

Table 16: *atp2b1a* knockdown and PMCA inhibitor treatment negatively affects kinocilium of neuromast. 84

Table 17: Auditory and vestobular-related phenotypes of *atp2b1a* morphant. 86

Table 18: The number of S-phase cells in neuromasts morphant increased. 93

List of Figures

Fig. 1: Schematic representation of enhancer trap (ET) construct. 20

Fig. 2: Calcium regulation at cellular level and PMCA. 22

Fig. 3: Development of zebrafish inner ear. 24

Fig. 4: Lateral line system of fish. 25

Fig. 5: Enhancer Trap (ET) transgenic lines with lateral line expression. 26

Fig. 6: Calcitonin-producing cells of the Ultimobranchial body (UB). 29

Fig. 7: Regulation of Ca^{2+} at tissue level. 31

Fig. 8: Chemical calcium indicator; Calcium Crimson AM. 55

Fig. 9: Expression pattern of *atp2b1a* transcript recapitulates that of *egfp* in SqET4. 71

Fig. 10: Control experiment showing the specificity of *atp2b1a* morpholino used throughout this study. 74

Fig. 11: Control experiment showing that the effect of *atp2b1a* morpholino is not due to activation of Tp53. 75

Fig. 12: Rescue of *atp2b1a* morphants using full-length *atp2b1a* mRNA. 76

Fig. 13: *atp2b1a* knockdown disrupted the rapid cell proliferation of hair cells in developing neuromast. 77

Fig. 14: *atp2b1a* is required for Ca^{2+} extrusion from mechanosensory hair cell. 79

Fig. 15: Formation of hair cells secondary structures was affected in morphants neuromasts. 83

Fig. 16: Mis-regulation of Ca^{2+} in mechanosensory cells by *atp2b1a* knockdown led to auditory / vestibular phenotypes of late *atp2b1a* morphant. 85

Fig. 17: *atp2b1a* is co-localized with *atoh1a* in hair cells of neuromast and inner ear 87

Fig. 18: *atp2b1a* acts downstream of *atoh1a* 89

Fig. 19: Increase in cell proliferation in neuromast peripheral cells in the *atp2b1a* morphant. 91

Fig. 20: Expression of *atp2b1a* correlates with regeneration of hair cells. 95

Fig. 21: *atp2b1a* is expressed in the ultimobranchial bodies (UB) of the developing zebrafish. 97

Fig. 22: Time-lapse recording of UB development in SqET4 (55-69 hpf) 98

Fig. 23: GFP-positive UB in SqET4 is connected to the pharyngeal dentitions. 101

Fig. 24: *atp2b1a* knockdown abolished EGFP expression in UB of SqET4. 105

Fig. 25: *atp2b1a* is required for calcification of early-forming bones in zebrafish larvae. 107

Fig. 26: General development was not delayed in injected *atp2b1a* morphants. 109

Fig. 27: Osteoblasts were detected at pharyngeal dentitions (PD) after 5.5 dpf. 110

Fig. 28: Bone matrix progression at developing operculum was severely affected in *atp2b1a* morphant larvae. 111

Fig. 29: *atp2b1a* knockdown resulted in mis-regulation of UB specific genes. 114

Fig. 30: *atp2b1a* regulates production of calcitonin gene-related peptide (CGRP) hormone. 115

Fig. 31: *atp2b1a* can be regulated by Delta-Notch signalling and is required for the normal development of optic tectum and sensory patches. 117

Fig. 32: *atp2b1a* is required for muscle development. 119

Fig. 33: Control experiment showing that lateral line phenotype of *atp2b1a* knockdown is independent from its muscle phenotype. 121

Fig. 34: Early function of *atp2b1a* is required for normal cell adhesion. 124

Fig. 35: *atp2b1a* could have roles in atrio-ventricular valves of the heart. 126

Fig. 36: *atp2b1a* is express in presumptive statoacoustic ganglion of the inner ear. 127

Fig. 37: Role of *atp2b1a* in the development of mechanosensory hair cells. 134

Fig. 38: Role of *atp2b1a* in calcification of pharyngeal dentition and bone. 139

List of Abbreviations

AB: Alcian Blue
AR: Alizarin Red S
BrdU: Bromodeoxyuridine
CaC: Calcium Crimson AM
cb: ceratobranchial arch
CE: 5(6)-carboxyeosin
CGRP: Calcitonin gene-related peptide
ch: ceratohyal
cl: cleithrum
cp: committed precursor
CT: calcitonin
dpf: days post fertilization
DIC: differential interference contrast
ET: enhancer trap
GFP: green fluorescent protein
hc: hair cell
hcp: hair cell precursor
hpf: hours post fertilization
IHC: immunohistochemistry
KD: knockdown
k: kinocilium
L1-L6: deposited neuromasts of posterior lateral line
mc: mantle cell
MO: morpholino
nm: neuromast
op: operculum
ot: optic tectum
ov: otic vesicle
PD: pharyngeal dentitions
pLLp: posterior lateral line primordium
pnm: proneuromasts
sc: support cells
WISH: whole-mount in situ hybridization
UB: ultimobranchial bodies
4V^{1}: first forming pair of pharyngeal dentitions
3/5V^{1}: subsequent forming pairs of pharyngeal dentitions

Publications

1. **William Go** and Vladimir Korzh, Plasma membrane Ca^{2+} ATPase, Atp2b1a regulates bone mineralization in zebrafish (submitted-in revision).
2. **William Go**, Dmitri Bessarab and Vladimir Korzh, *atp2b1a* regulates Ca^{2+} export during differentiation and regeneration of mechanosensory hair cells of zebrafish. *Cell Calcium* **48** (2010): 302-313.
3. Benjamin G.H. Choo, Igor Kondrichin, Sergey Parinov, Alexandra Emelyanov, **William Go**, Wei-Chang Toh and Vladimir Korzh, Zebrafish transgenic enhancer TRAP line database (ZETRAP), *BMC Dev. Biol.* **6** (2006):5.

CHAPTER 1

Introduction

1.1 Outline of this thesis

The present chapter illustrates the background, objectives and systems involved in this study. A detailed description of the materials and experimental methods used in this work is provided in Chapter 2. In Chapter 3, I have presented experimental evidence to show that SqET4 represents Tg(*atp2b1a*-EGFP) and based on that, I was able to address the functional role of Atp2b1a in the developing lateral line and ultimobranchial body. Functional knockdown of *atp2b1a* was achieved using specific antisense morpholino and small molecular inhibitor. A brief overview of other expression domains of *atp2b1a* is also included. In Chapter 4, I discussed all the findings. And in the final chapter, I have provided a concluding perspective on how these two seemingly unrelated models of development (i.e. otoliths formation and bone calcification) can be possibly converged.

1.2 Zebrafish and Enhancer Trap Transgenics

Several unique features of zebrafish (*Danio rerio*) have enabled researchers around the world to embrace this little organism as the model of choice for studying developmental biology. High on this list of advantages is the embryo's optical transparency, which have made *in vivo* imaging a practical and much simpler affair. And when coupled with high resolution imaging systems such as multi-channel confocal system, this marriage between powerful systems has often resulted in successful observation of both meaningful and crucial developmental events not possible with bigger animals. Successful advancements in zebrafish genome sequencing project have also

made understanding developmental biology-related questions from a genetic perspective possible.

Evidence of effective transposition of heterologous transposons *Tol2* from *Oryzias latipes* (Kawakami et al., 2000) and *Sleeping Beauty* from salmonid (Davidson et al., 2003) in the zebrafish genome opened new opportunities for reverse genetics and transgenesis based applications. The generation of Enhancer Trap transgenic zebrafish lines (ET lines) reported by the Korzh lab (Parinov et al., 2004) has created an excellent resource of ET lines for carrying out such analysis. In brief, they have successfully made use of a transposable element, namely *Tol2* transposon derived from medaka fish to generate a library of interesting *Tol2* insertion transgenic lines. This element uses conservative ("cut and paste") transposition mechanism, meaning it is excised from the donor site when the whole element moves to the new position. Enhanced green fluorescent protein (EGFP) was used as a reporter to fully utilize the nature of live embryos' optical clarity. When these random insertions occurred within the vicinity of an enhancer present in the genome, enhancers are considered metaphorically "trapped" to activate reporter gene expression even at considerable distance in orientation-independent manner and ideally, in a tissue specific manner.

Enhancers are highly conserved non-coding elements (HCNEs); sequences are of interest for their potential to regulate gene production (Bejerano et al., 2004; Sandelin et al., 2004; Woolfe etal., 2005). HCNEs in plants and animals are highly associated with transcription factor binding sites and other *cis*-acting regulatory elements. Conserved non-coding sequences can be important sites of evolutionary divergence (Navratilova et al., 2009) as mutations in these regions may alter the regulation of conserved genes, producing species-specific patterns of gene expression. Due to the random nature of *Tol2* genomic insertions, single and multiple insertions

can be expected. And in cases where single insertion has been identified through molecular method (i.e. TAIL-PCR), stable lines were generated and they can be experimentally verified to ascertain their potential of representing the trapped gene at the transcript level.

This simple construct (Fig. 1A) employs the *Tol2* enhancer which carries the EGFP reporter downstream of a *krt4* minimal promoter. Activity of this promoter is induced once it lands under control of a chromosomal enhancer (Bellen, 1999). Identification of the regulated genes can be challenging since enhancer can activate the reporter outside of genes. The key to identify the regulated gene is the enhancer trap line's expression should faithfully recapitulate the regulated gene's expression pattern, which many of such successful cases have already been reported elsewhere (Perrimon et al., 1991; Bellen, 1999).

1.3 Research Objectives

In this thesis work, I have focused on one such ET line, primarily due to its untapped potential in representing its trapped gene. SqET4 is the ET line, where EGFP expression takes place in mechanosensory hair cells (Parinov et al., 2004; Choo et al., 2006). The "Achilles' heel" of the SqET4 line, however, is the lack of information about the gene(s) expression pattern it mimics, and therefore the current deficit in understanding the developmental process reflected by GFP expression *in vivo*. Several questions need to be answered to anchor the fast-growing SqET4-related literature to a particular molecular mechanism: i) which gene's expression pattern is revealed by GFP expression in SqET4? ii) How are the transient hair cell precursors related to Atoh1-positive precursors? iii) How does this gene activity contributes to development and/or

mechanosensory hair cells regeneration? iv) Is this gene relevant within the context of auditory and (or) vestibular functions of the animal?

Since its inception, SqET4 has become widely embraced as a living marker for studying the molecular developmental program of these cells (Faucherre et al., 2009; Feijoo et al., 2009; Froehlicher et al., 2009; Gleason et al., 2009; Hernandez et al., 2007; Lopez-Schier and Hudspeth, 2006; Nagiel et al., 2008; Nechiporuk and Raible, 2008; Sarrazin et al., 2006). We mapped the insertion of SqET4 to a position adjacent to a plasma membrane Ca^{2+} ATPase. In addition to its expression in mechanosensory hair cells, I have characterized other expression domains of *atp2b1a*. Interestingly, 1 have found and studied a previously uncharacterized expression domain of *atp2b1a* which corresponds to the developing Ultimobranchial body (UB). The primary objective of this project aims to define developmental role(s) of *atp2b1a* in these tissues that expresses it.

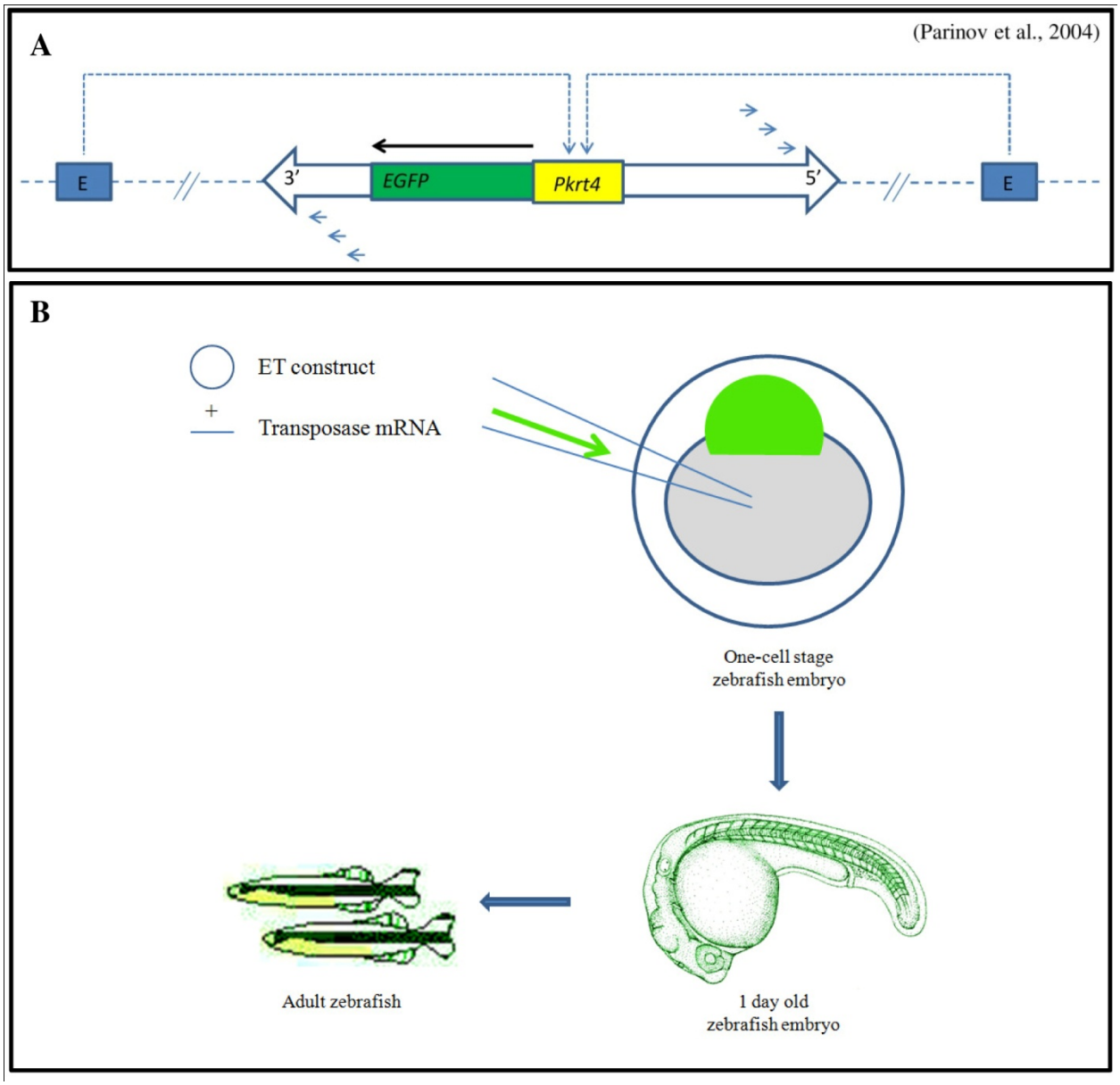

Figure 1: Schematic representation of enhancer trap (ET) construct. A) The *Tol2* element contains the EGFP reporter gene under control of a short 460-bp *krt4* promoter. Expression of the reporter is induced when it is inserted near an enhancer (Parinov et al., 2004). B) Generation of ET transgenic lines by co-injecting *Tol2* transposon construct and transposase mRNA to induce transposition.

1.4 Plasma Membrane Ca^{2+} ATPase

The plasma membrane Ca^{2+}-ATPases (PMCA1-4) in mammals are encoded by four genes (Atp2b1-4) and a diverse set of protein isoforms is produced in result of alternative splicing (Keaton et al., 1993; reviewed in Berridge, 2009). Despite the large molecular diversity within the PMCA family, the overall structure of all members is very similar. All PMCA isoforms have 10 transmembrane domains, with the largest cytoplasmic loop connecting TM4 and TM5 of particular significance because it contains the ATP-binding domain as well as a phosphorylation site that is phosphorylated during each pump cycle. At the C-terminus lies a calmodulin binding domain where it acts as a sensor for Ca^{2+} ions (Fig. 2B).

In mice, Atp2b1 is broadly expressed. Since Atp2b1 mutant embryos are embryonic lethal (Okunade et al., 2004) there is a paucity of information about a function of this gene during development of vertebrates. This is contrast to its relative Atp2b1b (PMCA2), which expression in mice is more restricted and mutation causes deficiency restricted to mechanosensory hair cells resulting in deafness and ataxia (Ficarella et al., 2007; Tempel and Schilling, 2007; reviewed in Hughes et al., 2006; Street et al., 1998). *Atp2b1* is duplicated in teleosts, which along with other factors such as evolutionary dependent differential expression in mice and zebrafish seemingly contributed into making one of the two Atp2b1-related genes of zebrafish – *atp2b1a* responsible for development of sensory hair cells in zebrafish (McDermott et al., 2007; Cruz et al., 2009; Go et al., 2010). This led to suggest that in teleosts Atp2b1a acts as a functional homologue of Atp2b1b (PMCA2) of mammals (Lafont et al., 2010). And yet *atp2b1a* is broadly expressed similar to its counterpart in mammals with transcripts being present not only in mechanosensory cells of the inner ear and lateral line, but also in the midbrain, somites, UB, heart and possibly, the statoacoustic ganglion where the nature of expression needs

to be further defined. Hence it is unclear whether Atp2b1a acts as a functional homolog of Atp2b2.

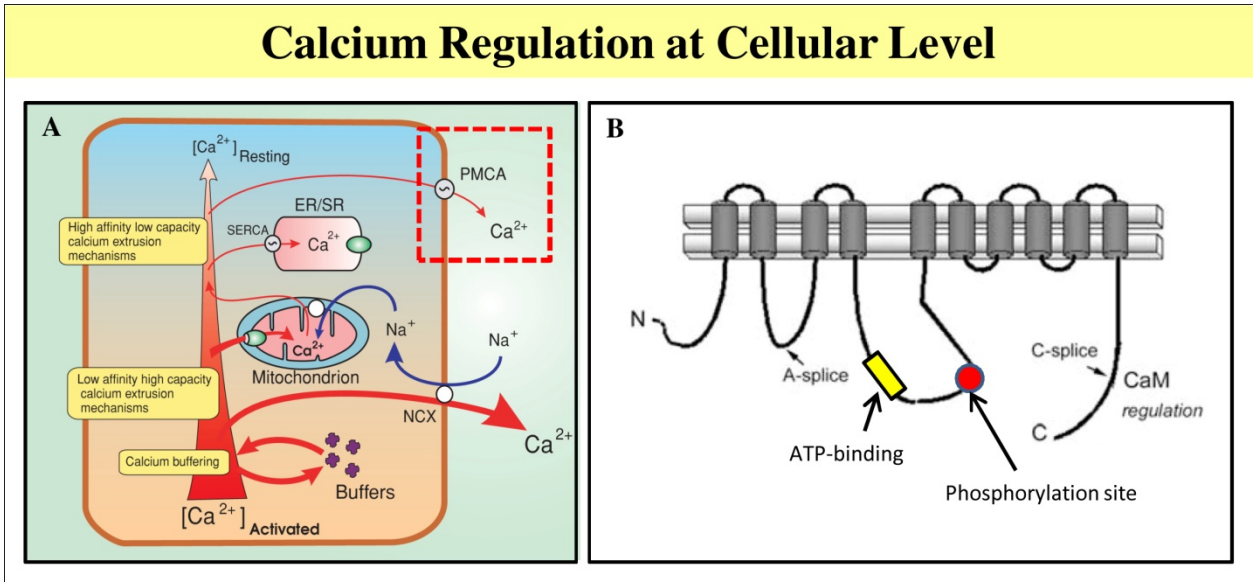

Figure 2. Calcium regulation at cellular level and PMCA. $[Ca^{2+}]$ gradient across cell membrane is tightly regulated to maintain resting $[Ca^{2+}]_I$ at 10 - 100 nM and excited $[Ca^{2+}]_I$ at 500 – 1000 nM. Ca^{2+} clearance can be achieved by a variety of "ATP-driven pumps" to prevent Ca^{2+} overloading. A) Ca^{2+} regulation at cellular level with PMCA playing a active role in maintenance of resting $[Ca^{2+}]_I$ (highlighted in red dashed box; reviewed by M. Berridge (2009). B) Structural features of the PMCA pump (Reviewed by Strehler et al., (2007).

1.5 Mechanosensory Hair Cells

Mechanosensory hair cells are present within the inner ear of all vertebrates as sensory patches. These sensory patches are named according to their location within the inner ear, such as the anterior and posterior macula and various cristae (anterior, posterior and medial) which develop later during development (Fig. 3). It is also present on the skin of fish and amphibian as part of

the lateral line system. The specific expression of SqET4 in mechanosensory hair cells of lateral line was what attributed to its popularity as an *in vivo* model of hair cells development.

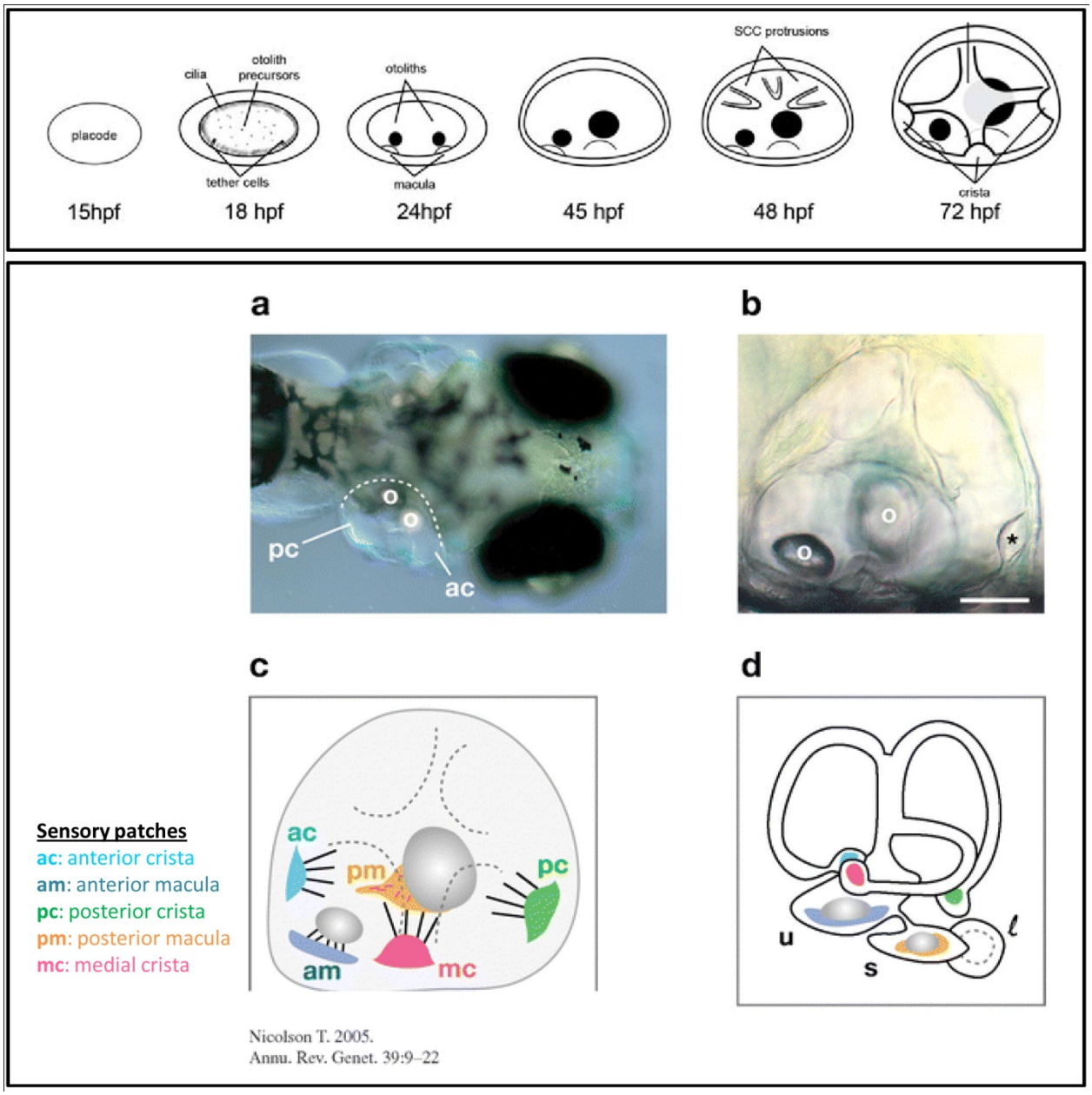

Figure 3. Developmental of zebrafish inner ear. Inner ear development commences with the initial appearance of the otic placode during embryonic stage. The entire hearing apparatus develops with increasing complexity till post-embryonic stages (72 hpf). (*A*) Dorsal view of a 5 dpf zebrafish larvae. Dashed line indicates the developing otocysts. (B) Lateral view of larval inner ear. Otoliths are visible (marked "o"). Asterix marked the neuroepithelium, posterior crista. (*C*) Diagrammatic representation of the larval ear illustrating all five sensory patches. Dashed lines indicate the semicircular canals formed. (*D*) Diagram of the adult zebrafish ear. The colours correspond to the same sensory patches in *C*. (Source: Nicolson T. 2005)

The lateral line is a sensory organ system that develops from the specification of early precursor cells and results in the terminal differentiation of lineage-committed precursors into specialized cells – mechanosensory hair cells (Itoh and Chitnis, 2001; Lopez-Schier et al., 2004; Haas and Gilmour, 2006; Froehlicher et al., 2009). Morphologically, the lateral line represents a linear arrangement of mechanosensory neuromasts distributed on the surface of the fish head and body (Fig. 4; reviewed in Moorman, 2001; Ghysen and Dambly-Chaudiere, 2007). Each neuromast consists of a central core of mechanosensory hair cells and a surrounding group of several subtypes of support cells (Hernandez et al., 2007).

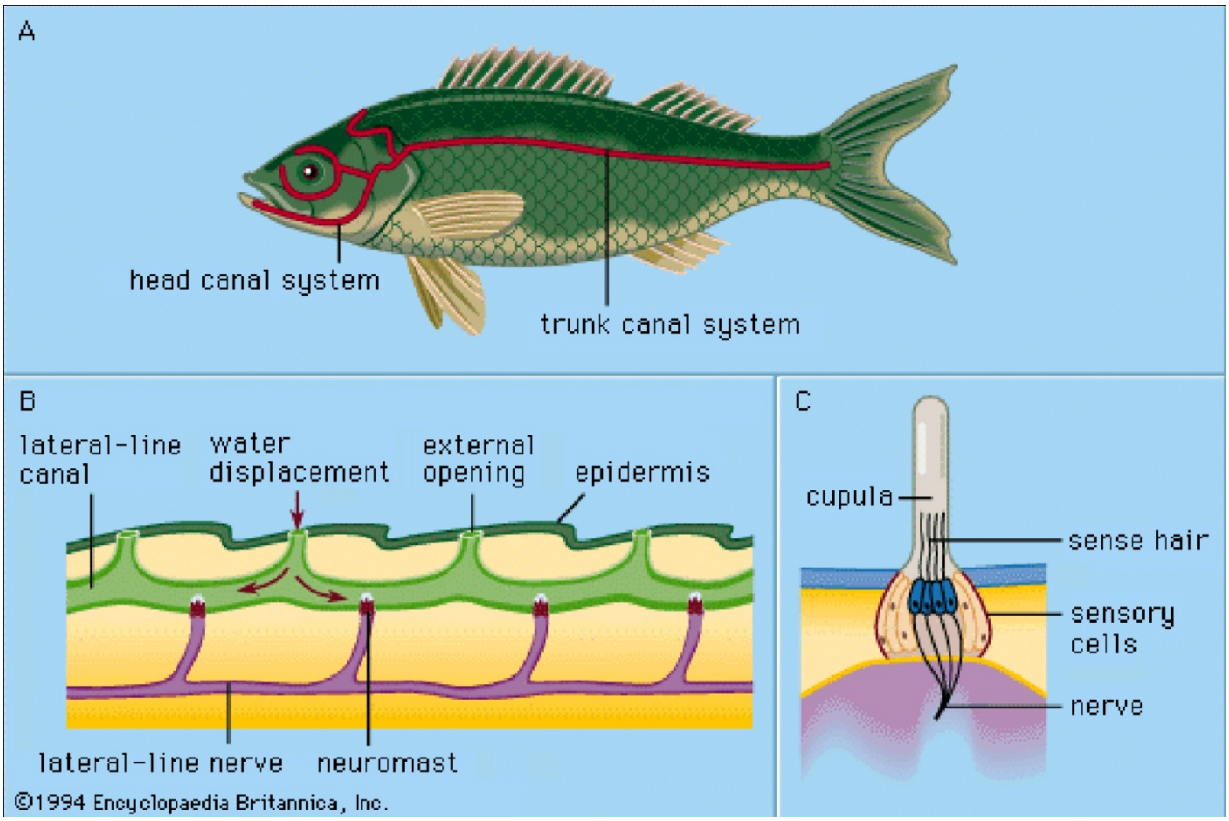

Figure 4. Lateral line system of fish. (A) Bodily location of lateral lines. 3 branches are apparent (anterior, posterior and dorsal lateral lines). *(B)* longitudinal section of a canal; *(C)* superficial neuromast illustrating mechanosensory hair cells as sense hair which are innervated.

The mechanosensory hair cells of the lateral line are highly differentiated and developed a special type of long cilium on its apex called, kinocilium. This is usually accompanied by numerous shorter stereocilia. These structures can be physically deflected by stimuli such as water current. This resulted in depolarization or hyperpolarization of the hair cell and enables transduction of stimuli into electrical signals (Fettiplace and Hackney, 2006). In fish and amphibians, these hair cells are embedded in a protective jelly-like protrusion called, the cupula (Fig. 4 & 5). In contrast, the support cells provide cohesive support (Cotanche et al., 1992; Warchol et al., 2007), perform secretory functions (Cotanche et al., 1987; Epstein and Cotanche, 1995) and generate new mechanosensory hair cells during normal development and regeneration (Balak et al., 1990; Raphael, 1992; Stone et al., 1994; Bermingham-McDonogh and Rubel, 2003; Fig. 5).

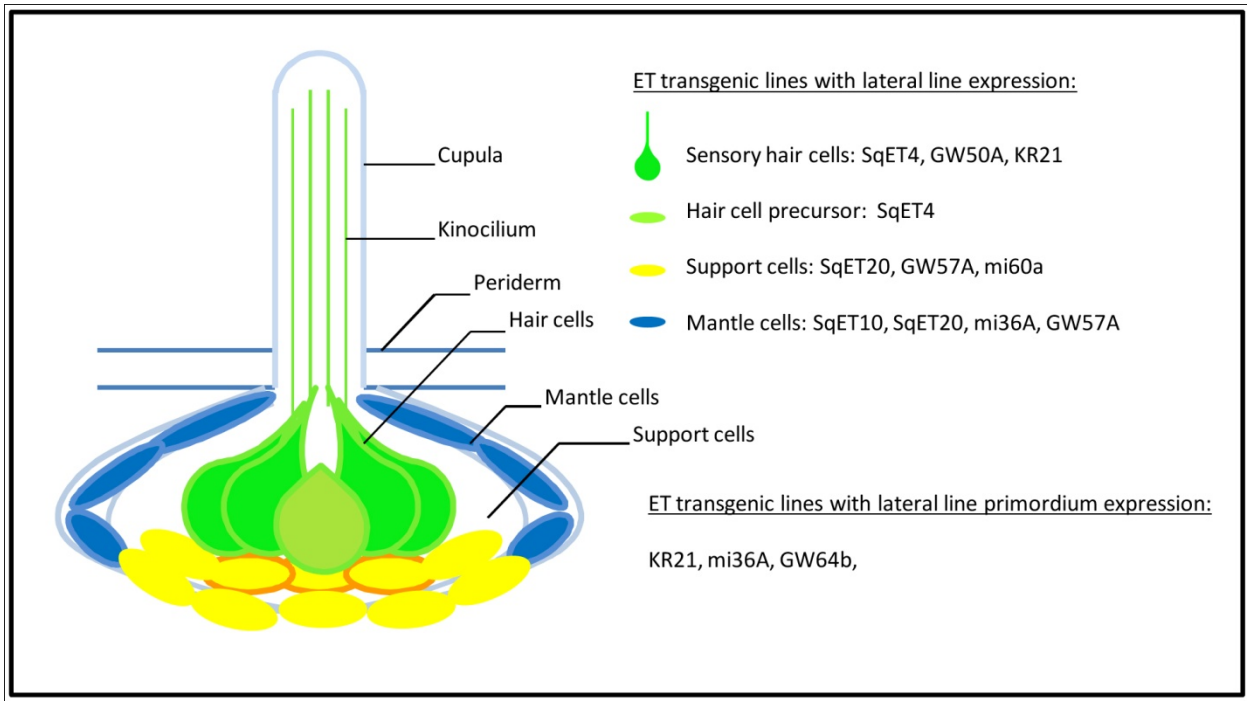

Figure 5. Neuromast and Enhancer Trap (ET) transgenic lines. A library of ET transgenic lines with characteristical expressions in various cell types of the zebrafish lateral line systems (Parinov et al., 2004; Choo et al., 2006; Go et al., 2010).

In zebrafish, the mechanosensory hair cells differentiate following terminal division of the transient hair cell precursor (Lopez-Schier and Hudspeth, 2006; Behra et al., 2009), which is reminiscent of that during *Drosophila* neurogenesis where the transient precursor, the ganglion mother cell (GMC), terminally divides to generate two neurons/glial cells (Bossing et al., 1996; Schmid et al., 1999).

The early events involved in the specification of mechanosensory hair cells are still not fully understood. Several signaling pathways govern this process, including Wnt (Ma and Raible, 2009), Fgf (Lecaudey et al., 2008) and Notch (Itoh et al., 2001), which results in activation of the transcription factor, Atoh1, in specified hair cell precursors that are required for mechanosensory hair cells differentiation (Millimaki et al., 2007). In the fly CNS, the homologue of *atoh1a – ato* – is indispensable in embryonic precursors and in the neurons they generate. Similarly, during cortical neurogenesis in mammals, radial glia produce a restricted, neuronal intermediate precursor cell (also referred to as a basal progenitor cell), which in turn gives rise to cells populating the embryonic subventricular zone (reviewed in Kriegstein and Alvarez-Buylla, 2009). In contrast, in the mouse inner ear, the term progenitor was traditionally used to define an earlier, common ancestor of the support cells and mechanosensory hair cells. Thus, in the inner ear of *Atoh1 (Math1)*-deficient mice, only mechanosensory hair cells, and not the common progenitors of mechanosensory hair cells and support cells, are believed to be absent (Bermingham et al., 1999; reviewed in Bertrand et al., 2002).

1.6 The Ultimobranchial body

UB is a derivative of the pharyngeal pouch which has been found in all vertebrates, at least during early stage of its development. At present, it seems unlikely to provide a consistent picture of the formation of UB since it varies differently amongst vertebrates. In many mammals including humans, it is an embryological structure of neural crest-derived lineage that gives rise to C-cells (reviewed by Bourque and Houvras, 2011), also known as parafollicular cells of the thyroid gland (Fig. 6). Fusion takes place between the developing thyroid diverticulum and C-cells after both components arrive at a position deep in the cervical mesenchyme (De Felice and Di Lauro, 2004). In vertebrates other than mammals (fish, amphibian and birds), UB remains separate from the thyroid gland (Le Douarin et al., 1974; Le Lievre et al., 1975; Alt et al., 2006) since migration of C-cells never took place.

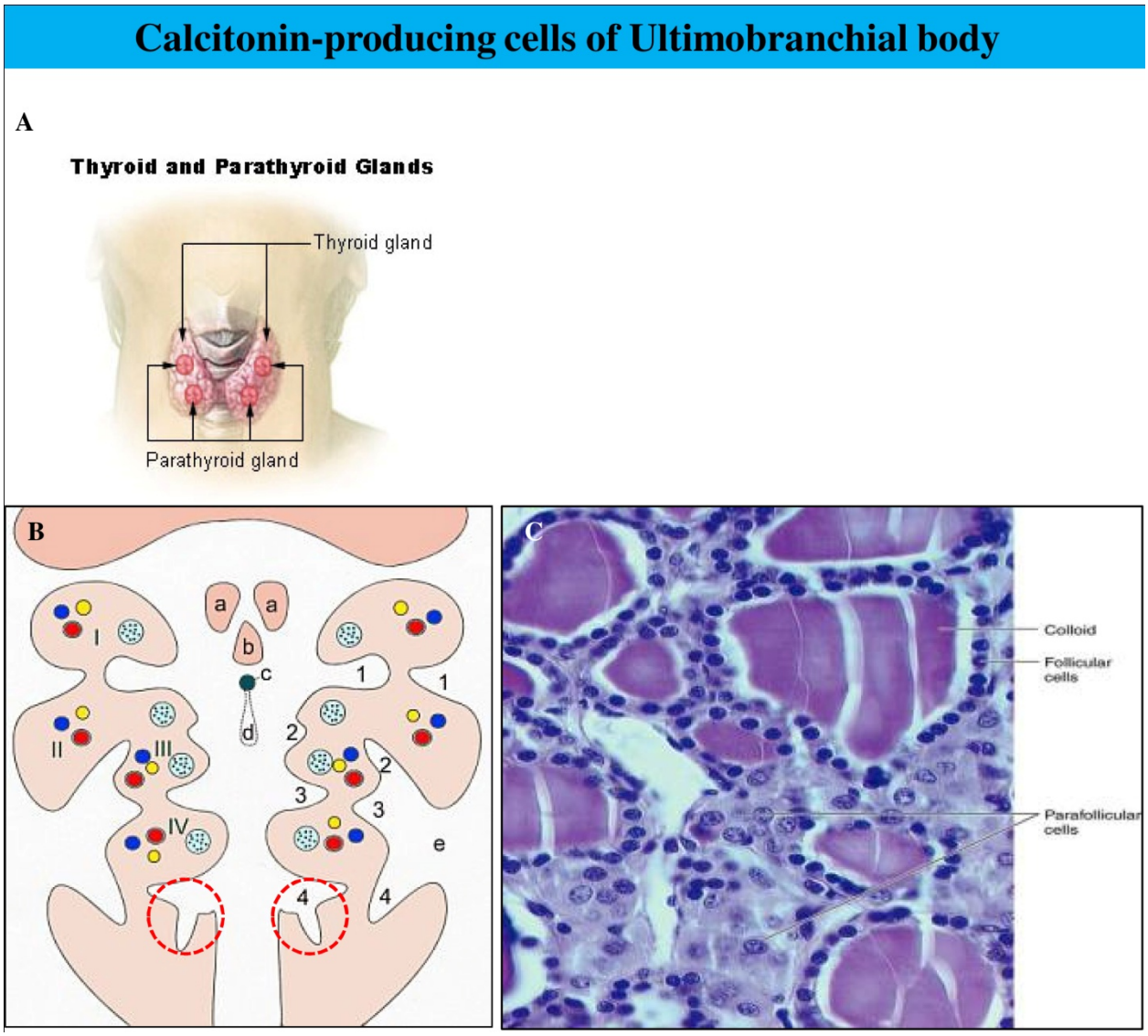

Figure 6. Calcitonin-producing cells of the Ultimobranchial body (UB). A) The thyroid gland controls how quickly the body uses energy, makes proteins, and controls how sensitive the body is to other hormones. It participates in these processes by producing thyroid hormones, the principal ones being triiodothyronine (T_3) and thyroxine (T_4). The thyroid also produces calcitonin, which plays a role in calcium homeostasis. B) Pattern of the branchial arches. I-IV branchial arches, 1-4 branchial pouches (inside) and/or pharyngeal grooves (outside). The parafollicular cells are the progeny of the ultimobranchial bodies, which arise from the rudimentary 5th pair of pharyngeal pouches (red dashed circle; source: Wikimedia Common). C) Micrograph of monkey thyroid follicles. (source: Basic Histology, a text and atlas, p. 425, Figure 21-18).

The importance of UB is recognized primarily due to its role in regulating Ca^{2+} at tissue level (Fig. 7). UB produces the hypocalcaemic polypeptide hormone, calcitonin (CT). CT is encoded by calcitonin gene-related polypeptide alpha gene (*calca*). In teleosts, calcitonin has been linked to hyper- and hypo-calcemia depending on physiological context (Wagner et al., 1997; Oughterson et al., 1995; Suzuki et al., 1999; Najib and Fouchereau-Peron, 1994; Lafont et al., 2010). *calca* also encodes the calcitonin-gene related peptide (CGRP) known for its effect as a powerful vasodilator. In mammals, *calca* is expressed in C-cells of the thyroid gland (De Felice and Di Lauro, 2004).

CT is known to play prominent roles in regulating free Ca^{2+} level in lower vertebrates (Fig. 7). And yet, among factors regulating Ca^{2+} metabolism, CT plays an important and yet incompletely understood role in mammals. Until now a lack of genetic markers of C-cells hampered the progress of understanding the *in vivo* functions of UB, other than its purported functions of secreting two Ca^{2+}-regulating peptide hormones; CT and calcitonin gene-related peptide (CGRP). In addition, the understanding of its related carcinoma, medullary thyroid cancer (MTC); a form of thyroid carcinoma which originates from C-cells is particularly challenging using mammalian models since the location of C-cells is much harder to define within the thyroid gland. Studying development of C-cells in lower vertebrates will theoretically be simpler since both organs remained separated during the animal's lifetime. Such approach presents an opportunity to understand the disease development of C-cells in the absence of a thyroid niche.

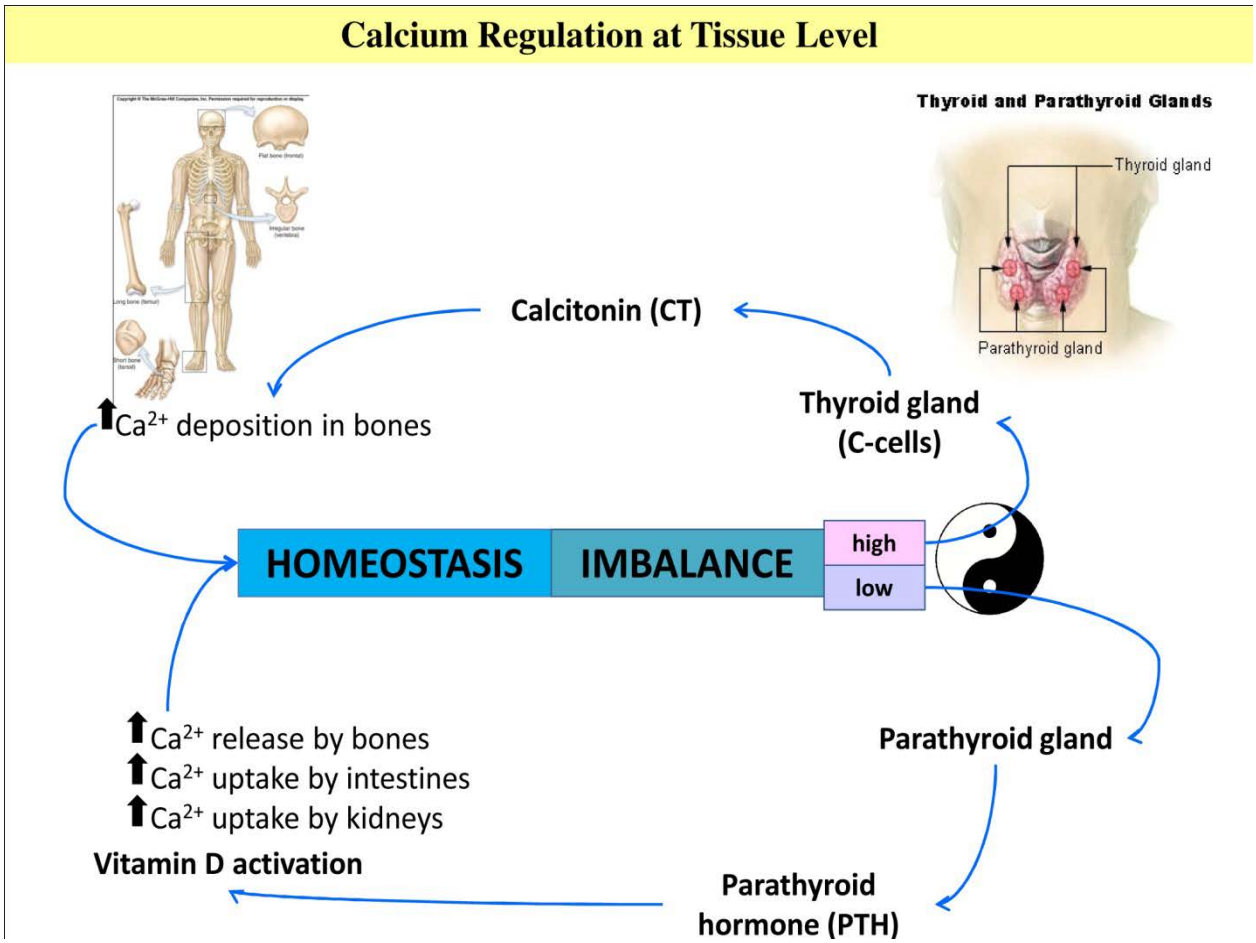

Figure 7. Regulation of Ca^{2+} at tissue level. Ca^{2+} homeostasis is controlled by three hormones: calcitonin, parathyroid hormone and vitamin D. Each of these hormones act on bone cells and other tissues to raise or lower the concentration of Ca^{2+} in the blood.

CHAPTER 2

Materials and Methods

2.1 DNA Applications

Table 1. Vectors and Commercial Competent Cells used in this study

Vectors
pGem®-Teasy (Promega,USA) pcDNA3.1™(-) (Invitrogen, USA) pEGFP-N2 (BD Biosciences Clontech, USA)
Host Bacteria
XL1-Blue (Stratagene) DH5α

Table 2. Bacteria Selection

Name	**Descriptions**
Carbenicillin Stock	10 mg carbenicillin sodium salt in 1 ml of water, filter sterilized.
Kanamycin Stock	10 mg in 1 ml of water, filter sterilized.
Isopropyl-1-thio-β-D-galactoside (IPTG)	20 mg/ml in sterile water
5-Bromo-4-chloro-3-indolyl-β-D-galactoside (X-Gal)	20 mg/ml in N,N dimethylformamide

Note. For Blue-White Selection of clones, IPTG and X-Gal were mixed at 1:5 (making 50 µl) and spread onto agar plates with appropriate selection antibiotics. The agar plates were dried in 37°C dry incubator before storage or use.

Table 3. Bacterial Culture Media

Media	**Components**
Luria-Bertani (LB) broth	Premixed from Media Prep
LB broth/carbenicillin	75 µg/ml carbenicillin in LB
LB broth/kanamycin	40µg/ml kanamycin in LB
LB broth agar	15 g agar in 1 liter of LB broth
LB broth agar/ carbenicillin	100 µg/ml ampicillin in LB agar
LB broth agar/ kanamycin	40µg/ml kanamycin in LB agar

LB broth/glycerol	20% (v/v) glycerol in LB broth
TSBG solution	85% (v/v) LB broth, 5% (v/v) DMSO, 10% (w/v) PEG, 10 mM MgCl2, 10 mM MgSO4, 20 mM glucose

2.1.1 Long-term Storage of Bacteria

Bacterial strains were stored long term at low temperatures (-80°C) in 15 to 40% (v/v) glycerol. A fresh colony was inoculated in 3 ml of LB or LB with specific antibiotics in a 15 ml tube. It was cultured at 37°C until late log or stationary phase (usually overnight). 0.5 ml of LB broth/glycerol was added to 0.5 ml of the bacterial culture (frozen stock will contain 25% glycerol) in a sterile labeled cryo-vial before being frozen at -80 °C. To revive bacteria from the -80°C stock, a sterile pipette tip was used to scrape some of the frozen medium and then streaked on appropriate culture plate e.g. L/A agar. The frozen stocks should not be thawed because each freeze-thaw cycle will result in a 50% loss in cell viability.

2.1.2 Competent Cell Preparation

A single host bacterial colony was inoculated into 3 ml LB and cultured overnight at 240 rpm, 37°C. 0.2 ml of the saturated culture was then inoculated into 200 ml pre-warmed LB in a 500 ml flask. The culture was incubated at 37°C, with vigorously shaking at 240 rpm until it reached exponential phase of approximately A600 0.5 (took approximately 3 hrs) and chilled on ice for 15 mins. The bacterial culture was harvested by centrifugation at 4000 rpm for 10 min at 4°C. The cell pellet was carefully resuspended in 15 ml of ice -cold autoclaved 1M $CaCl_2$ solution and

incubated on ice for 10 minutes and spun again at 4000 rpm for 10 mins. The bacterial cells were then resuspended in 4 ml sterile, ice-cold 0.1 M $CaCl_2$/15% glycerol. Finally competent bacterial cells were aliquoted in 100 µl and quick-freezed using liquid nitrogen and stored at -80°C until use.

2.1.3 Transformation of Bacterial Competent Cells

Transformation was carried out in 1.5 ml Eppendorf tube(s). 10 µl of ligation reaction was added to 100 µl of *E.coli* competent cells. This mixture was then incubated on ice for 30 mins. Cells were heat-shocked in 42°C water bath for 45 s. Cells were then immediately transferred to an ice bath for 2 mins. 900 µl TSBG recovery media was added into the tube and was then placed in a 37°C shaker for 1 hr at 240 rpm. Subsequently, 50 µl was plated onto LB agar plates with appropriate antibiotics. For blue/white screening of recombinants, 40 µl of X-Gal and 10 µl of IPTG were added to the bacterial suspension before the content was plated onto LB agar plates containing the appropriate antibiotics.

2.1.4 Polymerase Chain Reaction (PCR)

PCR reaction was carried out in Programmable Thermal Controller PTC-100 (MJ Research Inc. USA). Template DNA (genomic DNA / plasmid / purified DNA) or bacterial culture containing putative transformants (2 µl) were amplified in a reaction volume of 20-100 µl. Each reaction mixture consists of 1× PCR buffer (New England BioLabs Inc), 200 µM of dNTPs, 1 µM of 5'- and 3'- primers and Dynazyme (New England BioLabs Inc, USA) (2 units / 100 µl of PCR reaction). A master mix was usually prepared, dispensed into individual 0.2 ml PCR tubes and

respective DNA template was added to each reaction. The reactions were carried out for 35 cycles and each cycle begin with 0.5 min of denaturation at 94°C, followed by 0.5 min annealing at the desired temperature and extension at 72°C for x min (approximately 1 min for each kb of expected amplified product). In order to ensure complete elongation of all PCR products, a 5 min extension of 72 °C was included after the last cycle and the reaction samples were stored at 4 °C until further analysis.

2.1.5 Cloning of PCR Products

To clone PCR products, proper restriction sites were included at the ends of each PCR primer. The restriction sites selected are present in the multiple cloning site of cloning vectors and absent inside the DNA product. To ensure optimal restriction digest of PCR products, flanking nucleotide sequences were added 5' to the restriction site of the primer. The PCR products were separated on agarose gels and the desired DNA fragment was excised and purified with QIAquick® gel extraction kit (Qiagen, USA). Alternatively, PCR products were amplified by Taq DNA polymerase or Dynazyme (New England BioLabs Inc, USA), purified and directly cloned into pGem®-Teasy vector (Promega Corporation, USA).

Table 4. Ligation reaction set-up

Normal Ligation Set up	Rapid Ligation Set up
T4 DNA Ligase 1U, 2 µl	T4 DNA Ligase 3U/ µl, 1 µl
10× T4 DNA Ligase Buffer 2 µl	2X Rapid Ligation Buffer (Roche Diagnostics, Germany), 2 µl
Vector DNA 1×	Vector DNA 1×
Insert DNA At least 3× that of vector DNA	Insert DNA At least 3× that of vector DNA
dd$H_2$0 Top it up to 20 µl	dd$H_2$0 Top it up to 20 µl

Normal ligation was performed in Programmable Thermal Controller (PTC-100, Biorad) set at 16°C for 16 hr. Rapid ligation reaction (Roche) was incubated at room temperature for 1 hr or at 4 °C, overnight to obtain maximal number of transformants. Shrimp Alkaline phosphatase (Promega Corporation, USA) was used to dephosphorylate linearized vector to prevent re-annealing. And in order to melt any termini that may have re-annealed, vector and insert DNA in H_2O was warmed to 45 °C for 5 min in a sterile microfuge tube before the addition of 10× T4 DNA ligase buffer and the enzyme.

2.1.6 Restriction Enzyme Digestion

There are generally 2 types of restriction digest: a diagnostic and a preparative digest. A diagnostic restriction digest is performed on a small scale to screen for positive recombinants. The larger scale preparative restriction digest is performed to make recombinant constructs that require further manipulations such as sub-cloning into other expression constructs of interest.

Table 5. Restriction digestion set-up

Diagnostic Digestion (single RE)	Preparative Digestion (single RE)
DNA e.g. plasmid, 0.5 µg	DNA, 5-20 µg
10× Reaction Buffer, 2 µl	10× Reaction Buffer, 6 µl
Restriction enzyme, 2 U	Restriction enzymes, 10 – 40 U
100X BSA (if required), 1 µl	100X BSA (if required), 1 µl
Autoclaved H_2O Top up to 20 µl	Autoclaved H_2O Top up to 60 µl

The above reaction was treated as mentioned for diagnostic digestion and incubated at the recommended temperature (usually 37°C) for a standard period of 3 hr. After incubation, gel loading buffer was added to the reaction mix and the sample was loaded onto an agarose gel. Agarose gel electrophoresis was performed until digested fragments were well separated. The band of interest was cut out of the gel as an agarose block. Purification continued with QIAquick® gel extraction kit (Qiagen, Germany).

2.1.7 Agarose Gel Electrophoresis

To prepare 100 ml of a 1% (w/v) agarose solution, 1 g of agarose was added to 100 ml of 1×TAE and heated in a microwave. The solution was cooled to 55 °C and ethidium bromide was added to a final concentration of 0.5 µg /ml. The gel was allowed to solidify in a gel casting tray. Before loading of samples, the gel was covered with electrophoresis buffer (the same buffer used to prepare the agarose) and 1 µl of 6x gel loading dye was added to every 5 µl of DNA sample. Electrophoresis was performed at 100 volts until dye markers had migrated an appropriate distance. DNA band in the agarose gel was visualized under UV trans-illuminator at 304 nm.

2.1.8 DNA Gel Purification

DNA samples were separated by gel electrophoresis and the fragment to be cloned was cut out of the gel and purified by QIAquick® gel extraction kit (Qiagen, Germany). 3 volumes of buffer QG was added to each volume of agarose and incubated at 50 °C until the gel slice had completely dissolved. The sample was applied to QIAquick column to bind DNA. This was then spun down at 14000 rpm for 1 min to allow binding of DNA onto the QIAquick column. The flow through was discarded. Washing was done by the addition of 750 µl PE buffer into the QIAquick column and spun at 14000 rpm for 1 min. The flow through was discarded. An additional 1 min of centrifugation was carried out to remove any residual ethanol. 40 µl of nuclease-free water was added into the QIAquick column with sterile micro-centrifuge tube and allowed to stand for 1-2 mins. The column was then spun at 14000 rpm for 1 min and the DNA stored at -20°C for longer term. For short-term storage, DNA was stored at 4°C.

2.1.9 Small-scale Purification of Plasmid DNA

Small-scale preparation of plasmid DNA was carried out using AxyPrep Plasmid Miniprep kit (Axygen Biosciences, USA). 1 ml of overnight bacteria culture in LB medium with the appropriate antibiotic was harvested by centrifugation at 13000 rpm for 10 mins using the 5417C tabletop centrifuge (Eppendorf, Germany). After decanting the culture medium, the pellet was resuspended in 250 µl of cell resuspension solution (S1 with added 100 mg/ml RNase A). 250 µl of cell lysis solution (S2) was added to each sample of the bacterial resuspension and mixed by inverting the Eppendorf tube 4-5 times. Within 5 mins, 350 µl of Neutralization Buffer

(S3) was added into each tube and mix by inverting 4-5 times. The neutralized mixture (with white precipitate) was then spun down at 14000 rpm for 10 mins at room temperature. The supernatant was then decanted into a spin column with a 2 ml collection tube. The spin column with the collection tube was then spun down at 14000 rpm for 1 min at room temperature. The flow through was then discarded. 700 µl of Wash solution with ethanol (Buffer W2) was added into the spin column. This was spun at 14000 rpm for 1 min at room temperature. The flow through was again discarded. This washing step was repeated once. This tube was then spun at 14000 rpm for 2 mins at room temperature. The spin column was then transferred to a sterile 1.5 ml micro-centrifuge tube. Plasmid was eluted by the addition of 60 µl of nuclease-free water into the spin column. The spin column was then discarded and DNA stored at -20°C. The DNA was then quantified by using Nanodrop 1000 spectrophotometer (Thermo Scientific, US).

2.1.10 Midi-Scale Purification of Plasmid DNA

QIAGEN-tip 100 (QIAGEN, Germany) was used to isolate ultrapure plasmid for microinjection into zebrafish embryos. *E. coli* cells were lysed by the alkaline/SDS lysis treatment, followed by binding of plasmid DNA to QIAGEN anion-exchange resin. Plasmid DNA was eluted in a high salt buffer and then concentrated and de-salted by isopropanol precipitation. Briefly, 50 ml bacterial suspension containing transformed *E. coli* was lysed with alkali. The cell debris and chromosomal DNA was precipitated with SDS and potassium acetate. After pelleting the debris the plasmid DNA in clarified cell lysate was passed through the pre-equilibrated QIAGEN cartridge by gravity flow. The column was washed twice with 10ml Buffer QC and plasmid was eluted with 5ml buffer QF. Eluted DNA was precipitated with 3.5 ml of isopropanol at room temperature and centrifuged at 4,500 g, 4°C for 45 min. The DNA pellet was rinsed with 70%

(v/v) EtOH and centrifuged for 10 min at 13,000 rpm, room temperature. The pellet was dried and suspended in 100 µl sterile TE buffer, pH8.0. DNA was stored at 4°C for short-term or -20°C for longer term.

2.2 RNA Procedures

2.2.1 Isolation of total RNA from Zebrafish Embryos

Total RNA was extracted from dechorionated zebrafish embryos using RNeasy® mini kit (Qiagen, Germany). Zebrafish embryos were collected at desired stages and placed in 1.5 ml Eppendorf tube. Excess liquid was siphoned out from the tube. 350 µl of RLT buffer containing β-mercaptoethanol was added into the tube and the embryos were passed through a 23G sterile needle for at least 5 times to disintegrate embryos. The lysate was then spun down at 14000 rpm, RT, for 3 mins. The supernatant was decanted into a sterile 1.5 ml Eppendorf tube. 350 µl of 70% ethanol was added into the clear lysate and mixed well. This mixture was transferred to an RNeasy mini spin column sitting in a 2 ml collection tube. The column was then spun at 10000 rpm for 15 sec. The flow through was discarded. 350 µl of RW1 buffer was pipetted into the RNeasy column to wash, the column was centrifuged at 10000 rpm for 15 sec. The flow through was discarded. In-column DNA digestion was performed by adding 80 µl of RNase-free DNAse (10 µl DNAse diluted with 70 µl RDD buffer; Qiagen, Germany) incubation mix was then added directly onto the RNeasy silica-gel membrane and allowed to stand on the bench at room temperature for 15 mins. After which, another 350 µl RW1 buffer was added into the RNeasy column and spun down at 10000 rpm for 15 sec. The flow through was discarded. 500 µl of RPE buffer was pipetted on the column and spun down at 10000 rpm for 15 sec. The flow through

was discarded and the washing step was repeated with another 500 µl of RPE buffer. The column was then spun at 10000 rpm and for 2 mins and the flow through discarded. The column was then spun down for an additional 1 min to remove any residual trace of ethanol. Column was then transferred to a sterile 1.5 ml Eppendorf tube. Total RNA was eluted by the addition of 40 µl of RNase-free water onto the RNeasy membrane and spun for 2 mins. The RNA was then quantified by using the Nanodrop 1000 spectrophotometer (Thermo Scientific, US).

2.2.2 One-step RT-PCR

Total RNA (DNAse I treated) was isolated from zebrafish embryos using RNeasy® Mini Kit (Qiagen, Germany). cDNA for RT-PCR analysis was synthesized using Qiagen® OneStep RT-PCR kit (Qiagen, Germany) containing an optimized combination of Omniscript reverse transcriptase, Sensiscript reverse transcriptase and HotStartTaq DNA polymerase and the reaction was carried out according to the manufacturer's instructions. The technique was used to amplify *atp2b1a* transcripts from wild type and zebrafish embryos for making antisense probe in whole mount in situ hybridization experiments. Primers used are listed in Table 10. cDNA synthesis at 50°C for 30 mins, followed by denaturation at 94°C for 15 mins for 1 cycle followed by 40 cycles of [94°C for 1 min, 61°C for 1 min and 72°C for 1 min] and final extension at 72°C for 5 mins. The annealing temperature was changed according to the primer design.

Table 6. Primers Used in RT-PCR

Gene	Direction	Sequence (5' – 3')
atp2b1a	Forward	GAGAGATCTAGAAGACATGGCTAACAACTCATACAG
atp2b1a	Reverse	CTCTCTCCCTAGGTCAAAGGGACGTCTCTAG
β-actin	Forward	CTTCCTTCCTGGGTATGGAATC
β-actin	Reverse	CGCCATACAGAGCAGAAGCCA

2.2.3 First-strand cDNA Synthesis

First-strand cDNA was synthesized using the Superscript First Strand Synthesis Kit (Invitrogen, US). Briefly, 600 ng of purified total RNA was added to 10 mM oligo(dT), 10 mM dNTP mix and topped up to 10 µl with DEPC water. This mixture was incubated at 65°C for 5 mins and quick chilled on ice for another 3 mins. 25 mM $MgCl_2$, 10X First Strand buffer, 0.1M DTT & RNase Out (400 U/µl) were added to the mixture and incubated at 42°C for 2 mins. After which, 2 µl of Superscript II Reverse Transcriptase (50 U/µl) was added into the same tube and incubated at the same temperature for 1 hr, followed by 70°C for 15 mins. 1 µl of RNase H was added and the mixture was incubated at 37°C for 20 mins and chilled at 4°C. Aliquots of synthesized first strand cDNA were stored at -20°C until use.

2.2.4 Long-range PCR

Full length *atp2b1a* transcript was amplified from purified first-strand cDNA using the long-range Roche Expand Long Template PCR system. The PCR reaction mix contained 10X Buffer 1 (with 17.5 mM $MgCl_2$; suitable for amplifying template length ranging 0.5 kb to 9.0 kb), 10

mM dNTP mix, gene specific forward and reverse primers for *atp2b1a* at 10 mM each, first strand cDNA template, 3.75 U of Expand Long Template Enzyme mix and topped up to 50 ul with sterile ddH_20. The PCR mixture was incubated in the following temperature profile: initial denaturation at 94°C for 2 mins; 10 cycles of denaturation at 94°C for 10 s, followed by annealing at 55°C for 30 s and followed by elongation at 68°C for 4 mins (since predicted full length of amplicon was 4 kb). The reaction mixture was then subjected to another 25 cycles of denaturation at 94°C; 15 s, annealing at 55°C; 30 s, elongation at 68°C; 4 min with additional 20 s added to each successive cycle. The final elongation was completed at 68°C for 7 mins and cooled to 4°C for storage and use.

2.2.5 Messenger RNA Synthesis for Rescue Experiments

Sense mRNA was synthesized using mMessage mMachine kit (Ambion, USA) according to manufacturer's instruction. Table 11 details the reaction set up:

Table 7: Components of *in vitro* mRNA synthesis

Component	Amount
2X NTP/CAP	10 ul
10X reaction buffer	2 ul
Linearized DNA template	1 ug
Enzyme Mix	2 ul
Nuclease-free water	top up to 20 ul

Reaction mix was incubated at 37°C for 2 hours. 1 µl of Turbo DNase was mixed in and resumed incubation for another 15 mins to eliminate the DNA template. After which, the synthesized

mRNA was clean-up using Qiagen RNA clean up procedure and eluted at 30 µl with RNase-free water. Synthezied RNA was stored at -20°C and used within 1 month. Full length *atp2b1a* mRNA was designed to omit the priming site of *atp2b1a*-MO. In most cases, 1 nl of 500 pg/nl mRNA was co-microinjected with morpholino into zebrafish embryos.

2.2.6 Quantitative Real-time PCR

2 groups of pharynx explants (150/group) were excised from 3.5 dpf 4% PFA-fixed control and morphant larvae. Total RNA was extracted using Qiagen RNeasy kit and treated with DNaseI according to manufacturer's instruction. Quality of RNA was confirmed by Nanodrop absorbance measurement. cDNA was synthesized from total RNA with oligo (dT) priming using Superscript II reverse transcriptase (Invitrogen). Gene specific primer sets were designed based on Danio rerio ZV8 genomic assembly (see Table 12 for primer list). Primer sets were designed to span an exon-exon junction to avoid interference from genomic DNA and were tested for specificity using PCR (Qiagen) from cDNA template of AB embryos to verify production of a single band of the predicted size. Amplicons were PCR-purified (Fermentas) and sequenced for confirmation. Quantitative real-time PCR was performed using DNA Engine Opticon System (MJ Research) with SYBR green fluorescent label. Samples contained 1× SYBR green master mix, 0.1 - 0.5 µmol of each primer and 1 µl of test cDNA at 1 ng/µl for a final volume of 50 µl. Samples were run in triplicate (50 pharynx/pool) in coated 96-well plates (MJ Research). Data generated were compiled and analyzed for C_T values by using the accompanying Opticon Monitor software. Student's *t*-test was used to analyze differences in mean C_T values between

non-MO injected control and morphant pharynx tissues to determine significant differences in expression following morpholino knockdown. Significance was set at $P < 0.05$.

Table 8. Primers used for quantitative real-time PCR analysis

Gene	Primer (5'-3')	Location; size (bp)	Tm	Accession no.
atp2b1a	F) AGACATGGCTAACAACTCATACAG R) TCGCAGTTCCATAAGAGAGCGCAGCT	exon20-exon21; 112 bp	55 °C	NW_001878904
integrin αV	F) AAGATGAGCAGAGCCAGAAGCAGC R) AATCCTGAGCTCCCAACCAGCACT	exon2-exon3; 137 bp	55 °C	NW_001879461
calca	F) ATGGTTATGTTGAAGATCTCCGCTT R) CAATCTTCTCGCCTCGTAGTCGCT	exon2-exon3; 151 bp	55 °C	NW_001879254
cx43	F) TAGACGTCCAGGTCATCAGG R) CGACTACCCTGATGATACACAT	exon1 144 bp	55 °C	NW_003040660
dlx2b	F) CGCAGACCCAGGTGAAGATATG R) GTGGGAAATCCCAACCTGCT	exon2-exon3; 150 bp	55 °C	NM_131297
b-actin 1	F) CGAGCAGGAGATGGGAACC R) CAACGGAAACGCTCATTGC	exon3 102 bp	60 °C	NW_001878018

Note: Primer sets spanned an exon-exon junction to avoid errors due to contaminating genomic DNA. Primer sets were tested for specificity using standard RT-PCR and zebrafish embryo cDNA as template to verify production of a single band of the predicted size. Amplicons were sequenced verified.

2.3 Zebrafish

2.3.1 Fish Maintenance

Zebrafish embryos (*Danio rerio*) were obtained from the fish facility of the Institute of Molecular and Cell Biology. The fish were maintained according to the method described (Westerfield, 1995). Fishes were fed three times per day with brine shrimps or commercial fish flakes. They were kept under photoperiod cycle set at 14 hrs of daylight and 10 hrs of darkness. Crosses were set after the third meal at 1800 hr with a divider and wire mesh.
Divider was removed at desired time to stimulate spawning behavior. Embryos were then collected by a sieve and rinsed thoroughly to remove any waste materials attached to the chorion.

2.3.2 Stages of Embryonic Development

In developmental studies, the accurate staging series is a tool important for defining the timing of various developmental events. The embryos used were raised at 28.5°C and staged according to standard practice (Kimmel et al., 1995). Embryos which were used for analysis at stages beyond 36 hpf were treated with 1-phenyl-2-thiourea (PTU; 1.5 mg/ml) at 19 hpf to prevent the formation of melanin (Westerfield, 1995). The approximate stage of a live embryo was determined by examination under a dissecting stereomicroscope (Leica, Germany).

2.3.3 Microinjection into Blastula Stage Zebrafish Embryos

Micro-needles were pulled from borosilicate capillaries with filament (Sutter Instruments) using its Micropipette Puller (model P-97). For pan-embryonic microinjections, capillaries of inner diameter 0.58 mm were used while 0.50 mm capillaries were used for blastomeres injections. Morpholinos and plasmid DNA samples for injection were prepared at different concentrations in 1X Danieu solution (58 mM NaCl; 0.7 mM KCl; 0.4 mM MgSO4; 0.6 mM $Ca(NO_3)2$; 0.5

mM HEPES, pH 7.6). Samples were injected into the cytoplasmic stream of 1- 2 cell stage zebrafish embryos using a MPPI-2 pressure injection system (Applied Scientific Instrumentation, USA). Injected zebrafish embryos were raised in 1X egg water (1 ml contains 10% NaCl; 0.3% KCl; 0.4% $CaCl_2$; 1.63% $MgSO_4.7H_2O$).

2.3.4 Design of Antisense Morpholinos

Morpholinos (MOs) were obtained from Gene Tools, LLC, USA. The antisense oligonucleotide sequences were designed to bind to the 5'UTR or flanking sequences including the initiation methionine or sequence at exon-intron junctions. To minimize the possibility of non-specific effects, at least two MOs complementary were designed to non-overlapping sequences for each gene. MOs were resuspended from lyophilized powder, and then diluted to 1 mM stock in 1X Danieau's solution and stored in dark at 4°C as working solutions or -80°C for prolonged storage. The MOs were diluted to the appropriate concentrations and these were injected into the yolk cell of one to two cell stage embryos. The designs of MOs used were based on recommendations provided by Gene Tools, LLC

Morpholinos used in this study are listed in Table 9. ATG start site blocking MO, *atp2b1a*-MO was used for experiments since the splice MO (GTE22CA1MO) resulted in similar but more severe phenotype. *atp2b1a*-MO included the predicted ATG start codon. In all studies, 1 nl of 10 ng/nl control or 5 ng/nl of *atp2b1a*-MO or 3 ng/nl of zf-p53-MO were injected into 1–2-cell stage embryos.

Table 9. A List of Morpholinos Used in This Study.

Gene	Sequence (5'-3')	Reference
atp2b1a -MO	CCATGTCTCCCGACCACACCTTGTC	Go et al., 2010
5M-*atp2b1a*-MO	CGATCTCTCGCGAGCACAACTTGTC	Go et al., 2010
GTE22CA1MO	AACGCGCACTCACACCCGACAGTGG	Unpublished
5M_GTE22CA1MO	AAGGCCCACTCAGACCCCACACTGG	Unpublished
atoh1a-MO	ATCCATTCTGTTGGTTTGTGCTTTT	Millimaki et al., 2007
ascl1a-MO	CCATCTTGGCGGTGATGTCCATTTC	Amoyel et al., 2004
ascl1b-MO	TCGTAGCGACGACAGTTGCCTCCAT	Amoyel et al., 2004
calca-MO	CATGGTCCCCTTAAGATGCTCAGCT	Lafont et al., 2010
zf-p53-MO	GCGCCATTGCTTTGCAAGAATTG	Gene Tools LLC

Note: 5 Mismatches for control 5M-*atp2b1a*-MO were underlined

2.3.5 Embryo Anesthesia

When viewing live embryos after 19 hpf, the embryos may twitch or move which affects the process of imaging. Anesthetic was used to facilitate embryo manipulation. 400 mg of Tricaine (aka. MS-222; 3-amino benzoic acid ethyl ester) (Sigma, USA) powder was dissolved in 97.9 ml of sterile water and the pH was adjusted to 7 using Tris pH 8.0. Usually, 5 μl of this solution was added in a Petri dish with selected embryos and after a few seconds, the embryos could be transferred for viewing.

2.3.6 Behavioral Assay

Auditory and vestibular functions were assayed as described (Riley and Moorman, 2000). 2dpf larvae were stimulated by touch with a needle. Normal larvae show controlled linear motion by traversing across a 6 cm Petri dish in a straight line. Larvae with vestibular defect swam in rapid, irregular arcs, or in a circle. The ability to maintain a dorsal-side up posture for more than 30 seconds was checked to define the defect of balance. Auditory ability was tested at 7 dpf by tapping the side of the Petri dish. Touch response was used to define motor ability. Each individual larva was assayed three times and those with at least one normal response were considered to be normal.

2.3.7 16-cell Blastomeres Injection

Fertilized eggs were collected at the 1-cell stage and allowed to develop to the 8-cell stage either at room temperature or at 28°C. At the 8-cell stage, embryos were transferred to a 25 mm tissue culture dish. De-chorionation was unnecessary. About 30 embryos were transferred to a Petri dish with molded agar (1.5% agarose in egg water) injection wells prepared earlier. Wells of 1.5 mm are ideal. Excess water was removed by Kimwipes tissue paper. Since a micro-manipulator was mounted on the right hand side, embryos were then oriented with the blastomeres facing 45^{o} right, so that the central blastomeres can be easily recognized. Not more than 200 pl of reagents (MO + Texas Red tracer) was injected per blastomere per embryo. After injection, egg water was added slowly to the side of the dish to cover embryos and was left undisturbed in the agar wells until 2 hrs later in 28°C incubator to prevent injected embryos from bursting. After which embryos were collected in a glass Petri dish with egg water and allowed to develop to 4 hpf, then inspected under a UV florescence microscope. Properly injected embryos should have labeled

clones in the centre of the blasdoderm viewed from the animal pole and a perfect cone when viewed from the side. Only these embryos were selected and allowed to develop further. The others, where the clones were not in the centre were discarded. This was done to ensure that only ectodermal derivatives were labeled.

2.4 Functional Assays

2.4.1 Pharmacological Treatment

Embryos were treated with neomycin (neomycin sulfate, Sigma Aldrich) as described (Harris et al. 2003). The activity of PMCA was blocked via the administration of its inhibitor, 5(6)-carboxyeosin (CE; Sigma Aldrich). The chemical was dissolved in 0.1% DMSO (final concentration 0.05%) for stock and further diluted to the working concentration (50 µM) with embryo medium. For hair cells treatment, embryos were incubated in CE for 6 hrs at 28°C. Embryos were mounted ventral side faced up in 0.5% low melting agarose. For UB treatment, CE was administered at 10 µM and 3 small boluses (~500 pkl/bolus) were microinjected in succession into the pericardium chamber of embryos. Injection in small bolus helps prevent cardiac arrest. Vehicle control (0.1% DMSO) marked by Texas-Red tracer dye was injected similarly. Effect of CE treatment was observed after 6 hrs incubation at 28°C.

2.4.2 Acid-free Dual Staining of Bones and Cartilage

In order to visualize the progression of bone calcification over a period of developmental stages, an acid-free staining method was required. For most conventional cartilage staining, Alcian Blue 8GX has been the histo-dye of choice. But these staining protocols would require dissolving Alcian Blue 8GX powder in acetic acid, which would then makes it impossible to visualize any calcification signal in parallel. The dual-staining procedure use for this study was successfully adapted from Walker and Kimmel, 2006's work.

Briefly, an acid-free double stain solution was prepared in 2 parts. Part I was the Alcian Blue 8GX for blue cartilage staining which contained 0.4% Alcian Blue (w/v) in 70% ethanol, containing the crucial 150 mM $MgCl_2$ for clearing up non-specific Alcian Blue staining. Note that Alcian Blue 8GX powder does not dissolve readily in ethanol thus it has to be dissolved progressively with higher concentrations of ethanol. Part II was Alizarin Red S for red calcified bone staining which contained 0.5% (w/v) Alizarin Red S in ddH_2O. Eventually, 1 ml of Part I was mixed with 10 µl of Part II for the dual-staining solution. Larvae of at least 3 dpf were fixed with 4% PFA/PBS for 2 hr at room temperature. The fixative was later replaced by 50% ethanol and dehydrated for 10 mins with constant rocking. The alcohol was replaced with the dual-staining solution and stained overnight at room temperature with constant rocking. Pigmentation was removed on the next day by bleaching in 1.5% H_2O_2 in 1% KOH for 20 mins. The bleaching solution was replaced by a progressive glycerol exposure mixed in 0.25% KOH (i.e. 25%, 50%, 75% to 100%) and rocked overnight at room temperature for tissue clearance. For older larvae (e.g. 6 and 7 dpf), few nights of constant rocking was necessary to clear the tissues sufficiently to reveal specific bone staining.

2.4.3 Vital Dye Staining on Live Embryos

Vital dyes which detect specific signals were used during this study. Prime advantage of using vital staining procedure was the ability to obtain crucial information on live embryos which will otherwise be missed using fixed specimen. Data was collected and analyzed via various means of microscopy described in Section 2.8. Table 10 has listed the type of vital dyes used in this study, along with their working concentrations.

Table 10: Vital dyes used and their working dilution

Vital Dye	Signals or Structures stained	Working Dilution	Ordering info.
DASPEI	hair cells and ionocytes	1 mM in egg water	Invitrogen; D426
MitoTracker Red	mitochondria and cell membrane	1 µM in egg water	Invitrogen; I34154
Bodipy Texas Red	Cell membrane	1 µM in egg water	Invitrogen; I34407
Calcium Crimson AM	Intracellular Ca^{2+}	1 µM in egg water	Invitrogen; C3018
Rhodamine Phalloidin	F-actin, stereocilia	to be determined by user	Invitrogen; R415
Alizarin Red S	calcified bone	25 µg/ml in egg water	Sigma Aldrich; A5533
Calcein	calcified bone	25 µg/ml in egg water	Sigma Aldrich; C0875
Acridine Orange	Apoptotic cells	150 mg/ml in egg water	Sigma Aldrich; A6014

2.4.4 Bone Mineralization Assay

Dual-stage bone staining of the developing opercle was performed as described (Kimmel et al., 2010). Briefly, Alizarin Red S (AR) and Calcein were able to function as vital stains, highlighting bones that are in the process of calcification or calcified bones. AR is able to emit florescence signal at 580 nm when excited at between 530-560 nm while Calcein is able to florescent at 517 nm when excited at 494 nm. Vital stains were dissolved in 1X egg water from

stock solutions. Larvae were stained successively by first pulse exposed to AR (50 µg/ml) for 2 hours at 3 dpf, with a period of washing out before being incubated in Calcein (50 µg/ml) at 28°C up to 3 days until observation under a dual channel confocal microscope. The initial pulse to AR labeled the entire bone matrix present at the time of the pulse. It is important to note that this dye-bone staining appeared stable with little or no decrease detected in intensity over the subsequent 3-day incubation.

2.4.5 Live Ca^{2+} Imaging

Chemical Ca^{2+} indicator was used to obtain representative Ca^{2+} profile of live embryos, in particular the sensory hair cells of neuromasts and inner ear. Live embryos were collected at appropriate stages and stained with 1 µM Calcium Crimson AM (CC; Invitrogen, Molecular Probes; Fig. 8), dissolved in 1X egg water. After incubation at 28°C in the dark for 1 hr, embryos were washed 3 times, 10 mins each with 1X egg water to removed unstained dye and mounted for live confocal imaging as described in Section 2.8.1. High resolution confocal images were obtained as described in Section 2.8.2. Through such manipulation, sensory hair cells of the lateral line were able to pick up the staining efficiently. For visualizing hair cells located deeper within the confinement of the otic vesicles, it was necessary to microinject small volume of <200 pkl of the indicator directly into the otic vesicle. Single-line analysis measuring relative fluorescence level of signal emitted by CC was performed on hair cells by confocal software described in Section 2.8.2.

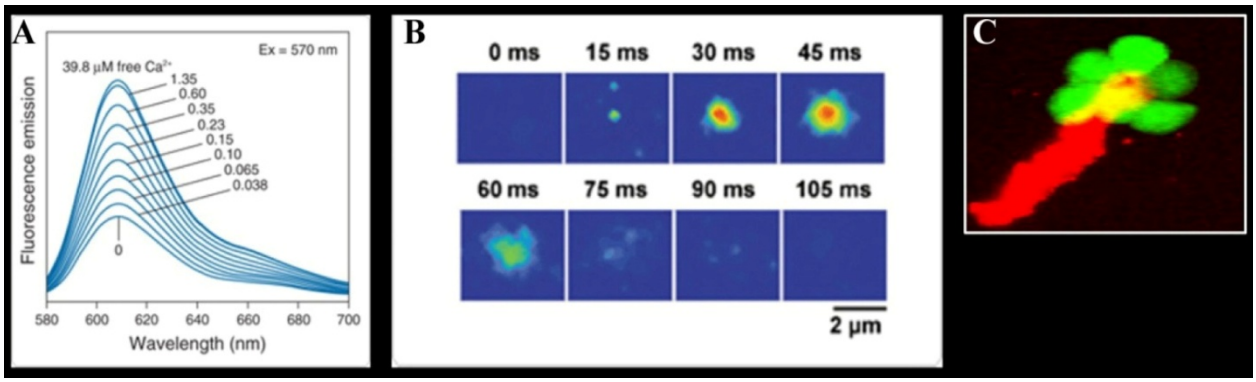

Figure 8: Chemical Calcium Indicator; Calcium Crimson AM. A) Ca^{2+}-dependent fluorescence emission spectra of the Calcium Crimson indicator. B) Fast confocal recording of spontaneous Ca^{2+} sparks in a rat ventricular myocyte (Invitrogen, Molecular Probe, USA). C) SqET4 vitally stained with Calcium Crimson AM (Go et al., 2010).The acetoxymethyl (AM) ester derivatives of fluorescent indicators and chelators make up one of the most useful groups of compounds for the study of live cells. Modification of carboxylic acids with AM ester groups results in an uncharged molecule that can permeate cell membranes. Once inside the cell, the lipophilic blocking groups are cleaved by nonspecific esterases, resulting in a charged form that leaks out of cells far more slowly than its parent compound. Frequently, hydrolysis of the esterified groups is essential for binding of the target ion. AM ester is colorless and non-fluorescent until hydrolyzed. This property is useful in diagnosing spontaneous hydrolysis during storage.

2.4.6 Birefringency of somite

Somite's integrity of larvae was assessed by its level of birefringency. Normal forming somite exhibit high level of birefringency post-somitogenesis and is observable under a polarized light source. In this case, an Olympus Stereomicroscope SZX-12 was fitted with a polarizer light filter (Olympus SZX-AN, Japan). Zebrafish larvae were contained in a glass Petri dish and birefringency of somites can be easily visualized through the eye piece of the stereomicroscope, which appeared as bright white fluorescence in dark field.

2.4.7 Hanging Drop Culture

Hanging-drop cultures were done with animal caps from embryos at 50% epiboly as previously described (Steinberg and Takeichi 1994). Briefly, embryos were injected with lysine-fixable fluorescein- or Texas Red conjugated dextran (mw. 70 kDa) into 1-cell stage embryos. *Atp2b1a*-MO was co-injected with fluorescein-dextran. Embryos were grown to 50% epiboly and the yolk cell was removed manually. The resultant animal caps (*n*=15 each for fluorescein and Texas Red labeled) were mixed together in an Eppendorf tube and mechanically dissociated in 300 µl of L15 medium with a 200 µl pipette. Drops of 30 µl each were placed on a plastic Petri dish cover and carefully inverted, creating hanging-drops. Dishes were then taped with surgical tape (3M Micropore™, NDC 8333-1530-1), to prevent contamination while still allowing airflow) and incubated at 28°C overnight. Fluorescent images were obtained by imaging with Olympus Fluoview FV1000 upright confocal system (Olympus, Japan).

2.5 *In situ* Hybridization

2.5.1 Antisense Probe Synthesis

7 to 10 µg of plasmid DNA was linearized at the 5' end of the cDNA insert by a preparative restriction enzyme at 37°C for 3 hrs. 1µg of linearized DNA was used to synthesize the DIG/fluorescein probe. The reaction was performed at 37°C for 2 hrs in a total volume of 20 µl containing 2 µl of 10X transcription buffer (Ambion, USA), 2 µl of DIG/Fluorescein-NTP mix [10 mM ATP, 10 mM CTP, 10 mM GTP, 6.5 mM UTP and 3.5 mM DIG/Fluorescein-UTP (Boehringer Mannheim, Germany)], 1 µl of RNase inhibitor (40U/ µl) (Promega, USA). 2 µl of

RNase-free DNase I was used to digest the DNA template at 37°C for 15 mins following this reaction. Antisense probes used in this study were generated from cDNAs and are listed in Table 11.

Table 11. A List of Molecular Markers Used in this Study.

Gene	Vector	Restriction enzyme	RNA Polymerase	Reference
egfp	pBluescript	SacI	T7	Teh et al.,
atp2b1a	pGEM-Teasy	SacII	SP6	Go et al., 2010
atoh1a	pGEM-Teasy	SpeI	T7	IMAGE clone: 7428977
sox2	pCMVSport6	EcoRI	T7	IMAGE clone: 6801649
tacstd	pGEM-Teasy	SacII	SP6	Villablanca et al., 2006
calca	pGEM-Teasy	SpeI	T7	Alt et al., 2006

2.5.2 RNA Probe Clean Up

Sample was adjusted to a volume of 100 µl with RNAse-free water. 10 µl of β-mercaptoethanol was added to 1 ml of RLT buffer. This was followed by the addition of 350 µl of the RLT buffer to the diluted RNA sample that was subsequently mixed with 250 µl of 96-100% ethanol. This whole volume was then transferred to an RNeasy mini spin column that had been inserted into a collection tube. The spin column and collection tube was spun at 10000 rpm for 15 sec. The flow through was then discarded. 500 µl of RPE buffer was pipetted into the spin column and spun at 10000 rpm for 15 sec. Flow through was discarded and replaced with another 500 µl of RPE buffer. The column was spun at 10000 rpm for another 2 min. The RNeasy column was then removed and placed onto a new 1.5 ml Eppendorf tube and 30-50 µl of RNase-free water was

added into the RNeasy column and allowed to stand for 1 min. RNA probe was then eluted out by micro-centrifuging the column at 10000 rpm for 1 min. The RNA probe was then stored at -80°C.

2.5.3 Fixation of Staged Embryos

Embryos were dechorionated manually using a pair of 26 gauge hypodermic needles and fixed overnight at room temperature. Staged embryos were chilled on ice for 5 mins to straighten their body and fixed in 4% PFA(paraformaldehyde) /PBS (0.8% NaCl; 0.02% KCl; 0.0144% Na_2HPO_4; 0.024% KH_2PO_4, pH 7.4) for 12 to 24 hrs at room temperature. Embryos younger than 15 hpf were fixed before dechorionation and the chorion was removed afterwards. Embryos older than 16 hpf were dechorionated before fixation. After fixation, the embryos were washed in PBST (0.1% Tween-20 in PBS) thrice for 5 mins each on nutator.

2.5.4 Proteinase K (PK) Treatment

This step is carried out for embryos that are older than 14 somites (>16 hpf). Embryos were treated with 10 μg/ml of PK (Roche) in PBST at room temperature. The time of exposure to PK is dependent on the stage of the embryos and the specific activity of PK, which vary from batch to batch. In general, the guidelines are listed in Table 12. Embryos were post-fixed in 4% PFA/PBS for 20 mins at room temperature. Embryos were then washed in PBST thrice for 5 mins each.

Table 12. Permeabilization of Zebrafish Embryos and Larvae by Proteinase K (PK)

Embryo stage (hpf)	Time of PK Treatment (mins)
<24	3
24-32	5
33-36	10
37-40	15
>41	20

It is important to note that for staining lateral line cells, PK treatment was usually avoided since it will removed some peripheral tissues which inevitably affects the final outcome of the staining.

2.5.5 Pre-hybridization

Pre-hybridization was performed by replacing PBST with pre-hybridization buffer [50% formamide; 5X SSC; 50 µg/ml heparin; 500 µg/ml torula RNA; 0.1% Tween-20; pH 6.0 (pH adjusted by citric acid)]. And the tube was placed at 68°C for at least 4 hrs.

2.5.6 Hybridization

2 - 4 µl of DIG-labeled probe (signal intensity dependent) was diluted in 300 µl of hybridization buffer and denatured at 70°C for 5 mins, followed by 5 mins on ice. Selected embryos were placed in a 1.5 ml Eppendorf tube with the original pre-hybridization solution removed and replaced with probe added in pre-hybridization solution. The reaction was incubated overnight at

68°C in a circulating water bath. The next morning, the embryos were incubated in four changes of washing solution containing decreasing percentage of formamide in 2X SSCT. The four washing solutions contained stepwise decrease in formamide from 50% formamide in 2X SSCT at the first wash to 12.5% of formamide in 2X SSCT at the last wash. All washings were conducted in the 68°C water bath for a period of 15 min per wash. This was followed by the fifth wash with 2X SSCT without formamide for 15 min. And the final wash of 0.2X SSCT at 68°C for 1 hr.

2.5.7 Preparation of Pre-adsorbed Anti-DIG Antibody

Commercial anti-DIG Fab-AP antibodies (Roche Diagnostics, Germany) should be pre-incubated with intact biological specimen, to decrease the staining background and to increase signal-to-noise ratio. In most cases, anti-DIG-AP antibodies was diluted to 1:200 in PBS containing 5% blocking reagent (Roche Diagnostics, Germany) and incubated with 4% PFA fixed zebrafish embryos on a nutator at 4°C overnight. After that, the antibody solution was transferred to a new tube and diluted to 1:2000 and 1:500 with PBS in 5% blocking reagent, 10 µl of 0.5 M EDTA (pH 8.0) and 5 µl of 10% sodium azide in a final volume of 10 ml to prevent bacterial growth. The pre-absorbed antibody was stored at 4°C and can be reused up to 3 times.

2.5.8 Incubation with Pre-absorbed Antibodies

After hybridization and post hybridization washes, the embryos were incubated in PBS containing blocking solution for a minimum of 1 hr at room temperature to remove background

signal generated from non-specific binding of antibodies. After removing the blocking solution, the embryos were incubated with pre-absorbed anti-DIG-AP antibody at 4°C overnight.

2.5.9 DIG and Fast Red Staining

After antibody incubation, embryos were washed 4 times 20 min each in PBS followed by 2 times 15 min each in detection buffer (100 mM Tris pH9.5, 5 mM Mg Cl2, 100 mM NaCl). NBT/BCIP color substrate development was performed in the presence of 0.3375 μg/ml of nitroblue tetrazolium (NBT) (Sigma-Aldrich, USA) and 0.175 μg/ml of 5-bromo, 4-chloro, 3-indolil phosphate (BCIP) (Sigma-Aldrich, USA) dissolved in detection buffer. Fast red staining was prepared by dissolving 1/2 of the fast red tablet (Roche Biochemicals, Switzerland) in 1ml detection buffer (100 mM Tris pH8.2, 5 mM Mg Cl2, 100 mM NaCl). The content was clarified by centrifugation and mixed with equal part of Naphthol AS-MX phosphate (Sigma, MO, USA) solution (500 μg/ml in fast red detection buffer). Color development was allowed to proceed in the dark and monitored occasionally under light microscopy until the desired intensities were achieved. For control and experimentally injected sets of embryos, the staining procedures were initiated and stopped at the same time. The staining reaction was stopped by washing 2 times 5 min each with PBST followed by 4% PFA fixation for a minimum period of 20 min before storing stained embryos in PBS containing 50% glycerol.

2.5.10 Two Color *In situ* Hybridization

In two-color whole mount *in situ* hybridization, two distinct RNA probes labelled with DIG or Fluorescein were applied to the same embryos in equal ratio. After incubation at 68°C overnight,

the probe in hybridization solution was removed and washing was carried out as stated in section 2.5.6. The DIG detection was carried out first and the procedure is as described in section 2.5.9. Following the DIG staining with NBT/BCIP, the embryos were washed with Maleic acid buffer (MA; 0.15M maleic acid; 0.1 M NaCl; pH 7.5) twice for 10 mins. To remove the phosphatase activity of first antibody, the embryos were incubated with glycine buffer (0.1 M, pH 2.2) for 30 mins at room temperature. After that, the embryos were washed with PBST four times for 10 mins each and then incubated in blocking buffer (5% Blocking reagent in MA buffer, Roche, Germany) at room temperature for 1 hr. Embryos were subsequently incubated with anti-Fluorescein-AP antibody overnight at 4°C. To detect the fluorescein signal, the embryos were washed with MA buffer (50 mM maleic acid; 100 mM NaCl) at room temperature for 4 times 20 min each. After which, the MA buffer was replaced with fast-red staining as stated in section 2.5.9.

2.6 Cryostat Sectioning

2.6.1 Mounting Specimen for Cryostat Sectioning

Fixed or stained embryos were first transferred into molten 1.5% Bacto-agar - 5% sucrose in a detached Eppendorf cap at 50°C. A syringe needle was used to adjust the embryo in a desired orientation in a gradually hardening agar. After the agar block solidified, a small trapezium-shaped agar block was cut with razor blade to mount the sample in the proper position. The block was then transferred into 30% sucrose solution and allowed to stand at 4°C overnight.

2.6.2 Freezing and Collecting Sectioned Specimens

Subsequently, the block was placed on the frozen surface of a layer of frozen tissue freezing medium (Tissue-Tek O.C.T., Sakura, Japan) on a pre-chilled (-20°C) tissue holder or chuck. The block was then coated with one drop of freezing medium and frozen in liquid nitrogen until the block had solidified completely. The frozen block was placed into a cryostat chamber (Leica, Germany) for 30 mins to be equilibrated with temperature of chamber that is at -25°C. Normally, 12 μm thick sections were cut and collected on a Leica CM1900 Cryostat (Leica, Germany) and the sections were transferred onto warmed polysine charged slides (Thermo-Scientific). The slides were dried at 42°C on the hotplate for 30 mins. The sections were rinsed briefly with PBST and cover slips were placed on the slides with several drops of 50% glycerol/PBS or Vectashield mounting medium with DAPI counter stain (Vecta Labs, US) for protection of fluorescence staining. The slides were sealed with nail polish and ready for observation under microscope.

2.7 Protein Applications

2.7.1 Immunohistochemical Staining

Fresh embryos were collected at appropriate stages and were fixed with 4% PFA/PBS overnight at RT. 5X PTU was added to prevent pigmentation for later stage embryos. The next morning, the embryos were washed in PBST thrice for 5 mins each and replaced with 100% methanol for storage at -20°C. Embryos were rehydrated in a stepwise fashion of decreasing MeOH concentration in 1X PBST (75%, 50%, 25% MeOH/1X PBST). To improve antigen retrieval by

antibody, embryos were equilibrated in 150 mM Tris-HCl, pH 9.0 for 5 mins and heat treated at 70°C for 15 mins in a water bath (Inoue and Wittbrodt 2011). Embryos were washed with dH_20 twice for 5 mins each and treated with ice cold acetone at -20°C for 20 mins to improve permeability. Acetone was washed away by rinsing six times with 1X PBST for 5 mins each and replaced with blocking reagent (Roche Diagnostics, Germany) for at least an hour. Primary antibodies were added at appropriate working dilutions in PBDT (1X PBS, 1% BSA, 1% DMSO, 0.5% Triton-X100, ddH_2O) and allowed to detect from overnight to 3 days in 4°C. After which, the primary antibodies were removed and washed with 1X PBST for 4 times at 20 mins each. Embryos were re-blocked with the same blocking reagent for another hour at room temperature. Appropriate Alexa Fluor-conjugated secondary antibodies were added. Secondary detection was allowed to occur for at least 2 hours to overnight in 4°C. After that, the antibodies were removed and the same washing steps followed. To preserve staining, embryos were kept in 50% glycerol/50% PBST or Vectashield mounting medium (Vecta Labs, US) at 4°C until use. Embryos were prepared for viewing and photography as stated in section 2.8. Table 13 lists the primary and secondary antibodies used in this study along with their working dilutions.

Table 13: Primary and Secondary antibodies used

Antibody	Host animal	Working dilution	Order info.
anti-acetylated tubulin	mouse	1:500	Sigma-Aldrich; T6793
anti-Sox2	rabbit	1:100	Millipore; AB5603
anti-Calcitonin	mouse	1:500	Thermo-Scientific; MA3-021A
anti-CGRP	rabbit	1:100	Millipore; AB15360
anti-GFP	mouse	1:200	Santa Cruz; sc9996
anti-GFP	rabbit	1:500	Clontech; 63246
anti-GFP	rabbit	1:500	Abcam; AB6556
anti-dsRed	rabbit	1:500	Clontech
Alexa Fluor 635 Phalloidin	N.A.	1:500	Molecular Probe; A34054
Alexa Fluor 488	mouse	1:200	Molecular Probe; A11017
Alexa Fluor 488	rabbit	1:200	Molecular Probe; A11008
Alexa Fluor 594	mouse	1:200	Molecular Probe; A11005
Alexa Fluor 594	rabbit	1:200	Molecular Probe; A11072

2.7.2 Cell Proliferation Assay (BrdU assay)

The whole-mount cell proliferation assay was performed on both control and morphant embryos at 55hpf, as described by Shepard et al (2004). Briefly, embryos were incubated in cold 10 mM BrdU/15% DMSO (Amersham Biosciences, RPN20) in embryo medium for 20 min before allowing embryos to develop at 28.5^{o}C for 15min. Embryos were then fixed with 4% PFA/PBS for 2 h before transferring to methanol overnight at 20^{o}C. Embryos were re-hydrated with graded methanol, digested in proteinase K and refixed. Embryos were then incubated in monoclonal anti-BrdU at 1:100 dilution and rabbit anti-phospho-histone 3 antibody of 1.33µg/ml overnight at

4 ^{o}C. BrdU and anti-pH3-labeled cells were detected using Alexa fluor 488 and Alexa fluor 594 secondary antibodies (Invitrogen, Molecular Probes), respectively. For imaging, embryos were mounted in the lateral orientation in VectaShield (Vector Laboratories Inc, H-1000). BrdU-labeled cells and anti-pH3-labeled cells were counted using 63X objective and Normarski optics of Zeiss LSM 510 Inverted Confocal Microscope.

2.8 Microscopy

2.8.1 Embryo Mounting and Imaging Using Upright Light Microscope

This procedure was performed for imaging stained embryos by whole mount in situ hybridized embryos. Stained embryos were transferred to 3% methyl cellulose on a concaved glass slide and conveniently orientated by manipulating embryos by dissection needles under a dissection microscope. For flat specimen, the yolk of the selected embryo was removed completely with needles. The de-yolked embryo was then placed onto a slide with a small drop of 3% methyl cellulose and adjusted to a proper orientation by a needle. Excess liquid was removed with tissue paper. Digital images were taken using a camera mounted to an AX-70 microscope (Olympus, Japan) with iSolution lite ver. 7.8 imaging software supplied by the MicroOptics. Brightness and contrast of images were adjusted as a whole by Adobe Photoshop CS ver.3 & 4.

2.8.2 Multi-channels Viewing and Confocal Microscopy

EGFP expression in live transgenic embryos was monitored under an Olympus SXZ16 or a Leica MZ FLIII stereomicroscope equipped with UV epifluorescence light source (ebq100, Leica). For detailed analysis, embryos were anesthetized as described in Section 2.3.5. For confocal imaging, embryos were live-mounted in 2% low melting agarose in Mat-Tek confocal dish for inverted configuration of the confocal system. Confocal images were acquired using Zeiss LSM510 and later, LSM700 scanning confocal systems (Carl Zeiss Inc., Germany) using lasers at appropriate wavelengths and bandpass filters. For time-lapse imaging, mounted embryos were covered with 1X egg water supplemented with PTU and triciane and maintained at 28°C using the fitted thermostat chamber. Time interval was specified over a 15 hr period and assembled into a final movie at a frame rate of 300 ms. Z-stacks images were taken at desired intervals using a 10X Plan-Neofluar 0.3 objective and 63X water immersion objective. Raw images were collected, processed and analyzed using the LSM510 Image Browser software and its later updated version, the ZEN 2009 lite version (Carl Zeiss Inc., Germany).

CHAPTER 3

Results

3.1 *atp2b1a* in Mechanosensory Hair Cells

3.1.1 Cloning and expression analysis of *atp2b1a*

The sequences flanking the *Tol2* insertion in SqET4 were obtained using TAIL-PCR (Parinov et al., 2004). Using BLAST analysis, the insertion was mapped to Chr. 4. This insertion is 97.4 kb away and in the opposite orientation to the Atp2b1a coding sequence located within the genomic clone DKEY-18O7 (Fig. 9A). We then cloned *atp2b1a* mRNA (GenBank accession no. HM449162). By RT-PCR, a low level of maternal *atp2b1a* transcript was detected (Fig 9B, Lane 1 & 2). It declined at 3hpf, and then increased at 5hpf (possibly due to an activation of zygotic transcription) followed by one more increase at segmentation stage (12hpf) (Fig. 9B).

Whilst *atp2b1* and *gfp* genes were in opposite orientation, their expression patterns were similar (Fig. 9A & C-K) and identical to a number of ESTs corresponding to *atp2b1a* (Rauch et al., 2003; Thisse et al., 2001; Thisse and Thisse, 2004). In sensory patches of the inner ear and in lateral line neuromasts, both transcripts were detected in the position of mechanosensory hair cells (Fig. 9C, D). In the L1 neuromast of 48hpf SqET4 embryo, a tight cluster of these cells was detected, with each cell projecting a kinocilium from its apical tip (Fig. 9E). Our analysis demonstrated co-localization of *atp2b1a*, *egfp* and EGFP in hair cells of the inner ear at 48hpf (Fig. 9F-H). These markers were observed in newly deposited neuromasts, as well as in a proneuromast of the posterior lateral line primordium (PLLP, black dashed line, Fig. 9I, J, K). During 3h period, when the primordium migrates from somite 6 (S6) to S8, the hair cell precursors divided in the trailing region of the primordium (Fig. 9, K-N). Thus, *atp2b1a* expression was initiated very early during development of the mechanosensory cells. This is in

concert with earlier observations from Lopez-Schier and Hudspeth (2006) that showed that GFP in SqET4 was expressed in transient progenitors prior to their terminal division, resulting in the formation of hair cells. These results demonstrate that SqET4 represents the Tg:*atp2b1a*-GFP line. As the expression of *atp2b1a* (and that of EGFP in SqET4) marks the initial stages of mechanosensory hair cells formation, we hypothesized that Atp2b1a is required for hair cell differentiation.

Figure 9: Expression pattern of *atp2b1a* transcript recapitulates that of *egfp* in SqET4. (A) Insertion of *Tol2* (triangle, green line) was mapped to the Chr. 4 near the *atp2b1a*. The sequence of 8-bp target site duplication is in lowercase. Arrows indicate the directions of transcription for *EGFP* and *atp2b1a.* The genomic clone, DKEY-18O7, contains the *Tol2* insertion and *atp2b1a.* The coordinates of the DKEY-18O7 sequence corresponding to the *Tol2* insertion and translation initiation (ATG) and termination (TGA) codons of the *atp2b1a* are shown above. Note that DKEY-18O7 sequence represents the reverse complement of *atp2b1a* sequence. (B) Semi-quantitative detection of *atp2b1a* expression using RT-PCR. (C & D) Both *atp2b1a* and *egfp* transcripts of SqET4 were detected in neuromasts of the anterior (data not shown) and posterior lateral line. (E) Mechanoreceptor of L1 neuromast of 48hpf-old SqET4 larvae showing a tight cluster of mechanoreceptor cells and kinocilium bundle. (F & G) Cross-sections of 48hpf-old SqET4 after WISH detecting *atp2b1a* and *egfp* in the inner ear hair cells. (H) Composite picture of 48hpf-old SqET4 showing expression of EGFP in mechanoreceptors of anterior and posterior macula. (I & J) Expression of *atp2b1a* and *egfp* in the newly deposited neuromast, as well as the mechanosensory hair cell precursor of the proneuromast (black dashed line). (K) Confocal scan of Bodipy-stained SqET4 (red) revealing the primordium of lateral line (38hph). (K - N) Time-lapse monitoring of neuromast deposition during 3h migration of primordium from somite 6 (S6) to somite 8 (S8), showing mitotic division of hair cell precursors (marked by EGFP of SqET4) during neuromast deposition upon proneuromast reaching the primordium trailing edge (line). (I-K) arrow indicates direction of prim1 migration. *Abbreviations: hc: hair cells; ov: otic vesicle; am: anterior macula; pm: posterior macula; s: somites; ao: anterior otolith; po: posterior otolith, nm: neuromast; pnm: pro-neuromast; prim1: primary primordium of posterior lateral line.*

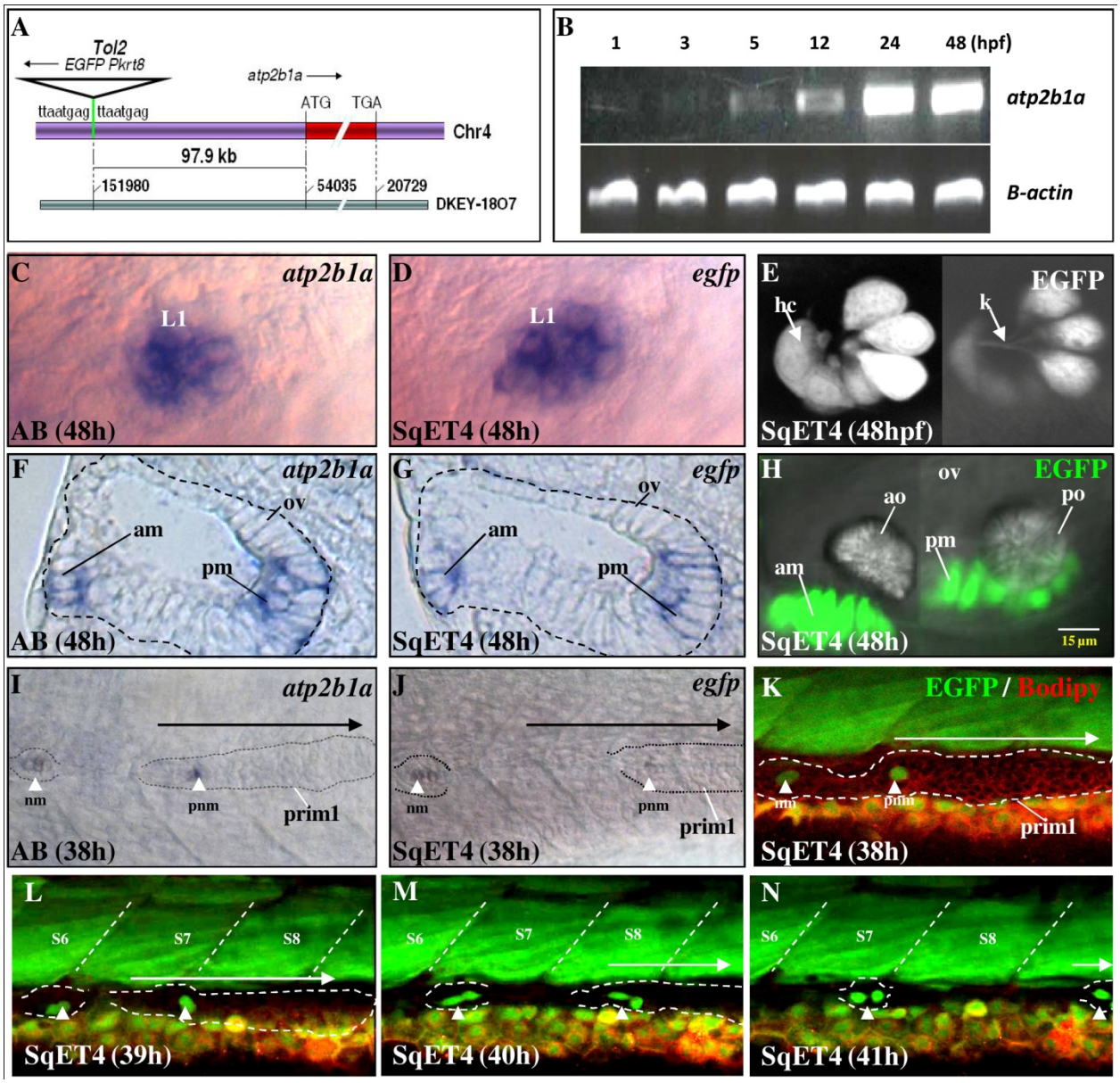

3.1.2 *atp2b1a* functions in the context of lateral line development

In the absence of mutants affecting *atp2b1a*, a role for this gene in hair cell development was studied using the morpholino (MO)-mediated knockdown (KD) approach. The translation-blocking MO efficiently down-regulated the GFP expression of the reporter construct (Fig. 10),

and affected GFP expression in the lateral line of SqET4 and in *tp53* morphants (Fig. 11C). Co-injection with *tp53* MO eliminates off-target effects that are associated with *tp53*-mediated apoptosis. This demonstrates both tissue- and target-specificity of *atp2b1a* MO. The position of neuromasts was affected in SqET4 morphants. We counted total number of neuromasts and total number of hair cells of L2 and L3 neuromasts of 18 embryos per treatment, staged at 48hpf. Morphant embryos displayed less neuromasts (reduced to 32%) and hair cells per neuromast (L2 and L3 combined: reduced to 33.3%); (Fig. 12A to B'; Table 14). Division of hair cells during neuromast formation was perturbed in *atp2b1a* morphant (Fig. 12B & 13). The effect of *atp2b1a* MO was partially reversed by co-microinjection of *atp2b1a* mRNA, which moderately restored neuromast position, caused a two-fold increase in neuromast number (increased to 58.7%), and a three-fold increase in hair cell number (L2 and L3 combined: increased to 73%); (Fig. 12C, C'; Table 14). Thus, Atp2b1a has a functional role in neuromast and hair cell development.

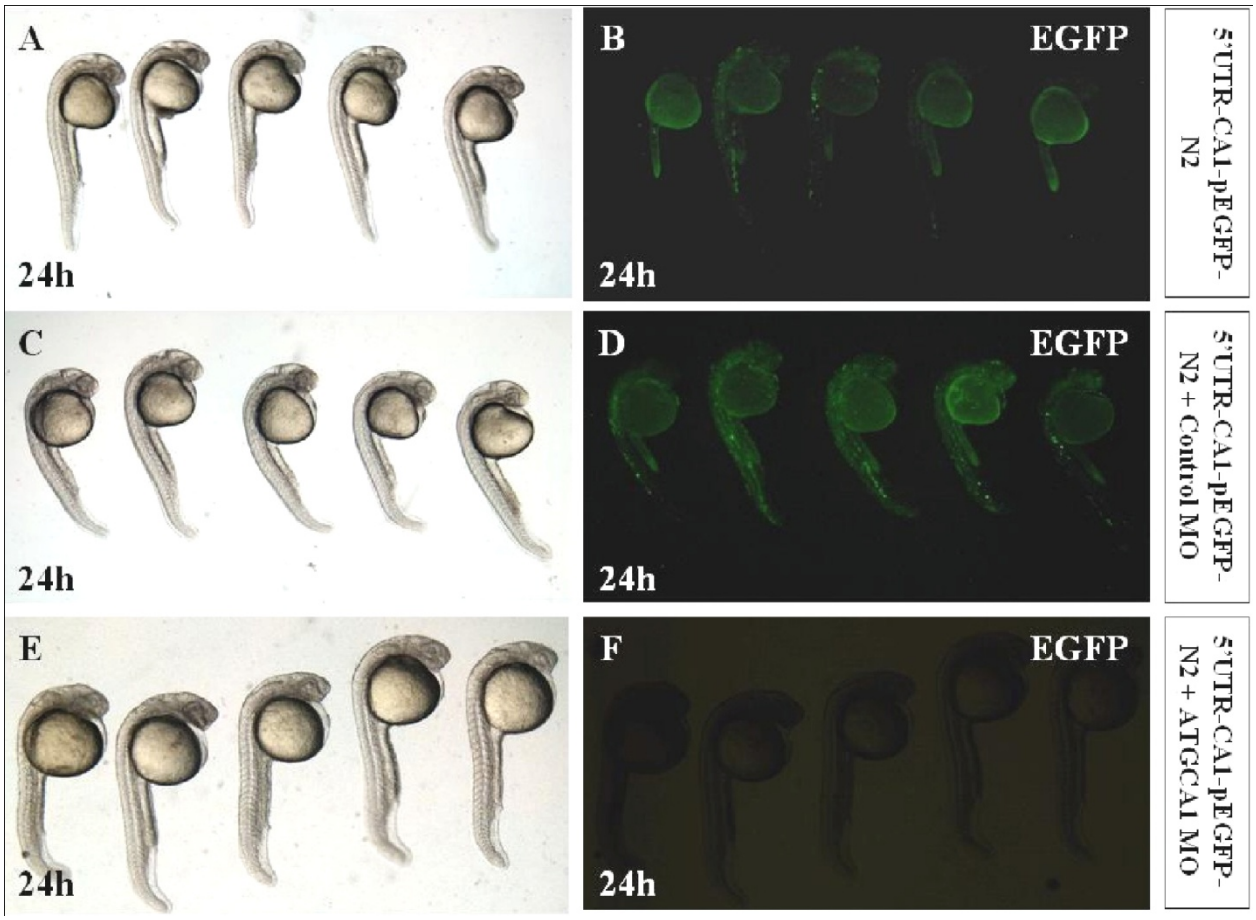

Figure 10: Control experiment showing the specificity of *atp2b1a* morpholino used throughout this study. A target construct containing the target sequence of the morpholino; 5'UTR-CA1 was cloned in-frame to pEGFP-N2 vector. (A & B) Brightfield versus florescence images of control embryos injected only with the above target construct. (C & D) Brightfield versus florescence images of control embryos co-injected with target construct and control morpholino. (E & F) Brightfield versus florescence images of control embryos co-injected with target construct and *atp2b1a* morpholino was able to shuts down EGFP expression completely.

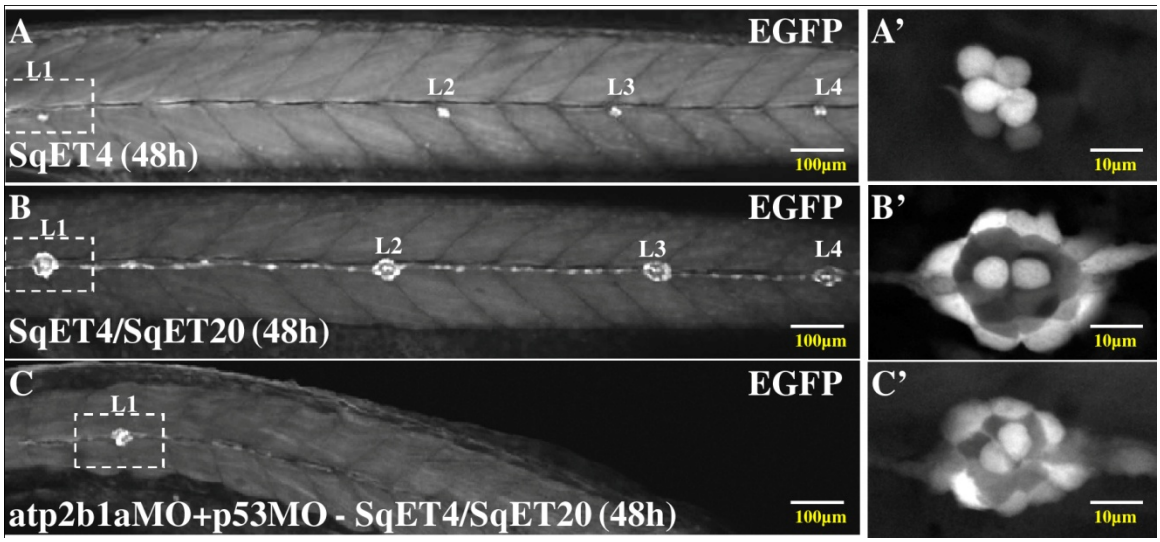

Figure 11: Control experiment showing that the effect of *atp2b1a* morpholino is not due to activation of Tp53. A & B illustrates the control situation of deployed neuromasts at 48hpf. B is a double transgenic of SqET4 crossed with SqET20 which provided additional EGFP signal from support cells of neuromast and inter-neuromast cells. Co-injection of *atp2b1a* morpholino with zf-p53 morpholino does not affect the outcome of *atp2b1a* morpholino knockdown phenotype in the PLL neuromasts (C). (A', B', C') Magnified view of L1 neuromast compares the division plane of hair cells. (n = 10).

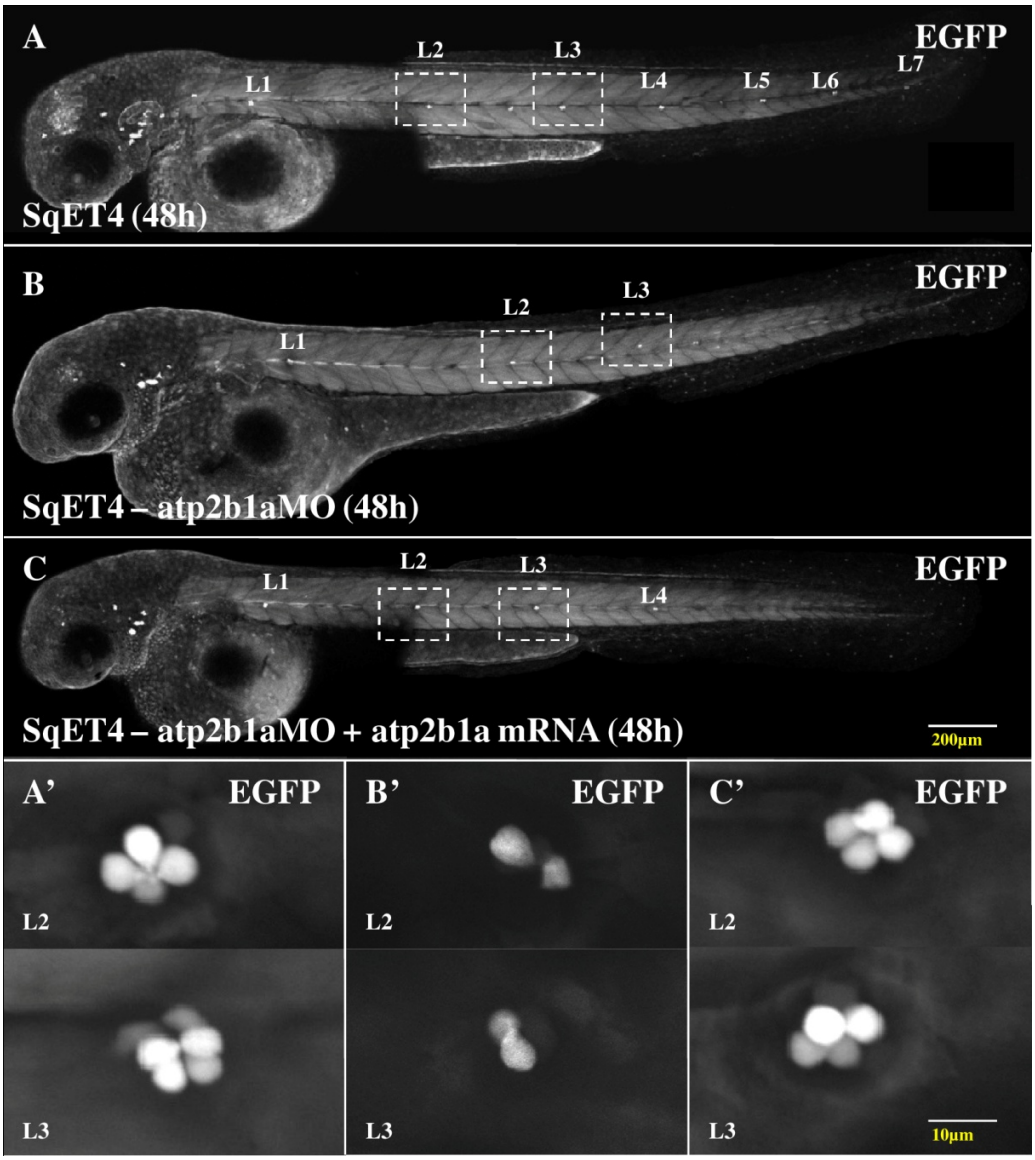

Figure 12: Rescue of *atp2b1a* morphants using full-length *atp2b1a* mRNA. (A) Confocal stack image of the PLL neuromasts (L1 to L7) in control SqET4 embryo. (A') Magnified view of L2 and L3 neuromasts of control SqET4. (B) The number of neuromasts in *atp2b1a* morphant is reduced (L1 to L3). The body axis of the morphant appears bended. (B') Magnified view of *atp2b1a* morphant L2 and L3 neuromasts show reduction of mechanosensory cells and intensity of GFP signal. (C) Co-injection of *atp2b1a* morpholino with *atp2b1a* mRNA increased the number of neuromasts (L1 to L4) found more anterior, similar to that in control, and the body axis has straightened. (C') Magnified view of L2 and L3 neuromasts of morphants after mRNA rescue demonstrate more intense GFP expression. (D, E) Statistical analysis of the *atp2b1a* mRNA rescue showed an increase in the number of neuromasts as well as mechanosensory hair cells of L2 and L3 neuromasts. Horizontal bar – S. D. (n = 61).

MO dose	No neuromast	One neuromast	Two neuromasts	>Three neuromasts
0.3pg	0	26.6%	5.2%	67.8%
0.6pg	16.4%	58.6%	9.5%	13.8%

Table 14: **Reduction of number of neuromasts caused by *atp2b1a* knockdown is dosage-dependent.** Number of neuromasts was estimated at 2 dpf from counting groups of EGFP positive mechanosensory hair cells of posterior lateral line of morphant embryos/larvae of SqET4 transgenic line. (N = 50)

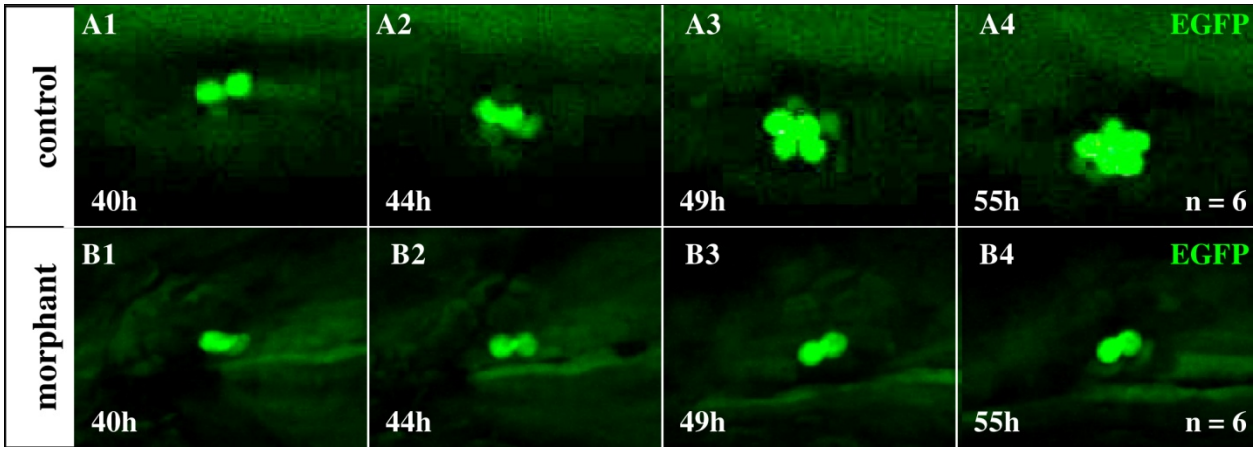

Figure 13: *atp2b1a* knock down disrupted the rapid cell proliferation of hair cells in developing neuromast. A1-A4 shows the time-lapse monitoring of the development of control L2 neuromast of SqET4 from 40hpf to 55hpf. Beginning with two mature (based on stronger intensity of EGFP signal) hair cells at 40h, L2 neuromast developed rapidly to a cluster of around 6 mature hair cells by 55h. (B1-B4) L2 neuromast of Atp2b1a morphant developed significantly slower than control with two mature hair cells at 40h and 55h. (n = 6).

3.1.3 *atp2b1a* regulates dynamics of Ca^{2+} in developing and mature hair cells

Given the reported activity of Atp2b1 proteins in Ca^{2+} export, we analyzed the Ca^{2+} levels in wild type embryos and *atp2b1a* morphants. *In vivo* staining of neuromasts by Ca^{2+} reporter dye (Calcium Crimson AM) revealed a signal associated with the cupula of hair cell bundle (Fig. 14A, orthogonal sections: Ai & Aii, 3D projection: Aiii), outside of the cell body (Fig. 14E to Eii). In contrast, in *atp2b1a* morphants, Ca^{2+} signal on cupula was reduced (Fig. 14B, orthogonal sections: Bi & Bii, 3D projection: Biii) and Ca^{2+} was predominantly detected inside the cells (Fig. 14F to Fii), signifying that Atp2b1a is largely responsible for export of Ca^{2+}.

Treatment of gastrulating embryos with the PMCA inhibitor, 5(6)-carboxyeosin (CE, Kurnellas et al. 2005) blocked Ca^{2+} export from hair cells and reduced the number of neuromasts and hair cells (Fig. 14F and Table 15), similar to that in the *atp2b1a* morphants. When assessed with Ca^{2+} reporter dye, a profile similar to morphant was resulted (Fig. 14C, orthogonal sections: Ci & Cii, 3D projection: Ciii, 14G to Gii). In contrast, thapsigargin, a SERCA-specific inhibitor, had no such effect on hair cells (data not shown).

Upon co-microinjection of MO and *atp2b1a* mRNA, Ca^{2+} was detected at some distance from hair cell bodies (Fig. 14D, orthogonal sections: Di & Dii, 14D projection: Diii), suggesting not only restoration of Ca^{2+} export, but the additional restoration of Ca^{2+} signal of cupula. Ca^{2+} signal of rescued morphant hair cells was detected largely outside the cell bodies; similar to control (14H to Hii).

Figure 14: *atp2b1a* is required for Ca^{2+} extrusion from mechanosensory hair cell. Calcium Crimson AM (CC) was used as an *in vivo* indicator of intracellular Ca^{2+} level in SqET4 transgenics. Ca^{2+} is predominantly localized within the cupula. (Ai & Aii) Orthogonal sections of control L1 neuromast (55hpf); (Aiii) 3D projection (42^{o} along Y-axis) of the same neuromast depicting the spread of Ca^{2+} along cupula. (Bi & Bii) Orthogonal sections of Atp2b1a morphant L1 neuromast (55hpf), (Biii) 3D projection of the same neuromast. (Ci & Cii) Orthogonal sections of carboxyeosin-treated L1 neuromast (55hpf), (Ciii) 3D projection of the same neuromast. Green and red box indicates plane of orthogonal section; blue box indicates z-depth of the confocal stack. In controls, intracellular Ca^{2+} is kept low. (Di & Dii) Orthogonal sections of a neuromast after *atp2b1a* mRNA rescue. (Diii) 3D projection of the neuromast. (E) Intensity profiling (x-axis: distance in microns VS y-axis florescence intensity) of EGFP v. CC in 5dpf control L1 neuromast across two planes of measurement (white dashed lines). Within hair cells CC was detected only at low level (Ei). The intensity of CC peaks (Eii) at the level of the stereocilia. (F) In morphants intracellular Ca^{2+} is high (3-fold difference). (Fi, Fii) Intensity profiling of EGFP v. CC in 5dpf morphant L1 neuromast across the plane of measurement. The intensity of CC at the level of hair cells is high. (N = 10). Intensity profiling of EGFP v. CC in 5 dpf 5(6)-carboxyeosin (CE) treated embryo (Gi, Gii). The intensity of CC at the level of hair cells is high. (N = 18). (Hi, Hii) Intensity profiling of EGFP v. CC in 5dpf *atp2b1a* mRNA rescued-morphant L1 neuromast across two planes of measurement. CC was low within hair cells (Hi). The intensity of CC peaks (Hii) at the level of stereocilia. (N = 10). Refer to Table 15 for post treatment results of neuromast and hair cell counts.

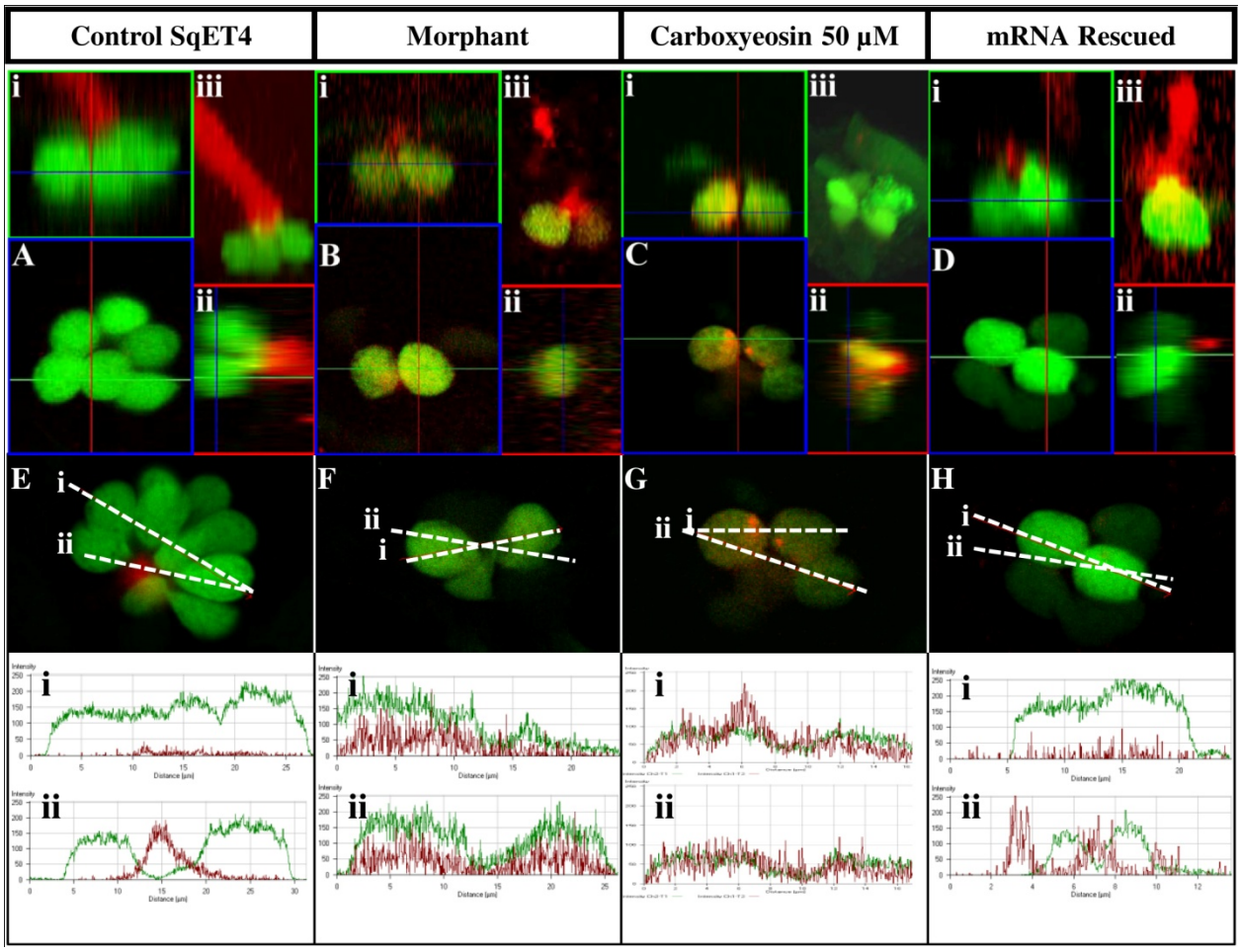
Control SqET4
Morphant
Carboxyeosin 50 µM
mRNA Rescued
A
B
C
D
E
F
G
H
i
ii
iii
Intensity
Distance (µm)

	Control (48hpf)	Morphant (48hpf)	CE-Treated (48hpf)	mRNA rescued (48hpf)
Number of 1^{o} neuromast	135 (100%)	43.2 (32%)	36 (26.7%)	79.2 (58.7%)
Number of hair cells (L2)	108 (100%)	34.8 (32.2%)	43.2 (40%)	75.6 (70%)
Number of hair cells (L3)	90 (100%)	31 (34.4%)	37.8 (42%)	68.4 (76%)

Table 15: Neuromast and hair cells count in embryos of SqET4 transgenics after *atp2b1a* knockdown, mRNA rescue and PMCA inhibitor (5(6)-Carboxyeosin) treatment. A number of primary neuromasts as well as hair cells within individual neuromast at 48hpf decreased after MO knockdown or PMCA inhibitor treatment at 6hpf. Upon co-injection of a morpholino and a full-length *atp2b1a* mRNA morphants phenotype partially improved. (Percentage values in bracket, N = 18 for all treatment).

3.1.4 Formations of kinocilium was affected in *atp2b1a* morphants

We have also examined the integrity of kinocilia and stereocilia of L1 neuromast by whole-mount immuno-staining with anti-acetylated tubulin antibody which labels kinocilium and Alexa Fluor 635 Phalloidin, which marks F-actin in the stereocilia respectively (López-Schier et al., 2004). Kinocilia in control L1 neuromast were in abundance, organized and well-projected (Fig. 15A & Ai). In both morphant (Fig. 15B & Bi) and PMCA inhibitor-treated larvae (Fig. 15C & Ci) situations, kinocilia were both sparse and truncated. Heights of kinocilia were measured from 3D-rendered images of L1 neuromast using Zeiss confocal software, where both morphant and PMCA inhibitor-treated had their kinocilia heights reduced by as much as 4 folds (Table 16). The number of stereocilia was counted from Phalloidin stained cuticular plates at the level of

stereocilia and both morphant and PMCA-treated larvae had stereocilia number reduced by almost 5 folds (Table 16). Rescued larvae have regained both its kinocilia's height and stereocilia to a level almost comparable to control L1 neuromast. Fig. 15Aii, Bii, Cii & Dii are enlarged images of actin signal (white dashed box), revealing in morphant and PMCA inhibitor-treated larvae, reduced number of actin-rich cuticular plates and in addition, the lack of hair cell polarity in these populations as seen in control and rescued larvae (yellow dashed line). Hence, Atp2b1a is required to regulate Ca^{2+} levels in mechanosensory hair cells and their environment and/or affect formation of secondary structures such as stereocilia and kinocilia (reviewed in Manor and Kachar, 2008).

Figure 15. Formation of hair cells secondary structures was affected in morphants neuromasts. The integrity of stereocilia of L1 neuromast for control and morphant larvae was accessed by anti-acetylated tubulin antibody (green) which labels kinocilium, and Alexa Fluor 635 phalloidin (red) which marks actin in the stereocilia. A, B, C & D compares control, morphant, 5,6 carboxyeosin-treated and mRNA rescued larvae respectively at maximum projection . Length of kinocilium was negatively affected by *atp2b1a* knockdown and Atp2b1a inhibitor treatment. Ai, Bi, Ci & Di shows merged signals of kinocilium and actin-rich cuticular plate. Aii, Bii, Cii & Dii are enlarged images of actin signal (white dashed box), revealing reduced number of actin-rich cuticular plates and lack of hair cell polarity as seen in control and rescued larvae (yellow dashed line). Scale bar at 5 µM.

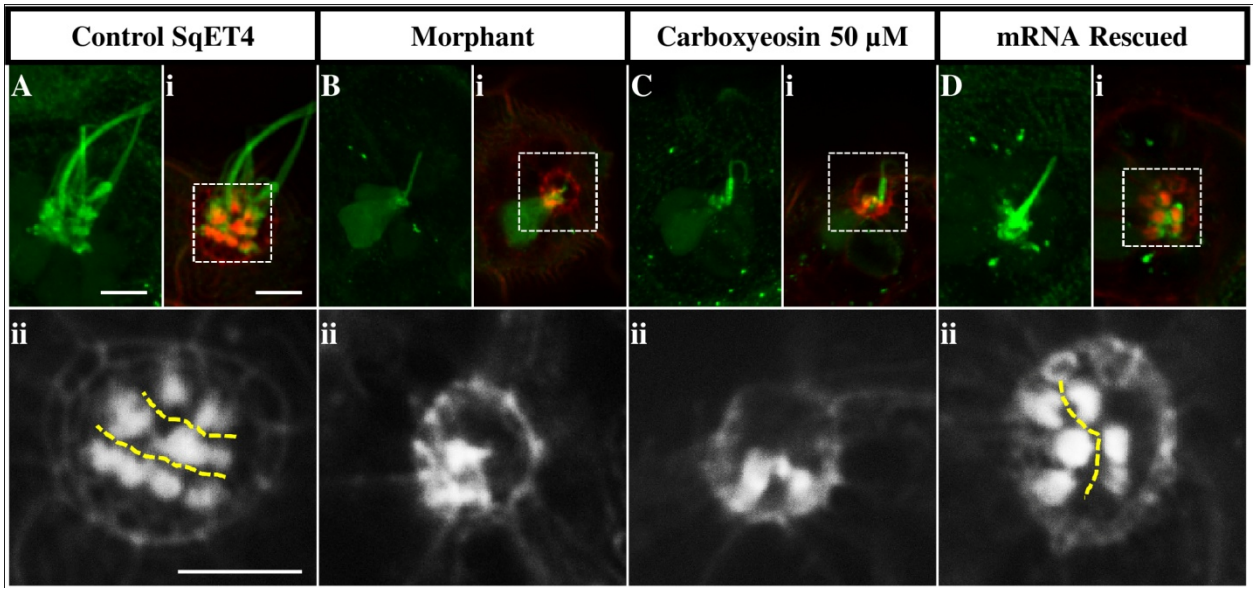

	Control (5 dpf)	Morphant (5 dpf)	CE-Treated (5 dpf)	mRNA rescued (5 dpf)
Height of kinocilia	24.7 µM (0.51)	6.12 µM (0.8)	5.96 µM (0.47)	20.8 µM (1.25)
Number of stereocilia	10.8 (0.84)	2.2 (0.45)	2.4 (0.55)	6.4 (0.55)

Table 16: *atp2b1a* knockdown and PMCA inhibitor treatment negatively affects kinocilium of neuromast. 3D rendered images were generated from z-stack of L1 neuromast at 5 dpf. Height of kinocilia of L1 neuromast was measured from GFP-signal of anti-acetylated tubulin staining on kinocilia using confocal software. The number of stereocilia was counted from neuromasts co-stained with Alexa Fluor 635 Phalloidin, which labels actin-rich cuticle plates at the level of stereocilia. (Standard deviation values in bracket, N = 5 for all treatment).

3.1.5 Late phenotypes of *atp2b1a* morphants

Next, we investigated the Ca^{2+} profile of mechanosensory hair cells in the inner ear after microinjection of Calcium Crimson AM into this organ. In morphants, mechanosensory cells of posterior macula failed to form. Ca^{2+} was only detected in mechanosensory cells of the anterior macula sensory patch (Fig. 16A - C"). The otoliths were smaller than control (Fig. 16C). In order to study the late auditory/vestibular phenotype in detail, morphant larvae were tested individually for their ability to maintain controlled linear motion during a startle response induced by gentle physical stimulus (i.e. touching the tip of larvae tail with a dissecting needle). Larvae that failed to respond to such stimulus at 2 dpf or swam in rapid, irregular arcs were classified into three phenotypes: circling, imbalanced and non-touch responsive (Riley and Moorman, 2000). The hearing ability was linked to the later development of the lagenar sensory patch (Whitfield et al., 2002). The hearing assay was therefore carried out at 7 dpf by tapping the side of the 10-cm Petri dish, and larvae that failed to respond were classified as deaf. Each larva was assayed three

times, and those that reacted normally at least once were considered to be unaffected.

Upon touch, the normal larvae traversed the plate in a straight line without rolling or veering (Riley and Moorman, 2000), but 2 dpf morphants were clearly affected, with 30% circling, 41.6% unable to maintain a dorsal side-up posture and 0.05% non-touch responsive, and of the 7 dpf morphants, 68.5% were classified as deaf (Fig. 16; Table 17). Thus, the initial abnormality of mechanosensory hair cells in the lateral line and inner ear of Atp2b1a morphants leads to later defects in the auditory and vestibular system.

Figure 16: Mis-regulation of Ca^{2+} in mechanosensory cells by *atp2b1a* knockdown led to auditory / vestibular phenotypes of late *atp2b1a* morphant. Calcium Crimson AM was injected into the otic vesicle to examine the Ca^{2+} profile of the inner ear. A strong Ca^{2+} signal was observed at the tips of kinocilium located at two sensory patches, as marked by EGFP of SqET4. Both anterior and posterior otoliths were strongly labeled by Calcium Crimson AM (A-B'). In morphant mechanosensory cells, a Ca^{2+} signal was consistently detected within the cell bodies. Otoliths (stained negatively for Calcium Crimson AM) were observed to be smaller than control (C-C"). In morphant mechanosensory cells of posterior macula failed to form. Table 17 details the classes of phenotypes observed. Embryo phenotypes were classified into four categories: circling, imbalanced, non-touch responsive and deaf (Riley et al. 2000). A significant proportion of the tested morphants were classified as deaf. Larvae were tested individually for their ability to maintain controlled linear motion during a startle response induced by a gentle physical perturbation. Larvae which failed to respond to such stimulation at 2dpf or swam in rapid, irregular arcs were classified. The deafness assay was performed at 7dpf due to the later development of lagenar sensory patch for more robust hearing ability (Whitfield et al. 2002). In normal response, the larvae traversed the plate in a straight line without rolling or veering. Each larva was assayed three times and larvae with at least one normal response were grouped as normal. (N.T. - not tested).

[a] Touching the tip of larvae tail with a dissecting needle.

[b] Deafness assay by tapping the side of the 10-cm Petri dish.

Abbreviations: ao: anterior otolith; hc: hair cells; k: kinocilium; ov: otic vesicle; po: posterior otolith.

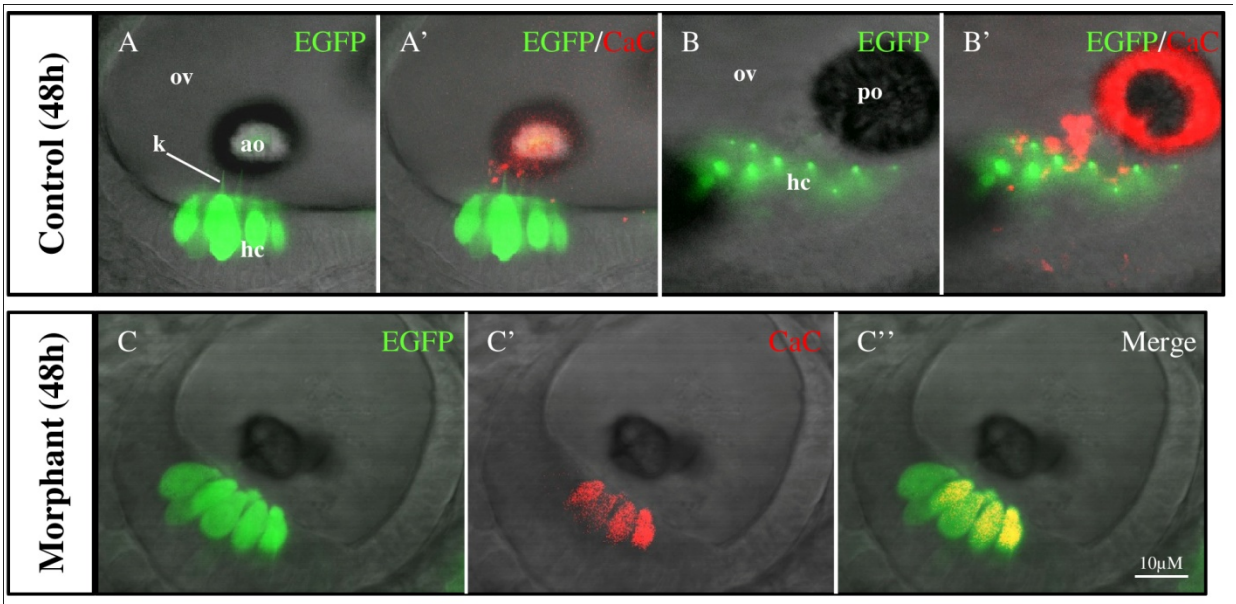

Table 17: Auditory and vestibular-related phenotypes of *atp2b1a* morphant.

	Control (2dpf)	Morphant (2dpf)	Control (7dpf)	Morphant (7dpf)
Circling [a]	0	54 (30%)	N.T.	N.T.
Imbalanced [a]	0	75 (41.6%)	N.T.	N.T.
Non-touch responsive [a]	0	9 (5%)	0	15 (8.3%)
Deaf [b]	N.T.	N.T.	0	**111 (68.5%)**
Total larvae	180	180	180	162

3.1.6 *atp2b1a* expression is downstream of and regulated by *atoh1a*

The proneural transcription factor, Atoh1a, acts as a determinant of hair cells (Millimaki et al., 2007). Thus, we decided to explore an interaction between *atoh1a* and *atp2b1a*. Double WISH shows co-localization of *atp2b1a* and *atoh1a* in mechanosensory cells of the ear and neuromasts (Fig. 17; A, B). Co-localization was also detected in proneuromasts located in posterior end of PLLP (Fig. 17; C)). While the expression of *atoh1a* in the anterior part of the PLL primordium

of *atp2b1a* morphants was relatively normal at 36hpf, there was an increase in the number of *atoh1a*-expressing cells in the posterior-most cluster corresponding to the pro-neuromast (Fig. 18; A, D) and L2 neuromast (Fig 18; H, L; *N=15*). Furthermore, *atoh1a* expression increased in the anterior and posterior macula of the inner ear in *atp2b1a* morphants (Fig. 18; G, K; *N = 5*). These findings suggest that the knockdown of *atp2b1a* blocked hair cell development at the stage of *atoh1a*-positive precursors.

Figure 17: *atp2b1a* co-localized with *atoh1a* in hair cells of neuromast and inner ear. Shown here by two-color *in situ* hybridization, *atp2b1a*‘s expression in the optic tectum does not overlap with *atoh1a*‘s expression in the cerebellum (A). Spatial co-localization of these two genes was detected in deposited supra-orbital neuromast as well as sensory patch of the inner ear (B, arrows). *atoh1a* is expressed in four distinct proneuromasts (C: black and white arrows) located within the pllp and co-localized with *atp2b1a* expression only in the proneuromast located at the posterior end of pllp as well as deposited neuromast L1 at 36 hpf. *Abbreviations: ot: optic tectum; cb: cerebellum; rl: rhombic lip; ov: otic vesicle; sp: sensory patch; OC nm: occipital neuromast; L1 nm: first deposited neuromast of posterior lateral line; pllp: posterior lateral line primordium*

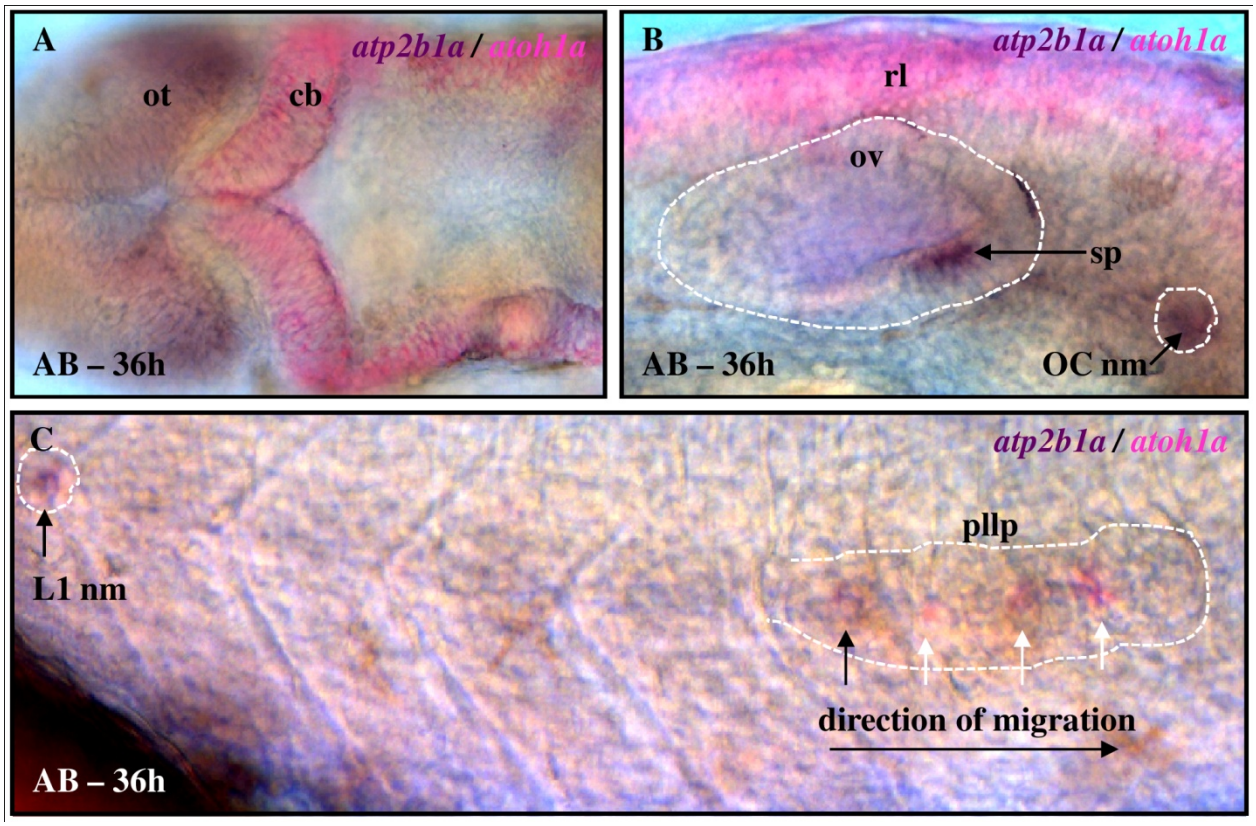

The knockdown of *atoh1a* blocked *atp2b1a* expression in the 36hpf PLL primordium (Fig.18B), without affecting the level of *atoh1a* expression (Fig. 18E; *N=15*). In SqET4 *atoh1a* knockdown abolished formation of neuromasts and hair cells (not shown). These experiments suggested that in precursors of mechanosensory hair cells *atoh1a* acts in an epistatic manner upstream of *atp2b1a*.

In order to assess the integrity of the migrating primordium and neuromast, *tacstd* was used as a marker. The zebrafish homolog of mammalian TACSTD (tumor-associated Ca^{2+} signal transducer), *tacstd* is expressed in cells of the migrating primordium and neuromasts (Villablanca et al., 2006; Fig. 18C, J), other than hair cells. In *atp2b1a* morphants expression of *tacstd* appeared to have expanded, based on its *in situ* hybridization signal (Fig. 18F, N; *N=10*).

In the screen for new ET lines (Kondrychyn et al., 2009; Poon et al., 2010), the SqET33-mi60a transgenic line with insertion close by *lnfg* (encoding a component of the Notch signaling) and GFP expression in support cells was identified. These cells also express Sox2 (Fig. 18I, Q); a transcription factor involved in self-renewal of undifferentiated stem cells (Hernandes et al., 2006). In control neuromasts, support cells formed a tight cluster immediately below and around GFP-negative hair cells seen as dark shadows (Fig. 18O). In morphant neuromasts, the support cells increased in number and dispersed between the mantle cells that form the outer rim of the neuromast (Fig. 18P). Furthermore, *sox2* expression increased in morphant neuromasts (Fig. 18M; *N=13*). Taken together, these results indicated that a block in hair cell differentiation in *atp2b1a* morphants leads to the accumulation of undifferentiated precursors.

Figure 18: *atp2b1a* acts downstream of *atoh1a.* (A) *atoh1a* expressed in several clusters corresponding to proneuromasts of the PLLP (white triangles). Knockdown of *atoh1a* removes *atp2b1a* expression completely in pro-neuromasts at 36 h (B), but does not affect intensity of its own RNA (E). (D) Knockdown of *atp2b1a* does not affect *atoh1a* expression in the proneuromasts. In the deposited neuromast at 48 h, *atoh1a* is expressed in a few central cells corresponding to hair cell precursors (H). In *atp2b1a* morphant, clusters of hair cell precursors are larger (L). (G &H) Cross-section of *atoh1a*-stained inner ear at 48 h revealed elevated expression of *atoh1a* in morphant saccular macula (yellow arrowhead). (C) *tacstd* is expressed in migrating PLLP as well as deposited neuromast. In 48 hpf *atp2b1a* morphant, expression of *tacstd* increased both in newly deposited neuromast (C & F) and mature neuromast (J & N), where a cluster of cells expressing *tacstd* expanded. (I) *sox2* at 48 h is expressed in the support cells of neuromast. *sox2* expression in morphants increased (M). (O) Support cells of the 5 dpf control L1 neuromast in SqET33-mi60a (white arrowhead). Hair cells appear as GFP negative shadows (blue arrowhead). (P) Support cells of morphant neuromast at 5 dpf in SqET33-mi60a. Morphant support cells spread to the outer rim of neuromast, unlike compact group of support cells in control restricted to the neuromast inner core (*N = 10*). (Q) Co-immunostaining shows colocalization of Sox2 and GFP in support cells of SqET33-mi60a. (Scale bar = 5 µm). Legends: migrating PLLP (black dashed line); otic vesicle (white dashed line); neuromast (yellow dashed line). *Abbreviations: sm: saccular macula; hcp: hair cell*

precursors; sc: support cells; pc: peripheral cells, hc: hair cells.

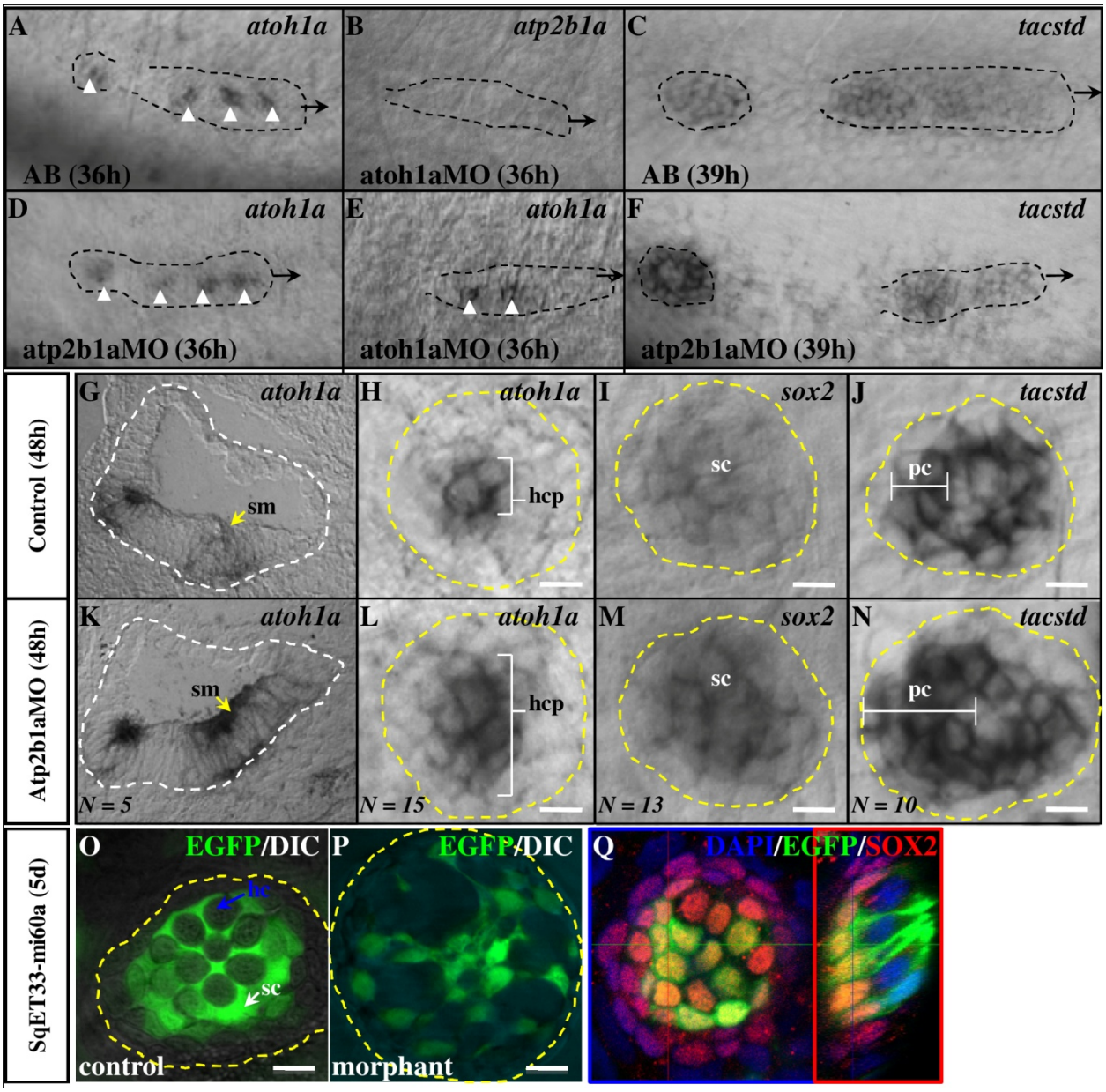

3.1.7 *atp2b1a* and cell proliferation in neuromasts

Recently, specific populations of neuromast cells were proposed to differentiate in the following sequence: mantle cell, support cell, hair cell precursor and hair cell (Ghysen and Dambly-Chaudiere, 2007). Given the obvious changes in cell number detected in these populations in the morphants, we sought to compare the cell proliferation rate in 55hpf control and morphant neuromasts using a short pulse (15 min) of BrdU labeling followed by an anti-phosphohistone H3 antibody, which detects cells in the M-phase of cell cycle. Under these conditions, very few M-phase or BrdU-labeled cells were detected in control neuromasts L1-3 (Fig. 19A, C, E) unlike that in morphants (Fig. 19B, D, F; orthogonal sections: B', D', F'; Table 18), where a several fold increase in cell proliferation was observed. This indicates that the *atp2b1a*-dependent mechanism of hair cell differentiation negatively controls the proliferation of hair cell precursors.

Figure 19: Increase in proliferation in neuromast peripheral cells in the *atp2b1a* morphant. A, C & E, Control neuromasts (L1-L3). B, D & F - *atp2b1a* morphant neuromasts (L1-L3). At a given point, control neuromasts contain very little, if any, BrdU-positive cells, unlike the morphant neuromasts. Z-stack images were taken at depth 8.0 - 13.3μm (depending of neuromast age). White arrows indicate BrdU-positive cells. Red arrows indicate pH3-positive cells. Analysis of positive cells was restricted within neuromast as demarcated by white dashed line based on DIC images of neuromasts. B', D' & F' shows orthogonal sections of morphant neuromasts that reveal BrdU-positive cells not visible in a single section. (Scale bar = 5 μm).

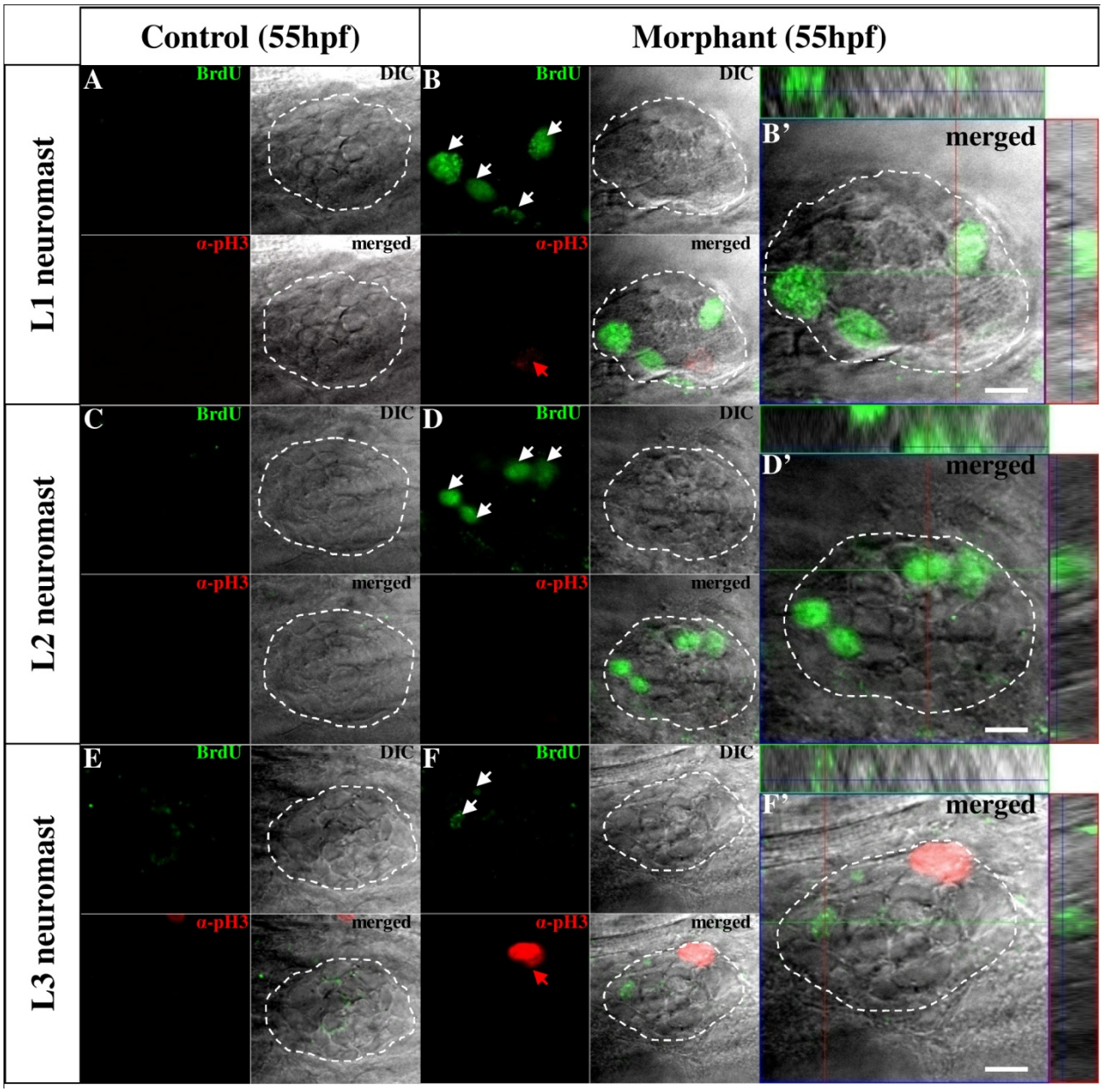
Control (55hpf)
Morphant (55hpf)
L1 neuromast
L2 neuromast
L3 neuromast
A
B
B'
C
D
D'
E
F
F'
BrdU
DIC
α-pH3
merged

	Marker	L1	L2	L3
Control (55h)	BrdU cells	0.27 (0.46)	0.33 (0.49)	0.61 (0.5)
	aPH3 cells	0.56 (0.51)	0.39 (0.61)	0.27 (0.46)
	Hair cells	5.17 (0.79)	4.56 (0.62)	4.20 (0.43)
Morphant (55h)	BrdU cells	3.11 (0.41)	1.94 (0.72)	1.50 (0.71)
	aPH3 cells	1.06 (0.87)	0.78 (0.65)	0.22 (0.43)
	Hair cells	2.06 (0.64)	1.83 (0.38)	1.78 (0.43)

Table 18: The number of S-phase cells in neuromasts morphant increased. The numbers of positive cells for BrdU and anti-phosphohistone3 were counted for L1, L2 and L3 neuromasts and mean was calculated and shown in the table. The number of hair cells was counted in embryos/larvae of SqET4 transgenic line from a separate experiment. (Standard deviation values in bracket, N = 18)

3.1.8 *atp2b1a* expression is induced during hair cell regeneration

The hair cells of the lateral line are the subject of cell regeneration investigations following insult with agents known to cause deafness in humans. To evaluate a role of *atp2b1a* in the regeneration of hair cells, embryos were exposed to sub-lethal concentrations of neomycin, which is known to ablate hair cells (Coffin et al., 2009; Harris et al., 2003; Owens et al., 2008). As expected, neomycin induced apoptosis of hair cells in neuromasts of the double transgenic embryos SqET4/ET20, where mantle (SqET20+) cells remained and hair cells (SqET4+) disappeared (Fig. 20A to B'). We then monitored the regeneration of hair cells in the L3 neuromast using the hair cell-specific vital dye, DASPEI (Fig. 20C to J), and whole-mount *in*

situ hybridization (WISH) using the anti-*atp2b1a* probe (Fig. 20K to R). Neomycin-ablated hair cells were observed post-treatment (Fig. 20D; black arrows). Regeneration was first detected one hour after treatment (T+1h) by DASPEI staining (Fig. 20E; white arrow), concomitant with the expression of *atp2b1a* (Fig. 20M; yellow arrow) that increased from T+1h to T+6h, followed by EGFP in SqET4 at around T+1.5h (data not shown). Thus, the expression of *atp2b1a* correlates with the initial phase of regeneration of hair cells, similar to that in the development of these cells.

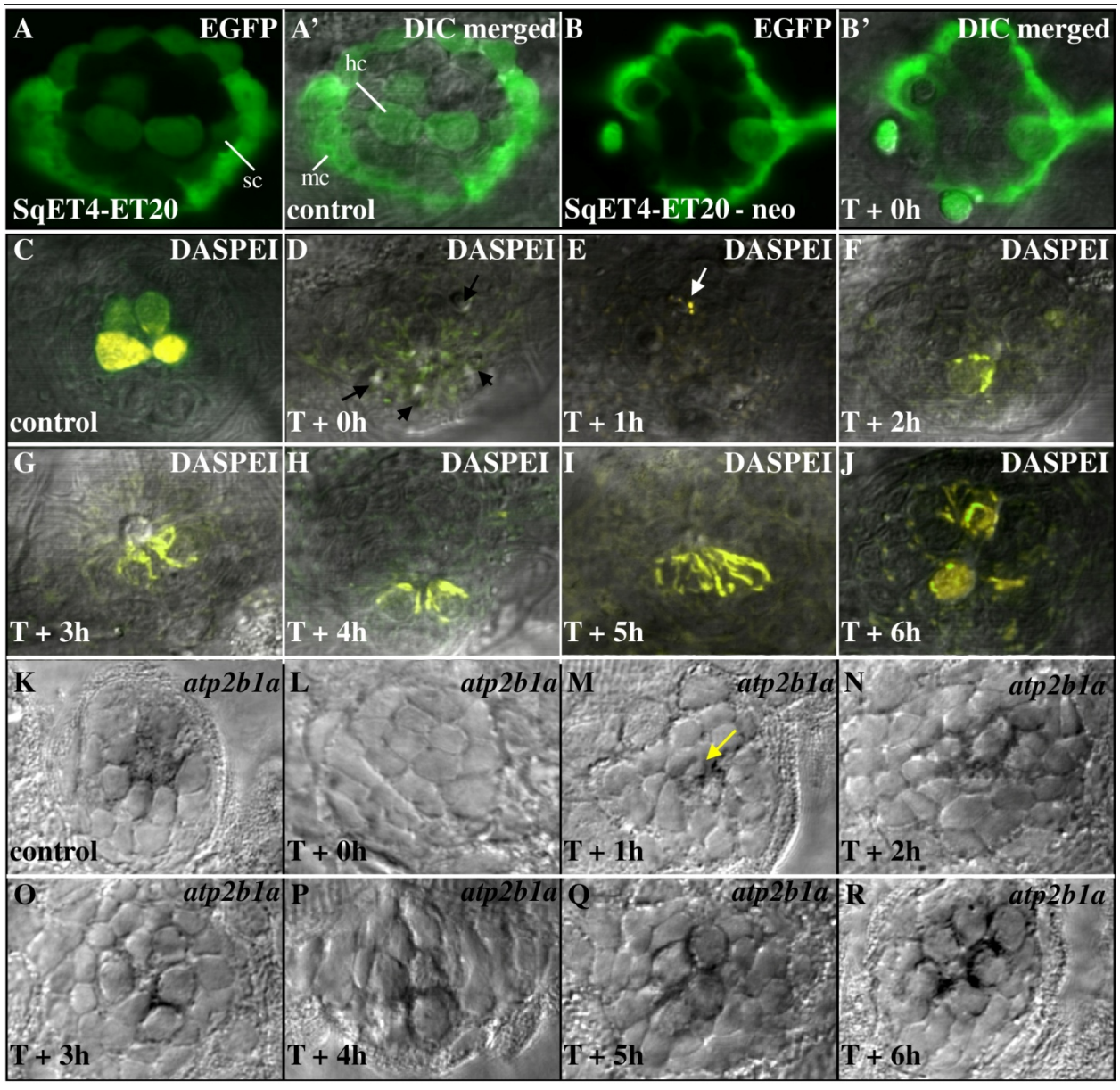

Figure 20: Expression of *atp2b1a* correlates with regeneration of hair cells. (A to B') Neomycin treatment eliminated hair cells of neuromasts, as shown here by double transgenic SqET4-ET20 with GFP-positive mantle, support (data not shown) and hair cells. (C-J) L3 neuromasts stained by DASPEI. Regeneration could be detected one hour post treatment (T+1h), when DASPEI staining (white arrow) was detected. (K to R) *atp2b1a* expression analyzed by WISH. *atp2b1a* transcript detected T+1h onwards (yellow arrow) increasing from T+1h to T+6h. *Abbreviations: hc: hair cells; sc: support cells.*

3.2 *atp2b1a* in Ultimobranchial Body (UB)

3.2.1 *atp2b1a* is expressed in UB of the developing zebrafish

atp2b1a functions during division of the terminal progenitor of mechanosensory hair cells and differentiation of these cells in the lateral line and inner ear (Go et al., 2010). At 72 hpf, whole-mount *in situ* hybridization (WISH) also detects small bilateral domains of strong expression of *atp2b1a* at the level of the atrial pole of the heart (Fig. 21A). In the lateral view these cells are in line with the posterior end of the otic vesicle (Fig. 21A). This expression domain is also present during later development (Fig.21E). In adults it was found next to the pharynx (not shown). Time-lapse imaging of SqET4 transgenics *in vivo* revealed that in this domain GFP began expressing at 55 hpf in a thin sheet of cells behind the heart and close to the yolk surface (Fig. 22). At 60.5 - 62.5 hpf these cells delaminate and form a separate cell cluster. Cross-section at this level shows the bilateral cluster ventral of the pharynx that contains *atp2b1a*-positive cells with characteristic glandular morphology (Fig. 21B). *calcitonin* (*calca*) is a known UB marker (Alt et al., 2006). It is expressed in the same population of cells as *atp2b1a* (Fig. 21C, D). In addition, immuno-detection of calcitonin peptide (CT) co-localized with EGFP signal of SqET4 at 6 dpf (Fig. 21G-I). We concluded that these domains of *atp2b1a* expression represent the developing UB.

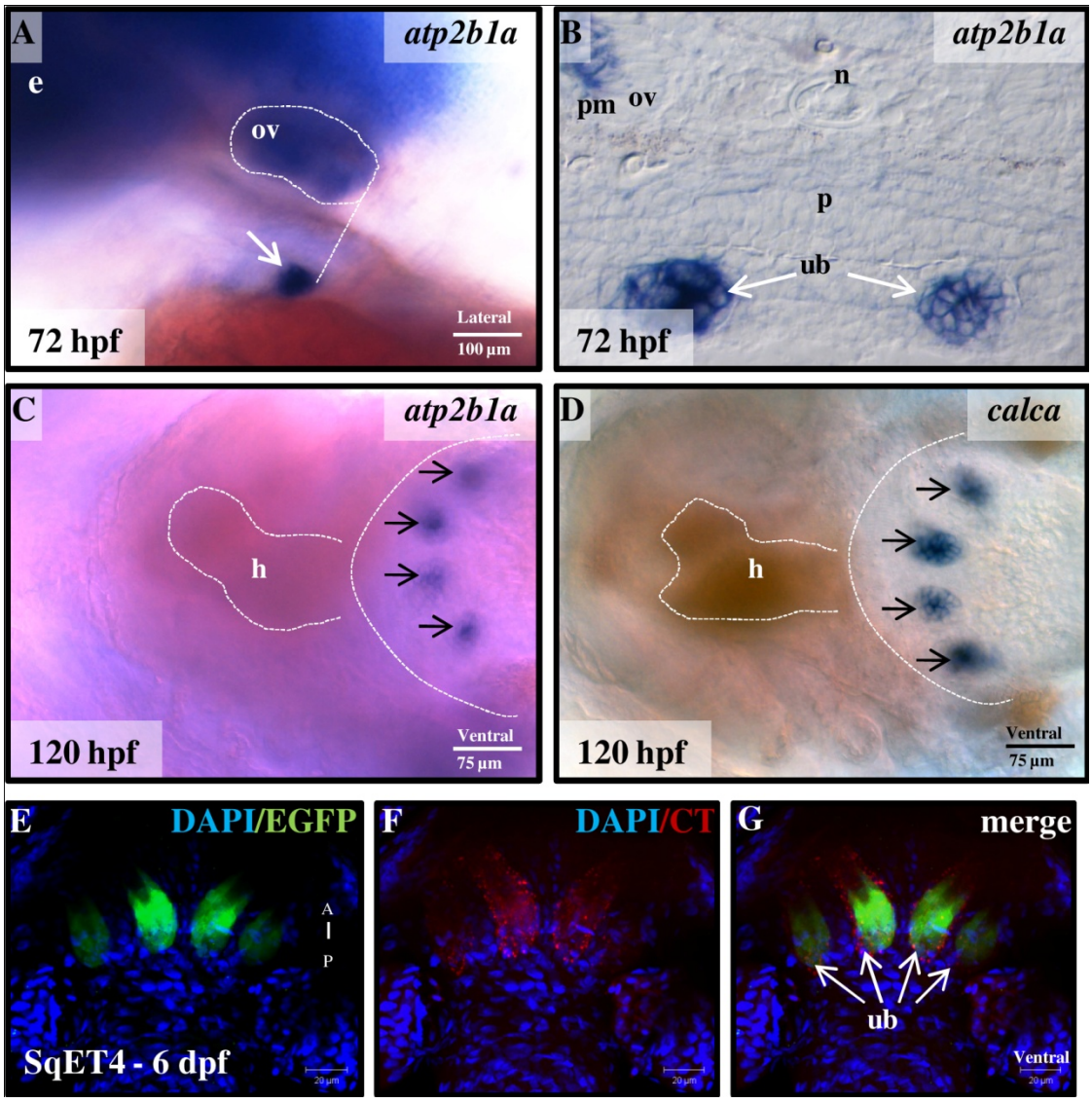

Figure 21: *atp2b1a* is expressed in the ultimobranchial bodies (UB) of the developing zebrafish. A depicts the strong expression of *atp2b1a* at UB at 72 hpf (A: white arrow). The expression at UB is in line with the posterior end of the otic vesicle (A: white encircle) when viewed laterally (A: white dashed line). (B) Cross section at the level of UB clearly shows that expression of *atp2b1a* is bilateral and *atp2b1a*-positive cells exhibit a glandular morphology. C shows a later stage larva at 120 hpf with four UB expressing *atp2b1a* transcripts (black arrows). D shows a similar stage specimen with four UB stained positive by UB molecular marker, *calca*. Immuno-detection of calcitonin (CT) shows co-localization with EGFP signal of SqET4 in UB (E-G; white arrows). *Abbreviations: e: eye; ov: otic vesicle, n: notochord; p: pharynx; pm: posterior macula; ub ultimobranchial bodies; h: heart*

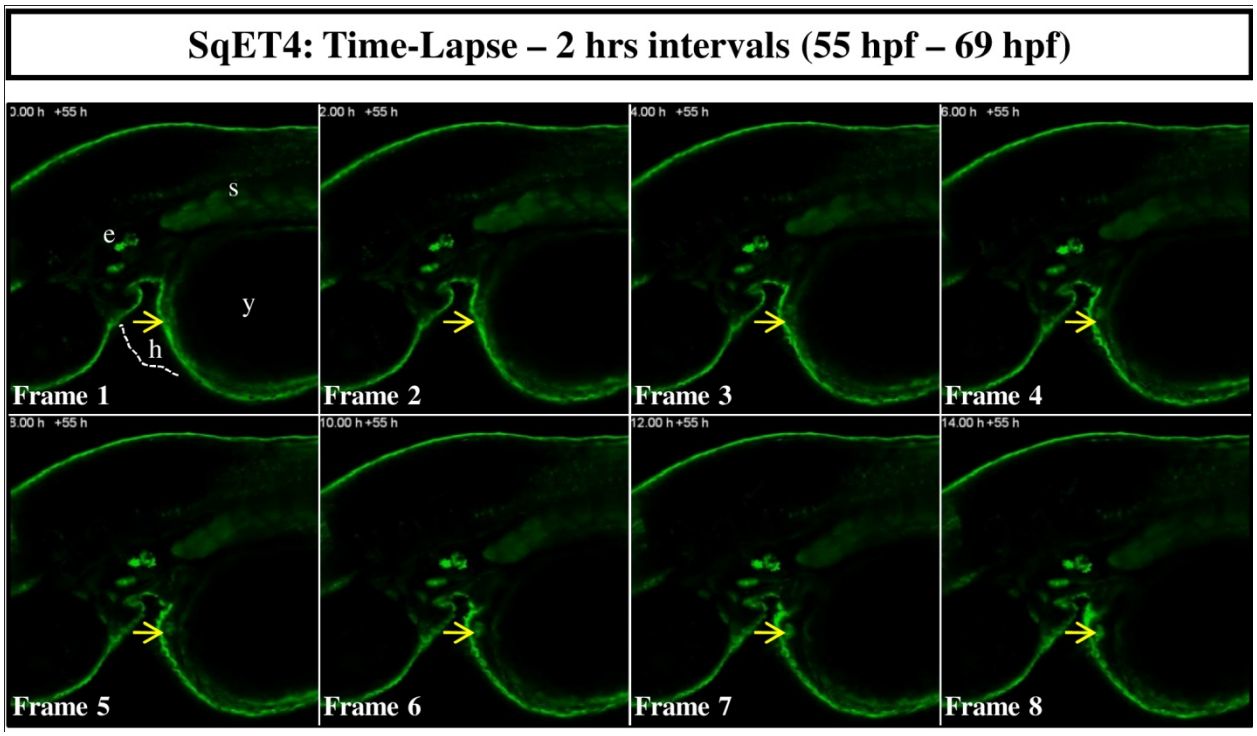

Figure 22: Time-lapse recording of UB development in SqET4 (55 – 69 hpf). EGFP reporter expression at UB was detected from 55 hpf onwards (white arrow) as a thin sheet of cells behind the heart (white dashed line) and close to the yolk surface and gradually developed into a ball-like structure. Shown here are frame-freeze at 2 hours intervals. A SqET4 larva was mounted on its left side. Movie was taken using Zeiss LSM 700 confocal system with 488 nm laser and fitted with temperature chamber set at 28 deg C. *Abbreviations: e: ear; h: heart; s: somites; y: yolk.*

3.2.2 Close 3D contact of UB and pharyngeal teeth

High-resolution confocal imaging at 96 hpf revealed the characteristic shape of UB representing a cluster of highly granulated cells thus suggesting that these cells are secretory. The cluster contains an inner lumen (Fig. 23A, B). Given expression of *atp2b1a* in UB, vital staining with Calcium Crimson AM (CaC) was performed. The staining revealed a single Ca^{2+}-rich tubular structure embedded in the lumen, which projects beyond UB (Fig. 23C, D). Nomarski imaging of larvae after *atp2b1a* staining by WISH also revealed similar tubules associated with *atp2b1a*-

positive UB clusters (Fig. 23E). To address whether this tubules could represent a blood vessels, SqET4 transgenics were crossed with *Tg(fli:EGFP)* transgenics expressing GFP in vascular endothelial cells (Isogai et al., 2001). In compound transgenics the Ca^{2+} staining did not co-localize with GFP expression. This ruled out the possibility that the tubule represents a blood vessel. Given the presence of Ca^{2+} signal at the surface of the tubule, it could represent a bone. Indeed, at 7 dpf Alizarin Red S (AR), a histochemical dye of calcified bones, stained the Ca^{2+}-rich tubule confirming that it contains calcified bone material (Fig. 23F, G). At this stage AR staining reveals some bones that are easy to identify, i.e. the 5^{th} ceratobranchial bone (Cb5) and cleithrum (Cl). These structures along with blood vessels provide useful landmarks suggesting that the UB-associated Ca^{2+}-rich tubule represents the first-formed pharyngeal tooth, $4V^1$ (Borday-Birraux et al., 2006). At 7 dpf, a strong association of *fli:EGFP*-positive blood vessels with both Cb5 and cl was detected. However, there are no *fli:EGFP* expression domains in the proximity of UB even after beginning of calcification of $4V^1$. This suggests that calcification of pharyngeal teeth does not involve vascular circulation. Therefore an alternative mode of Ca^{2+} ion transportation should be involved. This analysis revealed that the UB develops in close contact with the pharyngeal teeth $4V^1$ suggesting that Atp2b1a functions during early calcification of these structures.

3.2.3 UB cells provide Ca^{2+} for developing pharyngeal teeth

To determine whether *atp2b1a* plays a role in calcification of pharyngeal teeth two different approaches were used. First, the gene-specific knockdown of *atp2b1a* by the 5'-ATG antisense translation-blocking morpholino (MO) was performed (Go et al., 2010) and the Ca^{2+} profile in

UB was analyzed with Calcium Crimson AM in *atp2b1a* morphants (Fig. 23H). Second, 10 µM of PMCA inhibitor [5(6)- Carboxyeosin (CE)] was delivered locally in vicinity of UB by injection into the pericardium of 5 dpf larva (Fig. 23J) and the effect of this treatment was analyzed one day after injection (Fig. 23I). In both cases the specific Ca^{2+} signal detected in the pharyngeal dentition $4V^1$ of controls (Fig. 23D) was replaced by dispersed staining of morphant UB cells (Fig. 23H; N = 55) and CE-treated larvae (Fig. 23I; N = 10). Furthermore, CE treatment affected morphology of UB cells. The block of Atp2b1a resulted in Ca^{2+} retention in UB cells in illustration that UB supplies Ca^{2+} for developing pharyngeal teeth.

Figure 23: GFP-positive UB in SqET4 enhancer trap line are connected to the developing pharyngeal dentitions. High resolution confocal image shows a characteristic organization of UB, which consists of a cell cluster formed around an internal channel (A; yellow arrow). UB cells (green) appear to be highly granulated. (B) Orthogonal section of UB reveals an internal lumen. (C) Orthogonal view of UB stained with Calcium Crimson AM (CaC; red), the lumen is formed by the Ca^{2+}-rich tubular structure. (D) Vital staining of UB (green) with CaC (red) illustrates the close association between UB and the first pharyngeal dentitions. (E) Nomarski image of WISH of *atp2b1a* ; revealing pharyngeal teeth (orange arrows) association with *atp2b1a* expressing cells (red arrows). (F) Compound SqET4/Tg*(fli1:*EGFP*)* 7 dpf larvae; the 5^{th} ceratobranchial arch region with blood vessels AA5 and AA6. Green - a combined EGFP signal of two transgenes, red - Alizarin Red (AR) fluorescence. A diagram showing the composite signals from confocal z-stack, with blood vessels in green and AR-stained mineralized bones in red (G). The Ca^{2+} signal in the pharyngeal dentition $4V^1$ of controls is reduced in Atp2b1a morphants (H) and upon treatment by 5,6-carboxyeosin (CE) (I). In both K and L, Ca^{2+} signals were detected within intracellular spaces (white arrows). The morphogenesis of UB was affected by CE treatment as well. EGFP signal is from SqET4 (green), Ca^{2+} signal is visualized by Calcium Crimson AM (CC) in K and L (red signals). (J) Illustration of CE delivered into the pericardium by microinjection (marked by 0.05% DMSO control marked by Texas Red tracer) of 5 dpf larvae. *Abbreviations: nm: neuromasts; cb5: ceratobranchial 1-5; cl: cleithrum; $4V^1$: 1^{st}-forming pharyngeal dentition; e: eyes; AA5, AA6 and LDA; blood vessels at branchial arch region; UB: utimobranchial bodies*

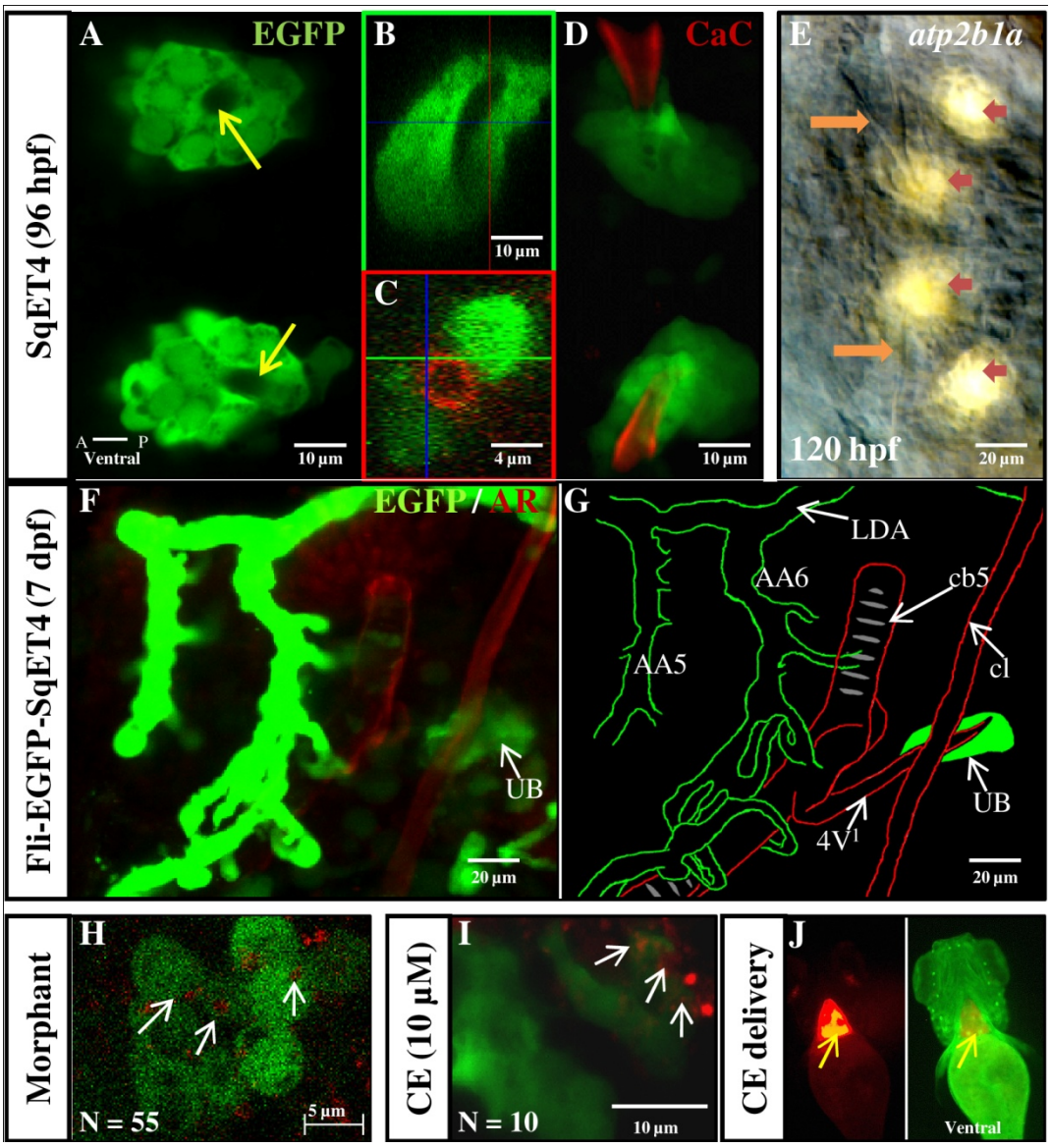

3.2.4 During early differentiation of UB cells *ascl1* acts upstream of *atp2b1a*

In order to understand a role of *atp2b1a* in UB development, we make use of the EGFP expression in both left and right UB of SqET4 transgenics as an indicator of knockdown efficiency. The control 5-mismatch MO had no effect on expression of GFP in the UB (not shown). In contrast, *atp2b1a* translation-blocking MO abolished GFP expression in the UB (Fig.

24A - B', C; $p < 0.05$). The GFP expression in the UB was rescued by co-injection of the full-length *atp2b1a* mRNA lacking the MO target site (Fig. 24C).

Atoh1a regulates *atp2b1a* transcription in mechanoreceptors (Go et al., 2010) suggesting that a member of a family of bHLH transcription factors could regulate transcription of *atp2b1a* in UB. Mash1 was previously reported to regulate calcitonin-producing cells (C-cells) in the thyroid gland of mammals (Kameda et al., 2007). In zebrafish C-cells are represented by UB (Alt et al., 2006). To find which transcription factor regulates an expression of *atp2b1a*, we injected antisense-MO for *ascl1a, ascl1b* (Amoyel et al., 2004) *and atoh1a,* (Millimaki et al., 2007). Either *ascl1a* or *ascl1b* knockdown inhibits GFP expression in the UB of SqET4 ($p < 0.05$) producing a phenotype very similar to that of *atp2b1a* knockdown (Fig. 24C). Co-injection with full-length *atp2b1a* mRNA in both cases did not result in any degree of rescue (Fig. 24C). This strongly suggests that *atp2b1a* expression is under control of Ascl1, which is similar to that in the C-cells of the mammalian thyroid gland. Such similarity illustrated conservation of this process in evolution between teleosts and mammals. On the other hand, knockdown of *atoh1a* was much less efficient (Fig. 24C) in inhibiting *atp2b1a*. *Atoh1a*'s expression is absent in UB, thus limits the similarity of the molecular machinery of differentiation of mechanosensory hair cells and UB cells.

3.2.5 *atp2b1a* knockdown caused a defect in calcification of bones

To understand further a role of Atp2b1a in calcification of bones in zebrafish larvae, the bone-cartilage dual staining with Alcian blue (AB) and Alizarin red (AR) (Walker and Kimmel, 2006) was used. In the 4 dpf controls dentine calcification starts from the pharyngeal teeth ($4V^1$) and

progressively spreads to the later forming 5th ceratobranchial bone (Cb5) and other pharyngeal teeth (3/5V1; Fig. 25A). We first determined that injected morphants were not developmentally delayed in respect of uninjected controls by comparing their hatching rates (Fig. 26A). In addition, sizes of developing liver (marked by *lfabp-RFP*) (Korzh et al., 2008) and pancreatic beta cells (*insulin-GFP*) (Verbruggen et al., 2010) were measured from confocal stacked images at 6 dpf (Fig. 26B). Liver and pancreas were chosen as positive markers of development as both organs do not express *atp2b1a*. In morphants calcification of dentition was delayed until 5 dpf, when a tiny signal was detected at the tip of 4V1. At 7 dpf this pharyngeal dentition is the only structure showing bone calcification in morphants (Fig. 25B; N = 10 larvae per stage analyzed).

Figure 24: *atp2b1a* knockdown abolished EGFP expression in UB of SqET4. (A & B) are maximal projection images of z-stack of 109 micron thick; comparing ventrally-mounted control SqET4 larvae and *atp2b1a* morphant SqET4 larvae at 72 hpf. Specific EGFP expression at the UB at 72 hpf was visible in control (indicated as Left UB and Right UB). In general, UB are bilateral and are positioned in line with the pectoral fins (dashed arc). (A') and (B') compares the EGFP intensity analyzed by confocal software. In comparison when *atp2b1a* was knocked down, EGFP expression was undetected at the same region of analysis. EGFP signal at UB was analyzed after knockdown of various transcription factors thought to be involved in regulating UB development; *atoh1a*, *ascl1a* and *ascl1b*. In addition, Calca knockdown shows no effect on EGFP signal. All injected larvae were similaly analyzed by confocal for EGFP intensity at the left and right UB and the resulting mean of EGFP intensity was being compared (C). EGFP signal at both UB was partially recovered by co-injecting *atp2b1a* morpholino with full-length *atp2b1a* mRNA without MO targeting site. The same mRNA failed to rescue neither *ascl1a* nor *ascl1b* morpholino injected larvae. N = 20 larvae per treatment were analyzed by confocal for EGFP intensity. *P* value was set at < 0.05. Error bar indicates standard deviation. *Abbreviations: ov: otic vesicles; ba: branchial arches; h: heart; y: yolk cell; pf: pectoral fins*

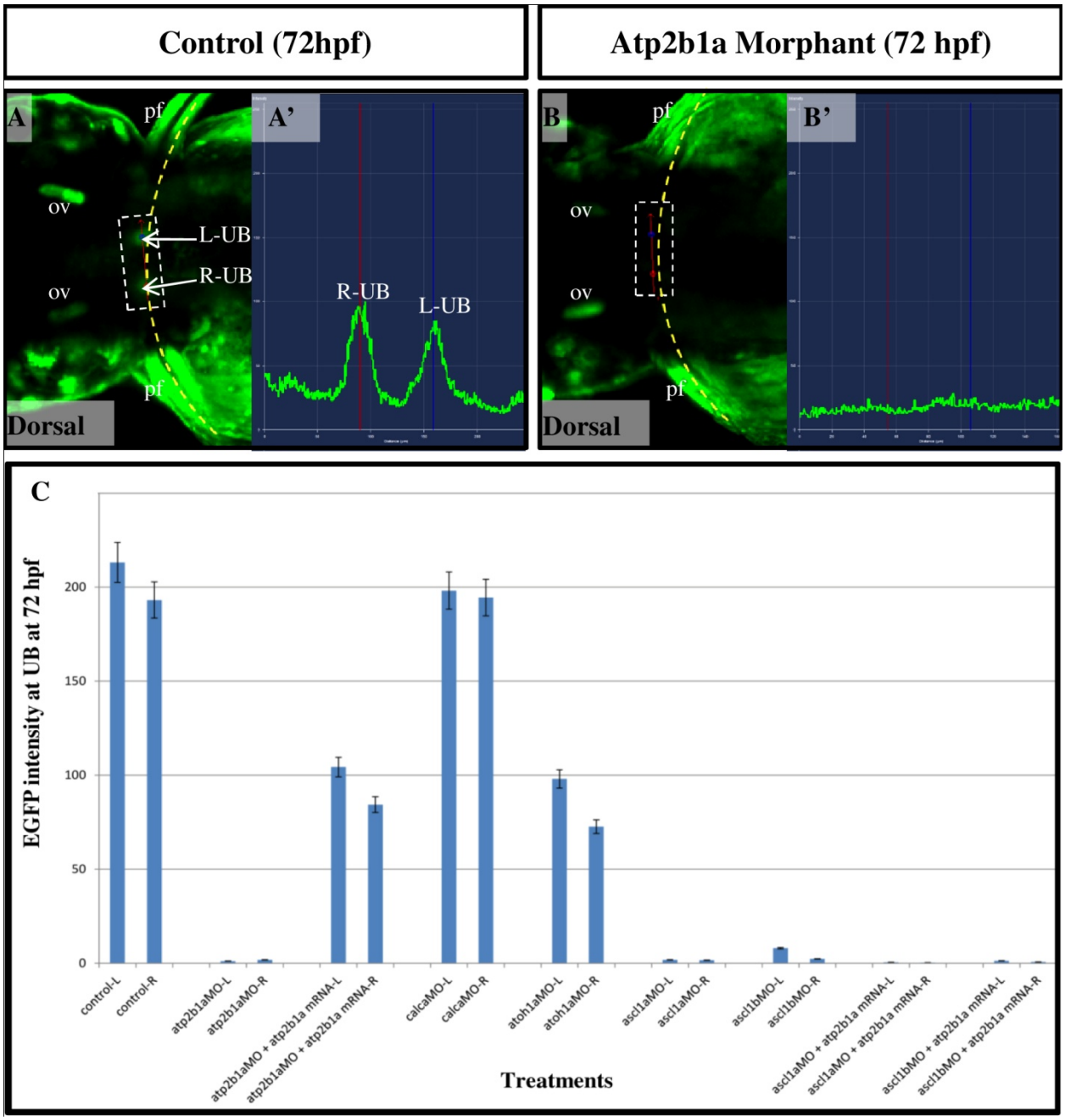
Control (72hpf)
Atp2b1a Morphant (72 hpf)
A
A'
B
B'
pf
ov
L-UB
R-UB
Dorsal
C
EGFP intensity at UB at 72 hpf
Treatments
control-L
control-R
atp2b1aMO-L
atp2b1aMO-R
atp2b1aMO + atp2b1a mRNA-L
atp2b1aMO + atp2b1a mRNA-R
calcaMO-L
calcaMO-R
atoh1aMO-L
atoh1aMO-R
ascl1aMO-L
ascl1aMO-R
ascl1bMO-L
ascl1bMO-R
ascl1aMO + atp2b1a mRNA-L
ascl1aMO + atp2b1a mRNA-R
ascl1bMO + atp2b1a mRNA-L
ascl1bMO + atp2b1a mRNA-R

Figure 25: *atp2b1a* is required for calcification of early-forming bones in zebrafish larvae. A & B compares bone calcification pattern (3-7 dpf) in control and morphant larvae as detected by Alcian blue (AB) and Alizarin red (AR) dual staining at the level of cb5. In controls, bone calcification starts in the pharyngeal dentitions *4V*^{1} and followed by *cb5* and later pharyngeal dentitions (*3/5V*^{1}). In morphants minimal level of calcification was detected with signal at the tip of 4V^{1} and absent in *cb5* and *3/5V*^{1}. Similarly, C & D compares calcification pattern at the head region (4-7 dpf) in control and morphant larvae. In control larvae, otoliths (oto) of the inner ear achieved complete calcification as early as 4 dpf while this is severely delayed in morphants. In addition, calcification of both ceratohyal (ch) and notochord (nc) was absent in morphant larvae. (n = 10). E) *atp2b1a* transcripts were detected at weak level in cartilages at 72 hpf. (F& F') Immuno-detection of EGFP in 4 dpf SqET4 detected expression in core of ch cartilage. B) Enlargement of image A) clearly shows the cytoplasmic localization of EGFP in these cells when co-localized with DAPI nuclear stain. *Abbreviations: cb1-5: ceratobranchial arches 1-5; 4V*^{1}*: 1*st*-forming pharyngeal dentition; oto: otoliths; ch: ceratohyal; nc: notochord; ch: ceratohyal; ub: ultimobranchial bodies*

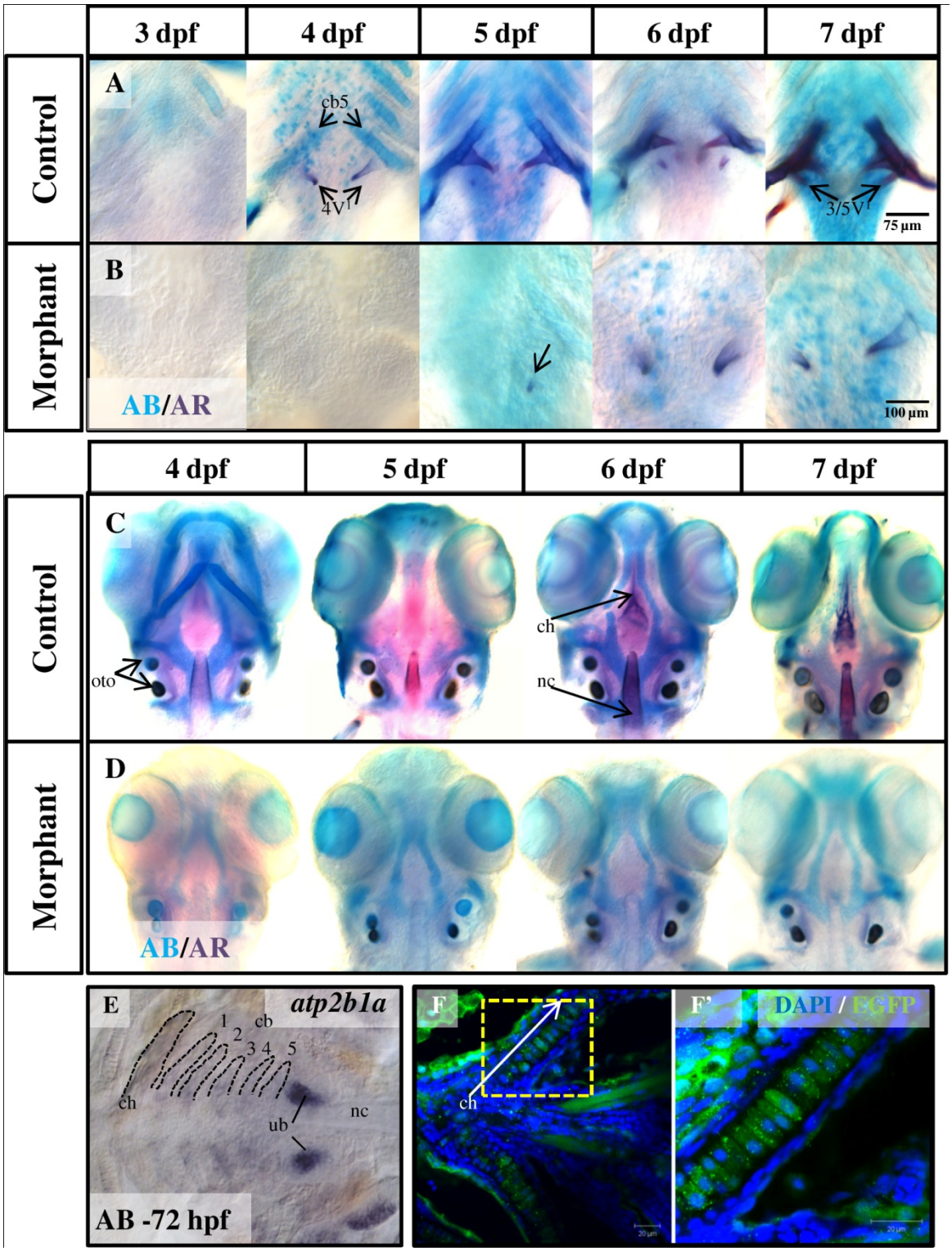
3 dpf
4 dpf
5 dpf
6 dpf
7 dpf
Control
Morphant
A
B
cb5
4V
3/5V
75 µm
100 µm
AB/AR
4 dpf
5 dpf
6 dpf
7 dpf
C
D
oto
ch
nc
AB/AR
E
atp2b1a
1
2
3
4
5
cb
ch
ub
nc
AB -72 hpf
F
F'
ch
DAPI / EGFP

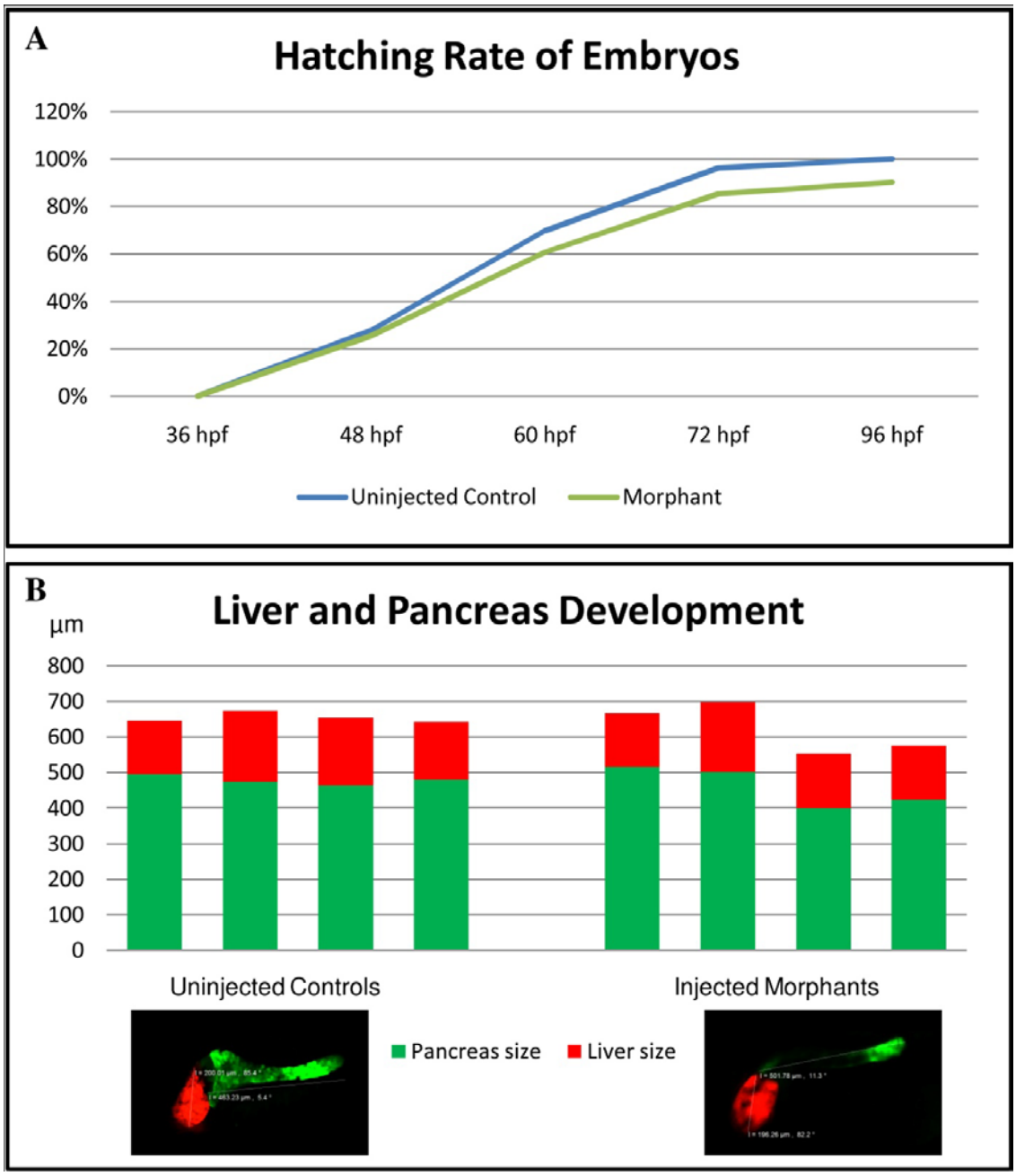

Figure 26: General development was not delayed in injected *atp2b1a* morphants. (A) Comparison of hatching rate between uninjected controls and injected morphants. Morphants' hatching rate followed closely of that in uninjected controls. Results were collated from two separate injection experiments where N = 380 embryos per group and expressed as percentage hatched. (B) Sizes of developing liver (marked by *lfabp*:RFP) and pancreas (*insulin*:GFP) were compared between controls and morphants larvae at 6 dpf. Measurements (µm) were made from confocal stack images taken by Zeiss LSM700 confocal system (see insert for illustration). All embryos were similarly raised in 28 ^{o}C incubator.

Supporting data obtained from the osteoblasts reporter line Tg*(osx-mCherry)* (Spoorendonk et al., 2008), reveals that an early calcification of pharyngeal teeth takes place in the absence of function of osterix-positive odontoblasts. These cells were not detected in PD at 4.0 dpf stage, but were present after 5.5 dpf, when they associate closely but do not overlap with UB (Fig. 27B). This indicated that Atp2b1a is required for calcification of structures adjacent to UB such as pharyngeal dentitions and Cb5.

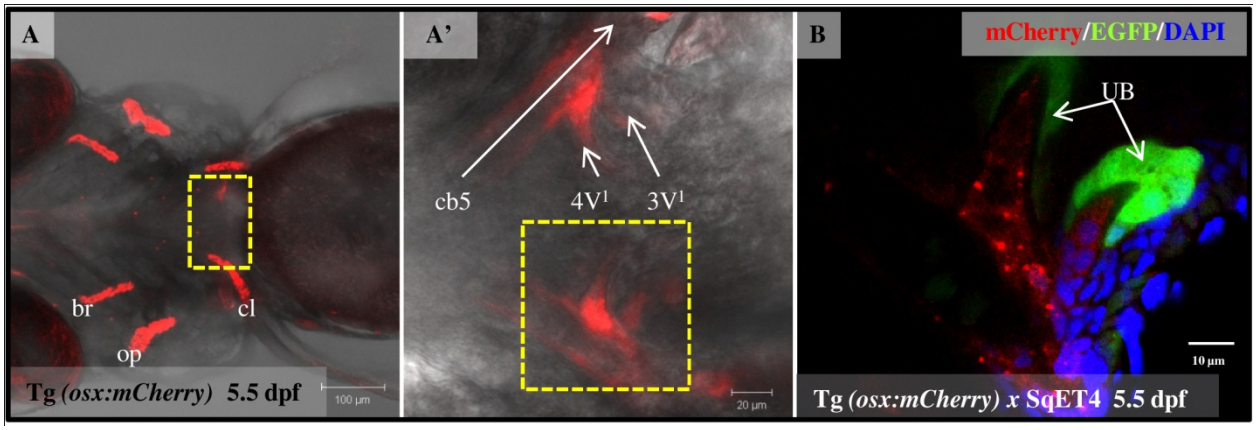

Figure 27: Osteoblasts were detected at pharyngeal dentitions (PD) after 5.5 dpf. A) Maximum projection image of Tg*(osx:mCherry)* transgenic line mounted ventrally indicate presence of osteoblasts at multiple bone-forming sites at 5.5 dpf; br, op and cl. Osteoblasts present at PD were not visible from this confocal stack. B) Osteoblasts at PD were visible on dissected pharynx tissue. C) Osteoblasts at PD associates closely but do not overlaps with UB. *Abbreviations: br: branchiostegal ray; op: operculum; cl: cleithrum; cb5: 5th ceratobranchial arch; 4V^{1}: first forming pair; 3V^{1}: second forming pair; UB: Ultimobranchial bodies.*

The progression of bone calcification in other early calcifying bones such as operculum was shown using Alizarin red (AR) and Calcein (green) vital staining (Kimmel et al., 2010). Larvae were stained successively, first, by Alizarin Red S for 2 hours at 3 dpf, and, second,

incubated in calcein up to 3 days until observation. Both ventral (v) and posterior apices (p) of the control operculum expanded in contrast to that in morphant (Fig. 28C, D). In addition, a negative effect on distribution of bone-matrix forming osteoblasts was observed in the operculum of *Tg(osx-mCherry)* (Spoorendonk et al., 2008) morphants. Here osteoblasts failed to reach the growing edges of v-p apices (Fig. 28E, F). This illustrated that UB not only regulates calcification of adjacent bones, but also exerts a long-range effect on bone calcification.

Figure 28: Bone matrix progression at developing operculum was severely affected in *atp2b1a* morphant larvae. A & B compares control and morphant situation, showing progression of calcification at a developing operculum (*op*) by differential live staining larvae by Alizarin red (AR) and calcein (green). Calcification at morphant operculum was severely retarded at ventral-posterior *(vp)* edges. C & D uses*Tg(osx-mCherry)* for comparing distribution of osteoblasts at *op*. In control larvae, osteoblasts were closely associated with the growing joint socket *(js)* and *vp* edges and were observed to outline predominantly at the expanding edges; *jp* & *jv* apices (E: red arrows), which were absent in morphant *op*. (D) In morphant larvae, *osx:mCherry*-expressing cells were only accumulating in *js* apex. C & D are maximum intensity projections of 70 micron z-stack. *Abbreviations: js: joint socket; v: ventral apex; p: posterior apex; e: eye; ie: inner ear; cl: cleithrum; op: operculum*

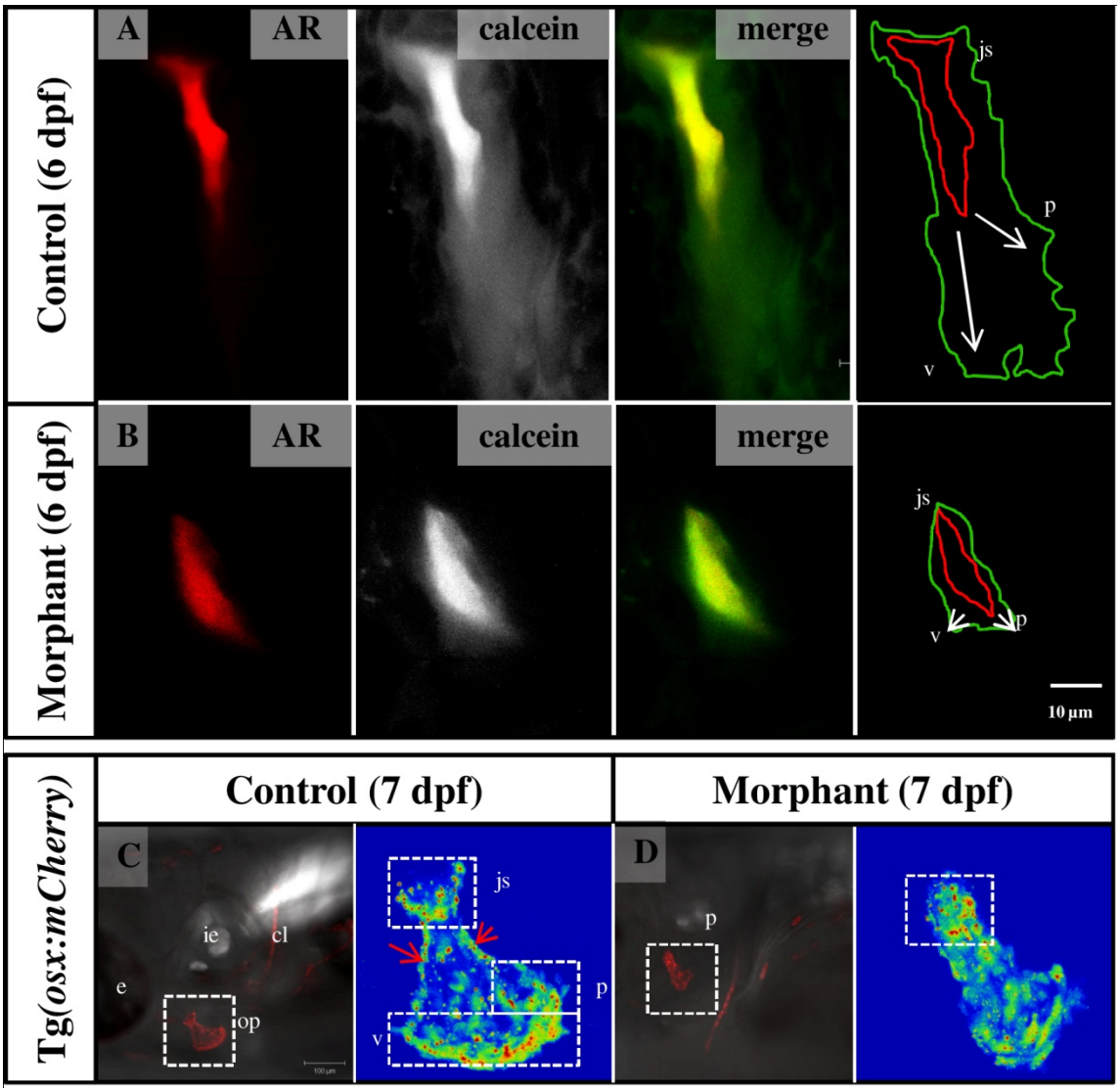

3.2.6 *atp2b1a* knockdown affects expression of genes expressed in UB and pharyngeal dentition

To check the effect of Atp2b1a deficiency on genes expressed in UB, such as *calca* (Lafont et al., 2010), and pharyngeal dentition; *itg αV, cx43* (Ablooglu et al., 2007); and *dlx2b* (Borday-Birraux et al., 2006) quantitative RT-PCR was used. To exclude a contribution of transcripts present in other tissues, total RNA was prepared from the pharynges isolated from 3.5 dpf larvae

(Fig. 29; N = 50 pharynges/pool; 3 replicates). Expression levels were normalized using the housekeeping gene, *β-actin1* and presented as fold-change. Quantitative RT-PCR showed 3-fold reduction in *atp2b1a* levels in the morphant, suggesting that *atp2b1a* regulates its own expression. The expression of structural genes of pharyngeal dentition was reduced too: *itg αV* - one-fold and *cx43* - more than 5-folds. Interestingly, expression of transcription factor *dlx2b* almost doubled, suggesting a feedback mechanism to compensate a loss of Atp2b1a activity. It seems that *dlx2b* may act as a transcriptional regulator of *atp2b1a* similar to *ascl1* (Fig. 24C). Importantly, *calca* transcriptional level was reduced almost 2-folds (Fig. 29).

At the same time, immuno-detection on calcitonin gene-related peptide (CGRP) indicated significant reduction in early bone-forming regions in the vicinity of UB, i.e. cleithrum, operculum and ceratobranchial bone (Fig. 30B). These results indicated that *atp2b1a* is required to regulate expression of *calca* and CGRP. To further explore a connection between *calca* and *atp2b1a*, *calca* morpholino (Lafont et al., 2010) was injected in SqET4, but *atp2b1a* expression was not affected (Fig. 24C), suggesting that in UB cells *atp2b1a* may act in an epistatic manner upstream of *calca*.

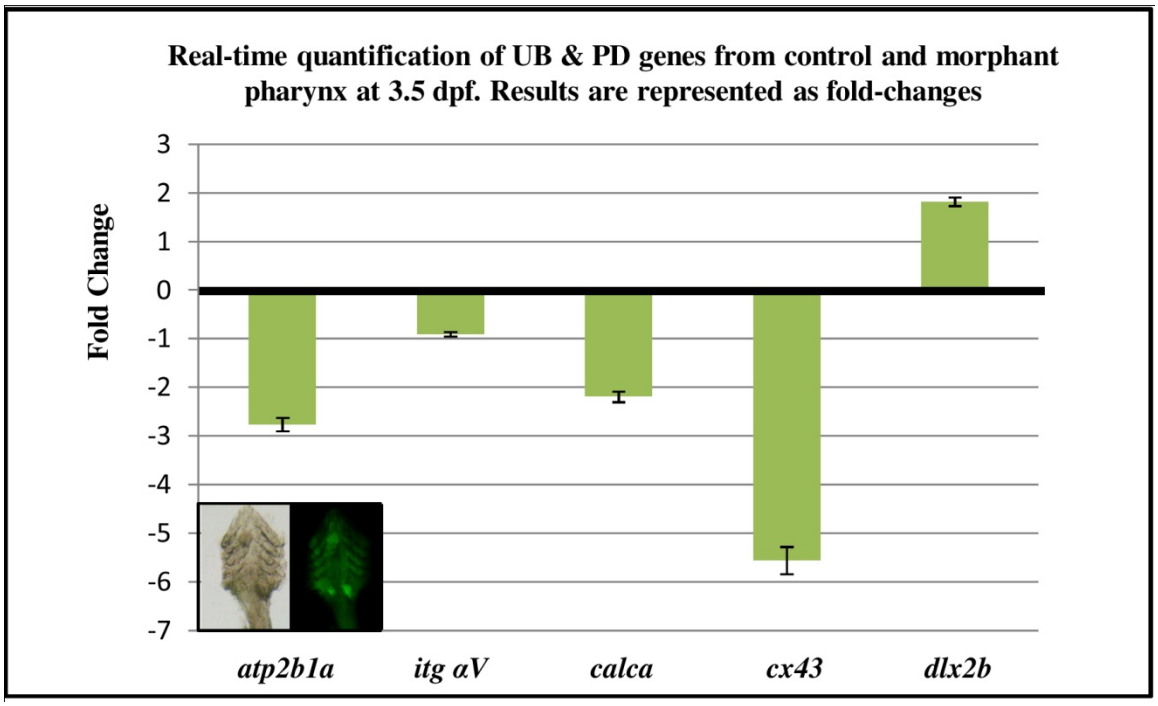

Figure 29: *atp2b1a* knockdown resulted in mis-regulation of UB specific genes. Real-time qPCR of UB *calca* from control and morphant larvae at 3.5 dpf. In addition, expression levels for known pharyngeal dentitions (PD) molecular markers (*itg αV*, *cx43* & *dlx2b*) were quantified from the same pool of test cDNA. Results are represented as fold-changes (mean ± SEM) compared to un-injected control group. cDNA was converted from total RNA extracted from pharynx explants (insert: pharynx excised from SqET4 with embedded UB) to exclude gene expression from non-related tissues (N = 50 pharynx/pool; 3 replicates; error bar represents S.E.M.). Expression levels were normalized with house-keeping gene, *B-actin1* (Table 8 for a list of gene-specific primers used).

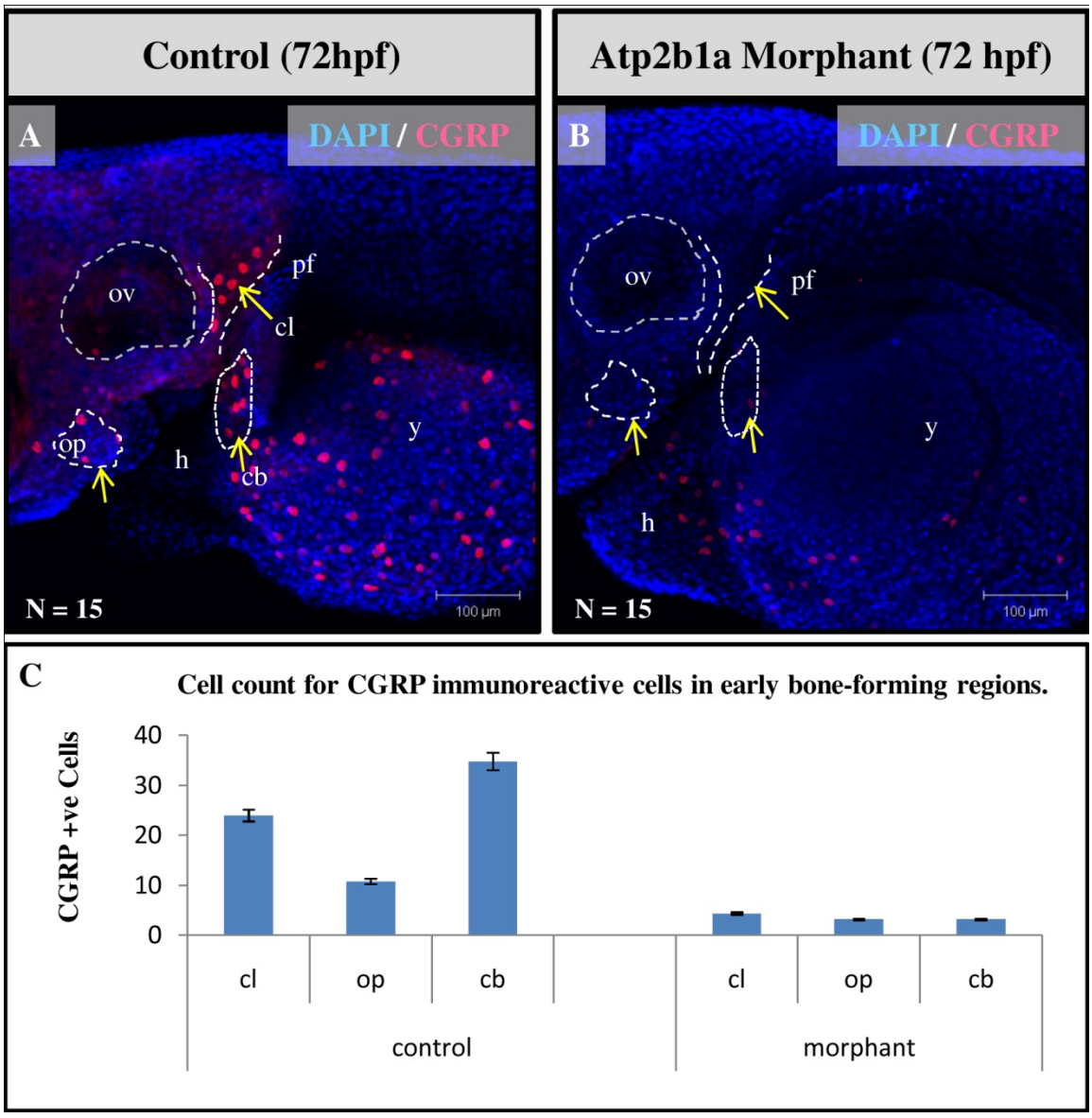

Figure 30: *atp2b1a* regulates production of calcitonin gene-related peptide (CGRP) hormone. (A) CGRP immuno-reactive cells of control embryos at 72 hpf. (B) Significant reduction in CGRP immuno-reactive cells was apparent at regions of developing bones (yellow arrows; cl, op and cb, (blue: DAPI; red: CGRP, scale bar: 100 µm). (C) Quantification (mean cell numbers) of CGRP immuno-reactive cells located in cl, op and cb respectively from both left and right sides of larvae (N = 15; error bar represents standard deviation). *Abbreviations: ov: otic vesicle; op: operculum; pf: pectoral fin; cl: cleithrum; cb: ceratobranchial; h: heart; y: yolk.*

3.3 Other Expression Domains of *atp2b1a*

As mentioned in earlier parts of this thesis, SqET4 has broader expression domains other than mechanosensory cells (Chapter 3.1) and ultimobranchial bodies (Chapter 3.2). Since these EGFP signals remain observable in adult stages, analysis in adult stages is thus possible. Without going into too much detail, I describe here these expression domains of SqET4 and the significance of the results. Some of which can be interesting to follow up if one wishes to do so.

3.3.1 *atp2b1a* can be regulated by Delta-Notch signaling and is required for the normal development of optic tectum and sensory patches

Not only is *atp2b1a* an excellent molecular marker for the developing optic tectum (from 19 hpf onwards, data not shown), but its expression in this region can be regulated by Delta-Notch signaling as evident in *mindbomb* mutants. Here, *atp2b1a* was significantly upregulated in both the mutant optic tectum and inner ear. In the inner ear, *atp2b1a*'s up-regulation represents a premature production of mechanosensory cells from support cells (due to a lack in lateral inhibition in *mindbomb*). But interestingly, the optic tectum experienced a similar over-production phenotype. These cells in optic tectum are *atp2b1a* positive, but their nature and their source(s) are currently unknown. On top of that, expression level of *atp2b1a* can be knockdown by *atp2b1a* morpholino, and thus affects optic tectum's development (Fig. 31G & H).

Figure 31: *atp2b1a* can be regulated by Delta-Notch signaling and is required for the normal development of optic tectum and sensory patches. (A) *atp2b1a* is express in the optic tectal region from 19h (not shown) and reaches its peak by 24h in the embryonic brain. (B) This expression faithfully recapitulates *egfp* expression of SqET4. In mindbomb mutants (*mib*^{ta52b}), mis-regulated delta gene expression results in failure of Delta-Notch signalling. Most dramatically, the sensory patches in mutant ear, which consist solely of hair cells, are produced in great excess and prematurely. This phenotype is apparent when mib is crossed with SqET4 transgenic line (C & D). *atp2b1a* transcript expression domain increase prematurely in mib mutant (E & F). Confocal images of SqET4 shows that knockdown of Atp2b1a affected the development of optic tectum when EGFP expression was significantly reduced (G & H). *Abbreviation: ot: optic tectum; ov: otic vesicles; e: eye*

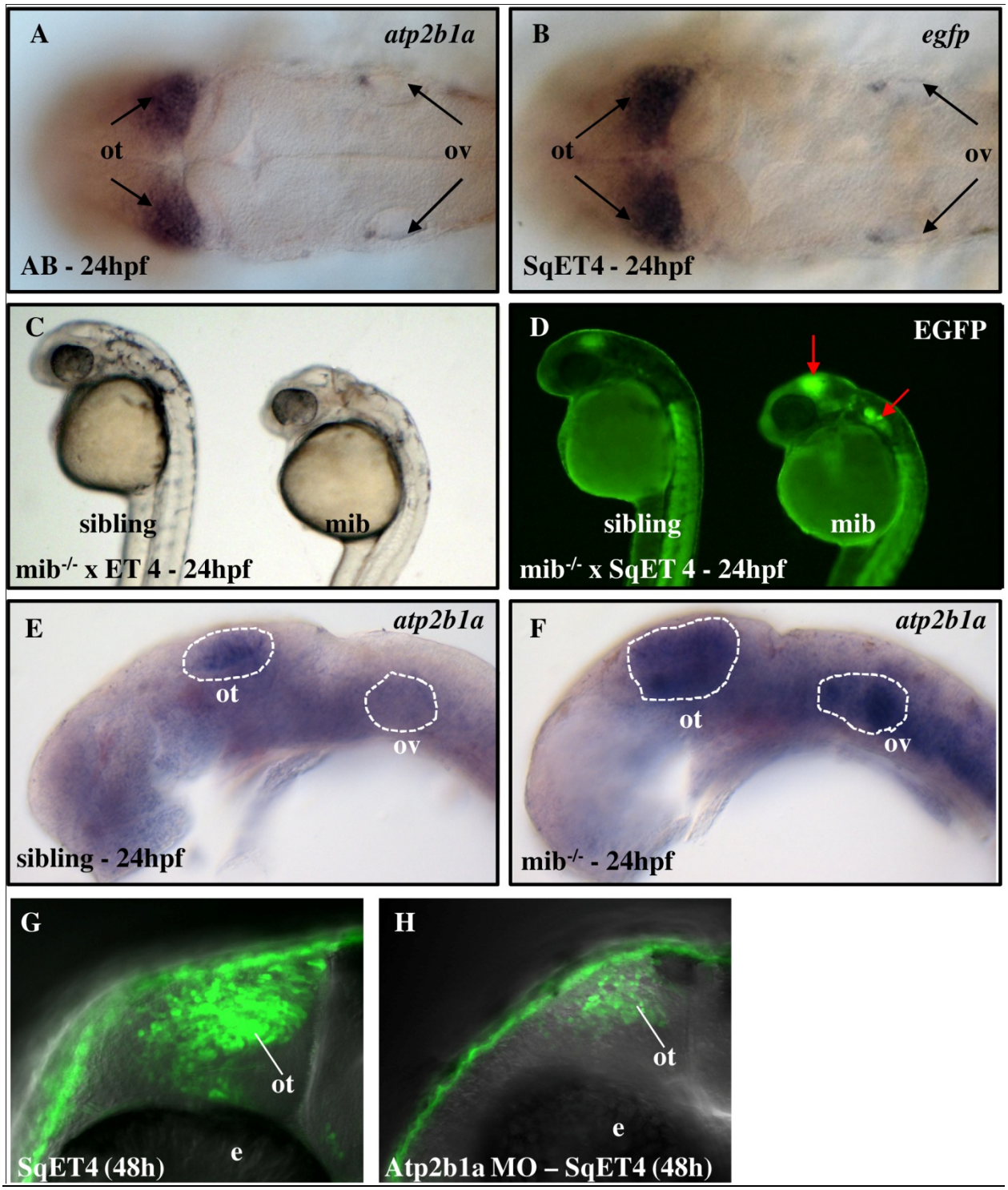
A
atp2b1a
ot
ov
AB - 24hpf
B
egfp
ot
ov
SqET4 - 24hpf
C
sibling
mib
mib-/- x ET 4 - 24hpf
D
EGFP
sibling
mib
mib-/- x SqET 4 - 24hpf
E
atp2b1a
ot
ov
sibling - 24hpf
F
atp2b1a
ot
ov
mib-/- - 24hpf
G
ot
e
SqET4 (48h)
H
ot
e
Atp2b1a MO – SqET4 (48h)

3.3.2 *atp2b1a* is required for muscle development

Here *atp2b1a* was shown to be expressed in early somites at 15 hpf, but SqET4's expression doesn't come on early enough in the same region. Nonetheless it is visible from 22 hpf onwards. *Atp2b1a* knockdown has resulted in some loss of somite integrity (as evident from lowered birefringence level in somites; Fig. 32D). And this was precisely the reason that drove me to take an alternate approach to ascertain the morphant phenotype seen in lateral line neuromast defects. Diffusion of morpholino was restricted to lateral line cells (and at the same time somites was avoided) by injecting morpholino in central cells of a16-cells blastomeres (Fig. 33).

Figure 32: *atp2b1a* is required for muscle development. Atp2b1a is expressed in the muscle lineage. (A) Flat mount of the anterior posterior part of the embryo at 12 somites. (B) Lateral view of trunk region above yolk extension at 24 hpf. Muscle birefringence is used to assess muscle integrity (C) Control embryo display normal level of birefringence whereas *atp2b1a* morphant show reduced birefringence (D). Confocal z-stack images of control SqET4 and *atp2b1a* morphant were taken from lateral view and then tilted to oblique angle (E, F) and orthogonal views of stacks of confocal images (E', F') to illustrating the defective horizontal myoseptum (white dashed line box) in *atp2b1a* morphant at 48hpf. Embryos were stained by Mito-Tracker Red to reveal mitochondrial-active neuromasts. Control (E, E') neuromasts were labeled with Mito-Tracker Red whereas mitochondrial-active neuromast was absent in *atp2b1a* morphant (F, F'). (Scale bar = 50 μm). *Abbreviations: s, somites; ac, adaxial cells*

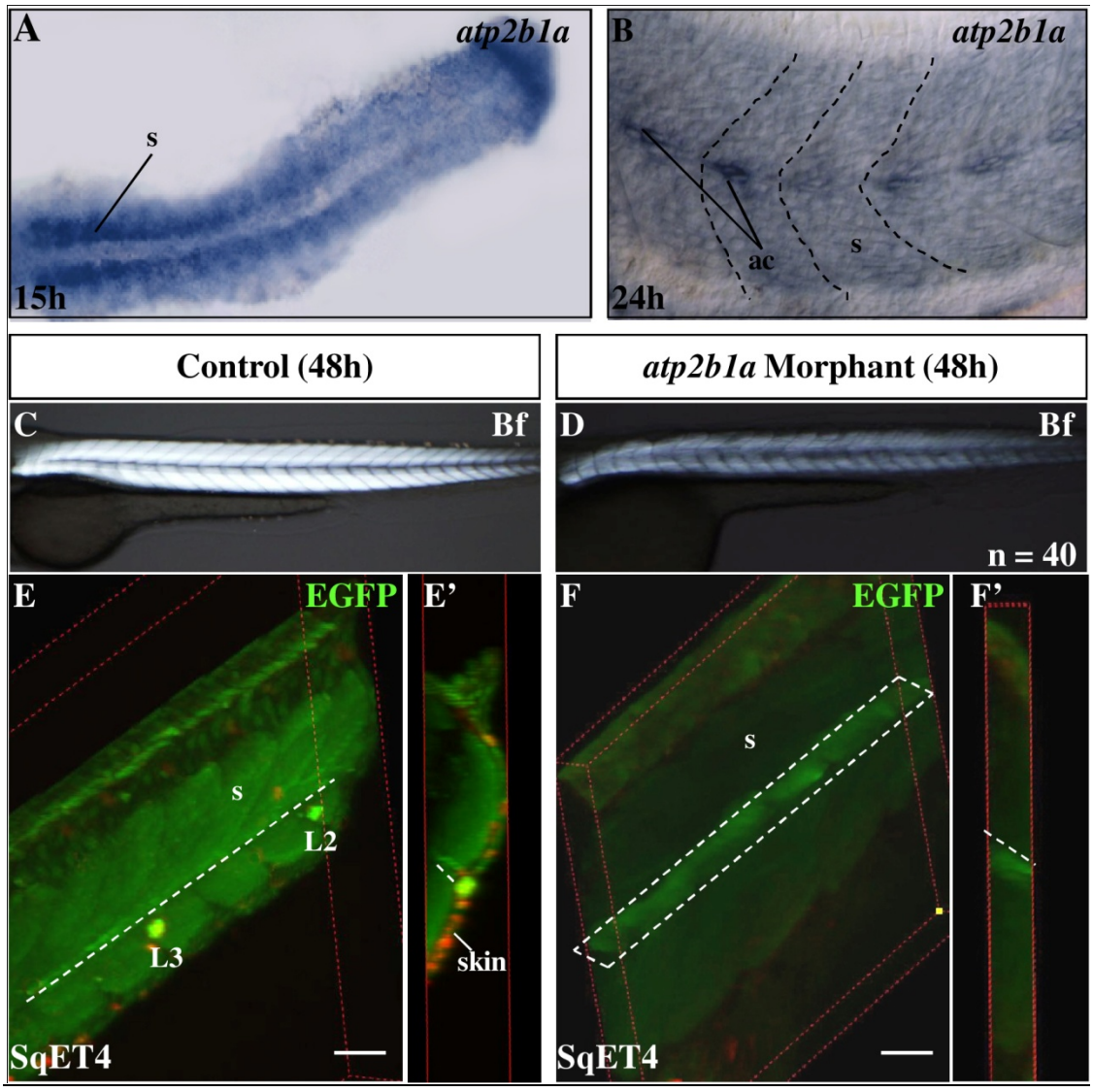
A
atp2b1a
s
15h
B
atp2b1a
ac
s
24h
Control (48h)
atp2b1a Morphant (48h)
C
Bf
D
Bf
n = 40
E
EGFP
s
L2
L3
SqET4
E'
skin
F
EGFP
s
SqET4
F'

Figure 33: Control experiment showing that lateral line phenotype of *atp2b1a* knockdown is independent from its muscle phenotype. 16-cell stage injection (Fong et al., 2005) was used to restrict distribution of morpholino to lateral line cells. One half of the injected SqET4 embryo was targeted. Texas-Red staining indicates the localization of the injected *atp2b1a* morpholino, showing that in this case the right half of the embryo (morphant side) is *atp2b1a*-deficient. The left half with low Texas-Red staining was used as an internal control (control side). The comparison of the anterior lateral line and inner ear at the morphant and control sides at 48hpf showed marked reduction of GFP in these organs at the morphant side (A). Similarly, (B) showed reduction of EGFP expression in neuromast L2 and L3 at the morphant side. (C) Comparison of the number of neuromasts deployed on the control and morphant (MO) side showed significantly fewer neuromasts at the morphant side by 3dpf. (D) Comparison of the number of GFP-positive hair cells within L2 and L3 neuromast showed significantly fewer hair cells on the morphant side by 3dpf. Horizontal bar represents standard deviation. (n = 32). (E, F) Neuromasts L2 and L3; (E, E') control morpholino; (F, F') morphants. Texas-Red (TR) staining indicates the localization of the injected morpholino in SqET4 at 48hpf, illustrating presence of neuromasts, but differentiation of mechanoreceptors is affected. (n = 20). *Abbreviations: AL; anterior lateral line neuromast, OV; otic vesicle, PM; posterior macula, L; posterior lateral line neuromast, hc; hair cell, s; somites*

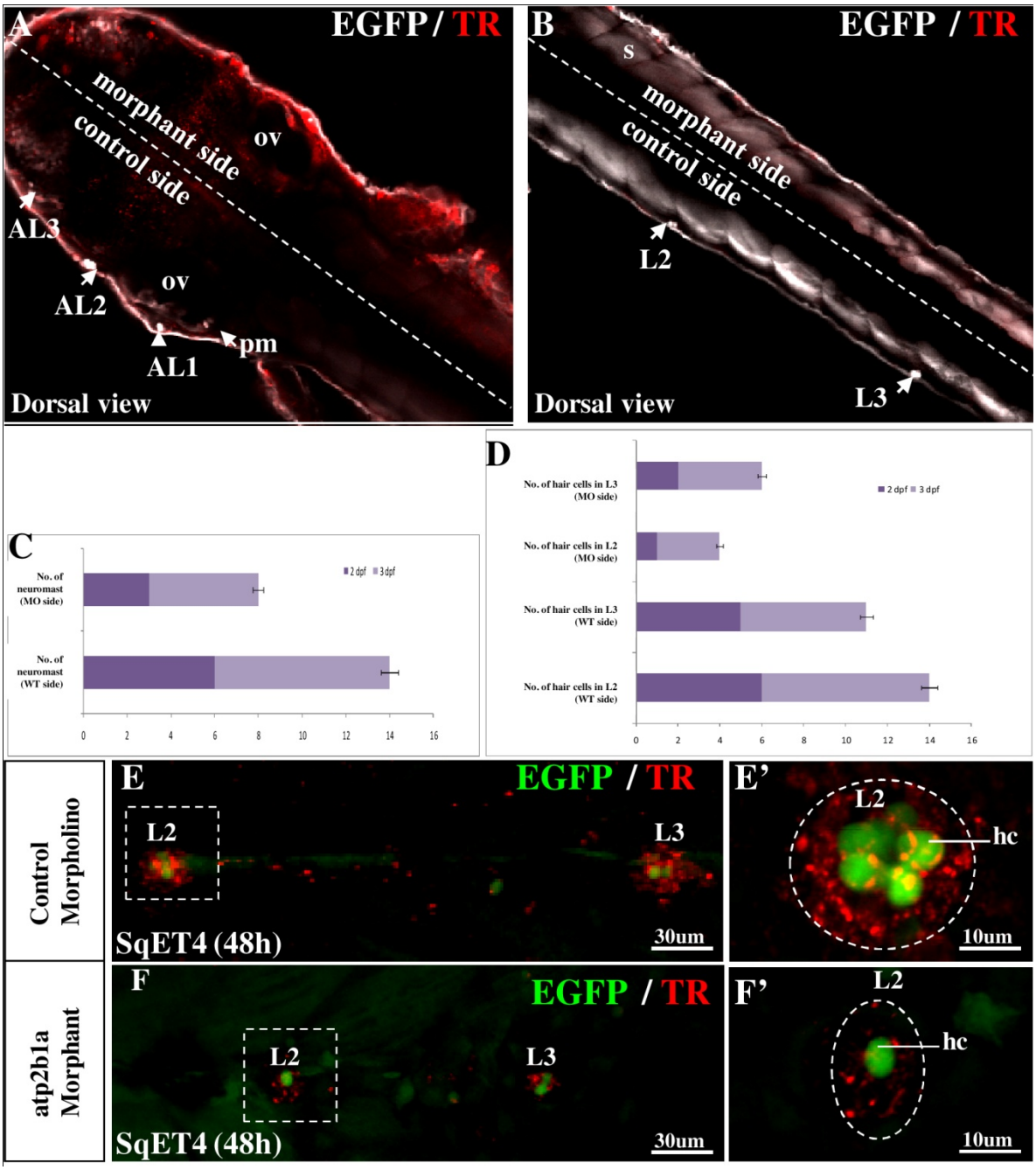

3.3.3 Early function of *atp2b1a* is required for normal cell adhesion

The reason why cell adhesion was looked into was due to an observation of sporadic lateral line neuromasts deposition pattern which differs very much from the normal, regulated pattern. We

hypothesized the reason could be due to a defective posterior lateral line primordium (pLLp) migration as result from the *atp2b1a* knockdown, since *atp2b1a* transcript (as well as in SqET4 expression) was first detected in the posterior end of a migrating pLLp. An experiment with hanging drop culture (Fig. 34A) was chosen to assay *atp2b1a*'s relevance to cell adhesion function. The experiment was found suitable as animal caps from embryos at 4 hpf were required to carry out the experiment. Since *atp2b1a* is maternally deposited, it should be present by 4 hpf for this assay. The results from this experiment fitted nicely with the homotypic binding model of c-cadherins (Ca^{2+}-dependent cell adhesion): i.e. modulating expression level where two cell lines expressing the same type of cadherin but in different amounts, also segregate from each other. The cells with the higher expression levels (Fig. 34F wild-type green cells) move to the interior of the aggregates while the cells with the lower expression levels (Fig. 34H; *atp2b1a* knockdown red cells) formed an outer shell. It is possible that a disruption of the level of extracellular Ca^{2+} required for normal cell adherence was achieved from *atp2b1a*'s knockdown.

Figure 34: Early function of *atp2b1a* is required for normal cell adhesion. A) Hanging drop experimental procedure. Animal caps were excised from two populations of donor embryos at 4 hpf, with donar 1 and donar 2 being wildtype embryos with different tracer dyes. Cells were dissociated and incubated overnight as hanging drop. Under such conditions, wildtype cells can form cell aggregates without any distinction between the two donars. In control (B to D), dis-associated cells at 4hpf labeled with fluorescein (green) and Texas-red-co-injected with 5-mismatched control morpholino (red) formed aggregates after 24 hours incubation in L15 medium supplemented with Pan/Strep antibiotics (hanging drop culture). Both red and green cells were able to intermix equally well to form cell aggregates (white arrows). By contrast, in morphant situation (F to H) where conditions were similar, except control morpholino was replaced by *atp2b1a* morpholino, red cells were only seen to associate with green wild-type cells by forming a "shell" outside the green cells aggregates (yellow arrows). E and I depicts a rotation at Z-axis by 60 degrees of z-stack images of these cell aggregates taken by confocal microscopy. White dashed circles singles out these cell aggregates, showing that in control (D), red cells were present with the core of the aggregates, whereas in morphant, red cells were excluded from the core of cell aggregates. (N = 60 cell aggregates/treatment).

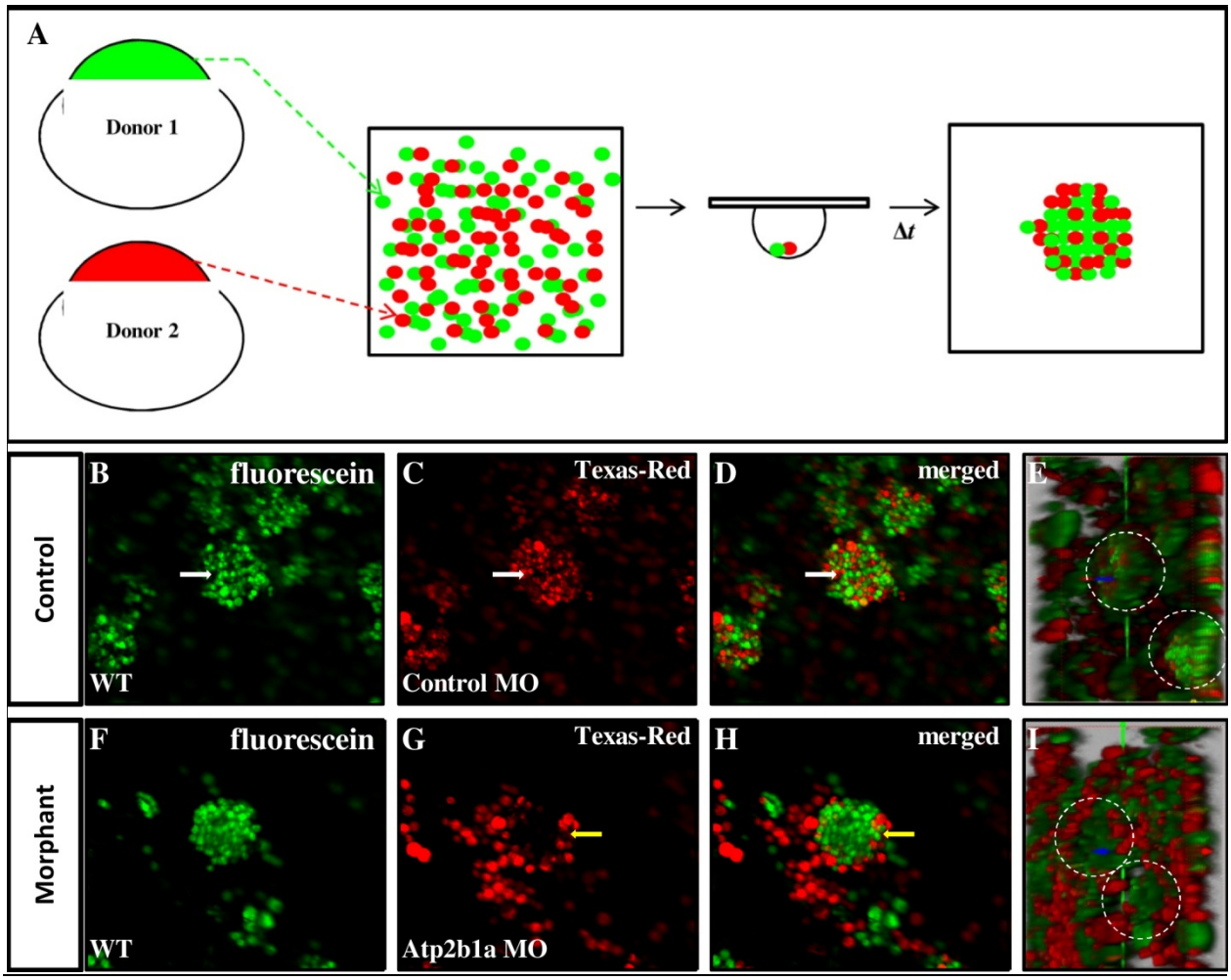

3.3.4 *atp2b1a* has roles in heart valves' function

SqET4 expresses weak EGFP signal in atrial-ventricular valve (AV valve) and this signal increases upon *atp2b1a* knockdown (Fig. 35B & B'). Morphologically, defective heart looping, pericardial edema, decrease heart beat and abnormal blood pooling were observed in these morphants.

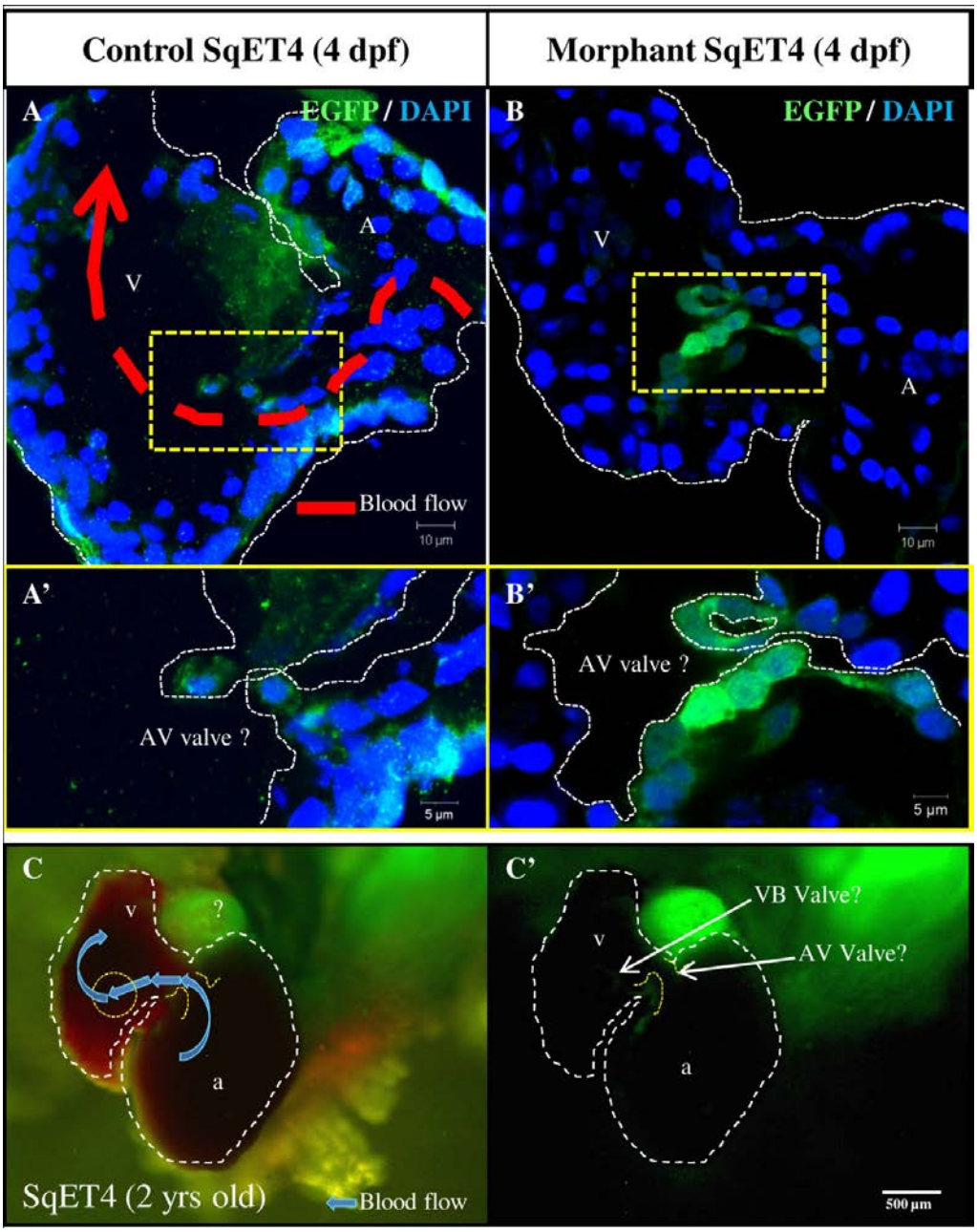

Figure 35: *atp2b1a* required for heart atrio-ventricular valves' function. (A & A') EGFP signal was detected in embryonic heart valves. (B & B') *atp2b1a* morphant phenotype of embryonic heart shows significant increase in EGFP signal in these presumptive heart valves, while heart looping was also being affected by the knockdown. (C & C') EGFP signal was also detectable in heart valves at adult stage. *Abbreviations: v: ventricle; a: atrium; VB valve: Ventricle-Bulbus valve; AV valve: Atrium-Ventricle valve*

3.3.5 *atp2b1a* is expressed in statoacoustic ganglion

SqET4 expresses EGFP in presumptive statoacoustic ganglion of the inner ear at larval stages. EGFP signal was detected in these presumptive neurons (until proven with appropriate markers) located dorsally from otic sensory patches from 4 dpf onwards. A posterior bundle of cells appeared initially as loose clusters of cells (Fig. 36A'). At a later stage, the anterior bundles of these neuron-like cells increase greatly in terms of number and the elaborateness of their axonal projections. Such elaborateness of axons in the inner ear correlates well with the on-going maturation of inner ear sensory patches, i.e. the anterior and posterior maculae. The anterior and posterior bundles were seen connected by a "bridge of axonal projections" (red dashed lines). *Atp2b1a* is similarly expressed in the same region at transcript level (Fig. 36C).

Figure 36: *atp2b1a* is express in presumptive statoacoustic ganglion of the inner ear. (A & A') EGFP signal was detected in presumptive statoacoustic ganglion located dorsally from otic sensory patches from 4 dpf onwards. A posterior bundle of cells appeared initially as loose clusters of cells. (B & B') At later stage, the anterior bundles of these neuron-like cells increase greatly in terms of number and the elaborateness of their axonal projections. Such elaborateness of axons in the inner ear correlates well with the on-going maturation of inner ear sensory patches, i.e. the anterior and posterior maculae. The anterior and posterior bundles were seen connected by a "bridge of axonal projections" (red dashed lines). (C) *In situ* hybridization of *atp2b1a* at 6 dpf demonstrated similar expression. *Abbreviations: ot: optic tectum; ov: otic vesicle; mb: midbrain; hb: hindbrain; nm: neuromasts*

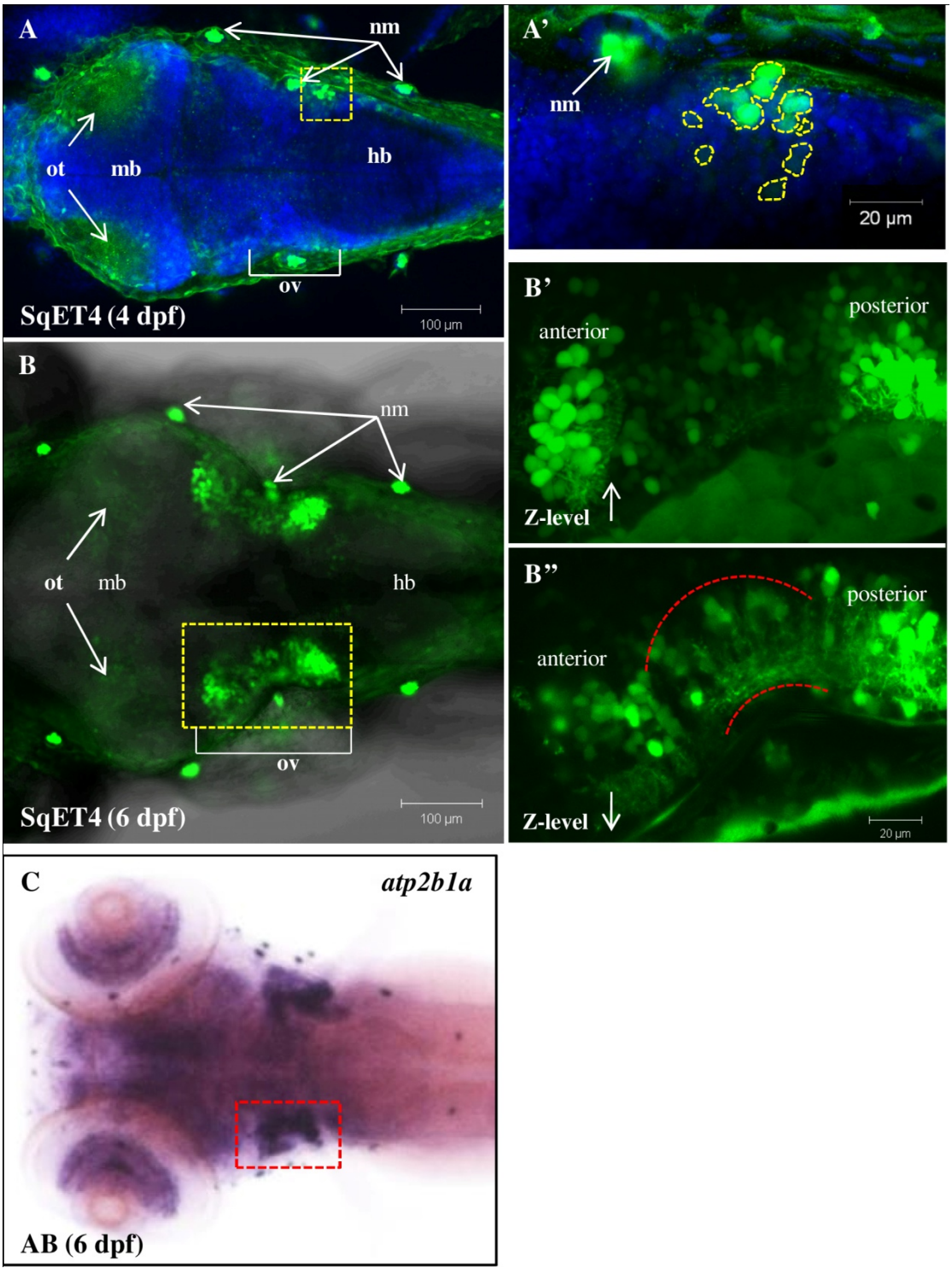
A
nm
ot
mb
hb
ov
SqET4 (4 dpf)
100 µm
A'
nm
20 µm
B'
anterior
posterior
Z-level
B
nm
ot
mb
hb
ov
SqET4 (6 dpf)
100 µm
B''
posterior
anterior
Z-level
20 µm
C
atp2b1a
AB (6 dpf)

CHAPTER 4

Discussion

4.1 *atp2b1a* in mechanosensory hair cells

SqET4 transgenics (Parinov et al., 2004) has grown to be a popular *in vivo* tool for studying the development and regeneration of sensory mechanosensory hair cells in the lateral line, including the evolution of mechanoreception, planar cell polarity, the terminal division of a transient hair cell progenitor, and hair cell regeneration (Faucherre et al., 2009; Feijoo et al., 2009; Froehlicher et al., 2009; Gleason et al., 2009; Hernandez et al., 2007; Lopez-Schier and Hudspeth, 2006; Nagiel et al., 2008; Nechiporuk and Raible, 2008; Sarrazin et al., 2006). As such, it became increasingly necessary to link the GFP expression pattern in this transgenic line with a particular molecular developmental mechanism. The proximity of the SqET4 insertion site and *atp2b1a*, along with the similarity of the *gfp* and *atp2b1a* expression patterns, suggested that SqET4 represents the Tg:*atp2b1a*-GFP line. By linking this marker with *atp2b1a*, we have demonstrated that the function of *atp2b1a* might be linked to some of the aforementioned events. Furthermore, this finding has linked SqET4 with the regulation of intracellular Ca^{2+}, a fundamental process of cell division, differentiation and physiology. The functional analysis of the zebrafish Atp2b1a has revealed its role in several aspects of mechanosensory hair cell development and physiology. Amongst these, hair cell proliferation and regeneration are of particular interest due to its established connection to deafness, which affects a large proportion of the human population.

One of the four mammalian *Atp2b* genes, *Atp2b2*, has been linked to deafness and ataxia (Ficarella et al., 2007; reviewed in Hughes et al., 2006; Tempel and Schilling, 2007). In mammals, *Atp2b1* is broadly expressed, and mutant embryos are embryonic lethal (Okunade et al., 2004). The duplication of this gene in teleosts, along with differences in embryogenesis and experimental approaches in mice and zebrafish, could have helped to contribute to the

implication of the second gene of this family, *atp2b1a*, in the development of sensory hair cells, and thus alluding to the role of Ca^{2+} signaling in this process. Early EST-based expression analyses demonstrated the presence of *atp2b1a* transcripts in mechanosensory cells in the lateral line, optic tectum, otic vesicle and somites (Rauch et al., 2003; Thisse et al., 2001; Thisse and Thisse, 2004). Based on the effect of the PMCA inhibitor, 5(6)-carboxyeosin, *atp2b1a* seems to be the only PMCA that is active in PLLP and primary neuromasts; this illustrates the involvement of different PMCAs in evolutionarily divergent fish and mice. For this hypothesis to be validated, further study of the activity of other members of the PMCA family in zebrafish is warranted.

Ca^{2+} ions at physiological, intracellular concentrations (10 -100 nM) regulate various aspects of cell physiology in a concentration-dependent manner, such as cell division and differentiation at low concentrations, and the inhibition of cell differentiation and even cell death at high concentrations (Kawano et al., 2006; Ntambu and Takova, 1996; reviewed in Florea and Busselberg, 2009; Slusarski and Pelegri, 2007). Based on preliminary results, apoptosis was put forward to explain the reduction of hair cells due to Atp2b1a deficiency (Cruz et al., 2009). This view is in conflict with our data showing that upon depletion of Atp2b1a the committed hair cells precursors fail to divide. Furthermore, even the weakly GFP-positive transient precursors failed to form (Fig. 13), suggesting that in the absence of Atp2b1a activity the process of hair cell differentiation stops prior to the formation of transient precursors of hair cells. Indeed, since Atp2b1a functions to export Ca^{2+} (Wanaverbecq et al., 2003; reviewed in Brini, 2009), its deficiency should induce an increase in intracellular Ca^{2+}, and lead to differentiation failure. Our experiments revealed that the knockdown of *atp2b1a* increased intracellular Ca^{2+} levels of hair cells (Fig. 14, 16), in parallel with a block in hair cell precursor division (Fig. 12,13), an increase

in *atoh1a/sox2/tacstd*-positive cells and disorganization of the support cells cluster (Fig. 18b). Mis-regulation of Ca^{2+} in differentiating hair cells has resulted in phenotypic lack of secondary structures such as stereocilia and kinocilia (Fig. 15), which are required for transducing sound waves and motion into electrical signals for the sense of hearing. Stereocilia length could be directly impacted by Ca^{2+}-dependent actin-myosin interactions in the stereocilia (Glenney et al., 1981; Oertner et al., 2005; Fettiplace et al., 2006; Grati et al., 2006; reviewed in Manor and Kachar., 2008).

In the inner ear, the same observation was made: an accumulation of *atoh1a*-positive cells in the saccular macula (Fig. 18K), which primary function is hearing (Riley and Moorman, 2000). This observation, coupled with the fact that 68.5% of morphant embryos were classified as deaf (Fig. 16), strongly suggests that Atp2b1a is required for development of auditory function. This implies that Atp2b1a plays a role in differentiation of hair cells in zebrafish, similar to Atp2b2 in the inner ear of mammals (Ficarella et al., 2007; Hughes et al., 2006; Tempel and Schilling 2007). These findings validate the use of this transgenic line as a model to assess the involvement of Ca^{2+} signaling in hearing-related disorders.

During neurogenesis in the fly CNS and the cortex of mammals, and during hair cell development in zebrafish, the transient precursors give rise to two differentiating neural cells in a process regulated by *ato/atoh1* (Bossing et al., 1996; Kriegstein and Alvarez-Buylla, 2009; Lopez-Schier and Hudspeth, 2006; Schmid et al., 1999; our results - Fig. 18L). In contrast, in the mice inner ear, the transient precursors of hair cells are currently not defined, although the intermediate “differentiating” hair cells have been recognized (Kelley, 2006). Thus, in the inner ear of *Atoh (Math1)*-null mice, only mechanosensory hair cells are believed to be absent (Bermingham et al., 1999; reviewed in Bertrand et al., 2002). This may be because the

intermediate precursor of hair cells remains elusive in this model species.

Overall, our results have demonstrated that the knockdown of Atp2b1a affected export of Ca^{2+} and blocked hair cell differentiation prior to formation of the transient precursors of hair cells. Thus, formation of this cell type depends upon Atp2b1a regulation of intracellular Ca^{2+}. At the same time this developmental process negatively regulates a number of support cells and Atoh1a-positive committed precursors. At first, this may sound paradoxical unless one considers that during normal development a pool of support cells is continuously depleted by the elimination of cells giving rise to transient precursors and eventually to hair cells. Thus, when this process is incomplete, the earlier types of precursors accumulate. It is not clear at the moment whether the differentiated hair cells actively control proliferation of the support cells in a negative feedback loop that may involve Notch signaling (Itoh and Chitnis, 2001; Li et al., 2010; Kelley et al., 2006).

We observed that *atp2b1a* expression was induced in regenerating hair cells (Fig. 20). This observation is consistent with that of Ma and Raible, 2009, reporting a marked elevation of *atoh1a* expression in the first 24 h after neomycin treatment. During hair cell development, Atoh1a acts in an epistatic manner upstream of Atp2b1a, similar to that which is observed during regeneration of these cells. So, it seems that a functional link of these two genes represents an important part of a universal, developmental program that is responsible for formation of hair cells in various situations.

Previous studies have noticed that, despite the progress in understanding the various transient states through which differentiating cells pass on the way to becoming mechanosensory hair cells, an understanding and discovery of corresponding *in vivo* markers has lagged behind

(Ghysen and Dambly-Chaudiere, 2007). Our work closed this gap at two important nodes: (1) by characterizing a function of Atp2b1a we not only linked it with SqET4 at the level of transient committed hair cell precursors. Importantly, these results illustrated a role of Atp2b1a in regulation of export of intracellular Ca^{2+}during differentiation of mechanosensory hair cells (Fig. 38). (2) The characterization of the SqET33-mi60a transgenic line presented a possibility to monitor *in vivo* not only the final phase of differentiation of mechanosensory hair cells, but to record much earlier events taking place at the level of support cells.

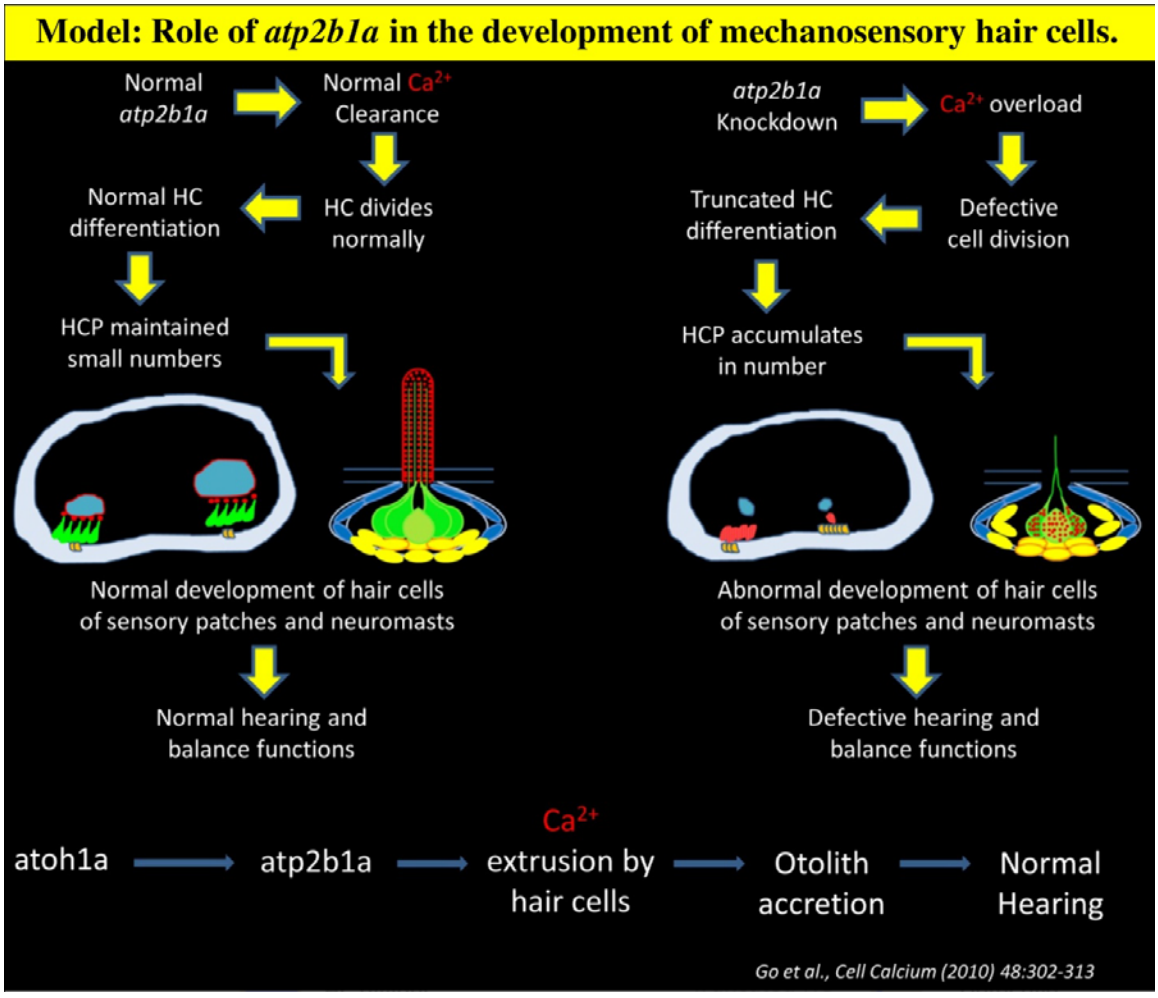

Figure 37: A model for *atp2b1a*'s role in the development of mechanosensory hair cells.

4.2 *atp2b1a* in Ultimobranchial body (UB)

The function of calcitonin-producing cells (C-cells) in zebrafish has never before been experimentally dealt with largely due to a shortage of useful genetic markers. This study represents a first attempt to fill this gap. We began the study of *atp2b1a* role in the UB by characterizing the GFP expression in the UB of SqET4, which starts as early as 55 hpf (Fig. 22), whereas WISH detects *atp2b1a* transcripts in the UB from 72 hpf (Fig. 21). Thus expression of GFP reveals an activity of the regulatory machinery behind expression of *atp2b1a* almost one day earlier than mRNA could be detected by WISH. This may be due to a relatively low level of *atp2b1a* transcripts in the UB. Such observation is important since *calca* encoding the calcitonin polypeptide alpha (CT) is a known definitive marker of C-cells in zebrafish (Alt et al., 2006). Its transcript expression could be detected from 60 hpf, or slightly after GFP expression in the same region making this transgenic line a sensitive tool for detection of events related to activity of Atp2b1a. Immuno-co-localization of CT with SqET4 in UB has reinforced this idea (Fig. 21).

High-resolution imaging of UB demonstrated that it consists of secretory cells assembled as distinct clusters with characteristic inner lumen occupied by a Ca^{2+}-rich pharyngeal tooth (PD; Fig. 23). This suggests a direct involvement of UB in calcification of PD mediated by Atp2b1a. In mammals, Ca^{2+}-ATPase was histochemically detected in cells forming teeth - ameloblasts and odontoblasts (Borke et al., 1993; 1995). This suggests that a role of Atp2b1a in formation of PD is evolutionary conserved. Atp2b1a could perform a binary function in PD formation. First, by exporting Ca^{2+} Atp2b1a supplies an essential component of calcification and, second, acting as phosphatase in hydrolysis of ATP, it provides Pi for tissue mineralization (Nakano et al., 2007).

Atp2b1a may regulate the formation and function of UB at several levels. First, this enzyme seems to be involved in regulation of formation of UB similar to that in neuromasts of the lateral line and sensory patches of the inner ear, where it was shown to act during formation and division of the terminal progenitor of mechanosensory cells. Second, retention of Ca^{2+} in *atp2b1a*-expressing morphant cells indicates a deficiency of Ca^{2+} export in target tissues (Go et al., 2010).

A perturbation of Atp2b1a function results in Ca^{2+} retention inside UB cells of morphant as well as PMCA inhibitor-treated larvae (Fig. 23). Supporting data obtained from the osteoblasts reporter line Tg*(osx-mCherry),* reveals that an early calcification of pharyngeal teeth takes place in the absence of function of osterix-positive odontoblasts. These cells were not detected in PD at 4.0 dpf stage, but were present after 5.5 dpf, when they associate closely but do not overlap with UB (Fig. 27). We show that calcification of PD has commenced between 3.5 to 4.0 dpf (Fig. 25). Therefore, a transition between the odontoblast-independent phase of calcification to the odontoblast-dependent phase of this process could therefore occur already after initiation of calcification and, perhaps, under its influence. This morphogenetic switch taking place between 4.0 to 4.5 dpf possibly signifies the beginning of enameloid mineralization, which in zebrafish is relatively short (Isokawa et al., 1970; Inoue et al., 1973; Van der Heyden et al., 2000). Taken together the presented evidence strongly suggests that an early odontoblast-independent phase of calcification starts in sites associated with UB.

In the *atp2b1a* morphants calcification was affected also in other anterior bones without sites of Atp2b1a expression in close vicinity such as operculum, where appearance of osterix-positive osteoblasts was affected (Fig. 28). Mouse osteoblasts are known to express E-cadherin. This renders these cells to be responsive to extra-cellular Ca^{2+} providing means for cell adhesion

(Babich et al., 48). It is likely that osterix-positive osteoblasts in operculum require adequate levels of extra-cellular Ca^{2+} to maintain integrity, cell adhesion and signalling through cadherin-mediated interactions during formation of this bone. This also suggests that UB had a long-range effect on calcification. Two plausible explanations should be discussed here. First, UB may provide enough Ca^{2+} to support bone calcification at a distance due to Ca^{2+} diffusion along a concentration gradient or by active cellular transport (Martin 1994). Since UB is not vascularized at least until 7 dpf this process seems to be independent of vascular circulation (Fig. 23). Second, UB secretes two hormones regulating Ca^{2+} metabolism - CT and calcitonin-gene related peptide (CGRP) (Grunditz et al., 1986). CT acts via its receptor CTR present in bones, whereas CGRP could act on carbonic anhydrase to regulate mineralization (Cudennec et al., 2006; Lafont et al., 2010). Not surprisingly the level of *calca* transcripts and CGRP was sharply reduced in the *atp2b1a* morphant (Fig. 29 & 30). The knockdown of *calca* caused no effect on the levels of *atp2b1a* in UB (Fig. 24) suggesting that *atp2b1a* acts upstream of *calca*. Thus, a failure of UB formation in morphants would account for deficiency of calcitonin and CGRP transcripts.

To gain information on possible transcriptional regulation of *atp2b1a* in UB, an analysis of a related bHLH transcription factor, Mash1 was considered as another candidate due to its involvement in C-cells development in mouse (Kameda et al., 2007). In zebrafish Mash1 is represented by the two related genes *ascl1a* and *ascl1b*. Based on the analysis of these morphants, it seems that these genes share a responsibility for regulation of *atp2b1a* in UB. Evidently, supplementing either *ascl1a* or *ascl1b* morphants with *atp2b1a* mRNA was unable to rescue both phenotypes in UB (Fig. 24).

To obtain better resolution on the analysis of molecular markers of pharyngeal teeth, only pharynges containing EGFP-marked UB (isolated from SqET4 larvae) was analysed (Fig. 29).

Dlx2b is a transcription factor required for normal morphogenesis of pharyngeal teeth of zebrafish (Jackman and Stock 2006). *Dlx2b* transcript level increased by two-folds in *atp2b1a* morphants, suggests a feedback mechanism to compensate the loss of Atp2b1a activity. Fgf signalling pathway has been shown to act upstream of teleost *dlx2b* in oral and pharyngeal teeth (Jackman et al., 2004). It would be interesting to see if such feedback regulation involves Fgf signalling components to promote activation of Fgf-responsive Ca^{2+} channels such as those observed in neonatal rat cardiomyocytes (Merle et al., 1995) and *Xenopus* nervous system (Lee et al., 2009). In contrast, the structural genes of PD (*connexin 43* and *integrin αV subunit*) were down-regulated (five-folds and one-fold, respectively). This was expected due to a collapse of structural integrity of UB in morphants (Fig. 23).

PMCA being a highly specific outwardly directed transporter for Ca^{2+} has been suggested to play a key role in bone mineralization (Carafoli 1991; Abramowitz and Suki 1996). Three isoforms of PMCA have been found in osteoblastic cells, primarily PMCA1, but also PMCA2 and PMCA4 (Nakano et al., 2007; Stains et al., 2002). Whereas a function of PMCA1 in mammals was confirmed during mineralization of osteoblasts in culture (Nakano et al., 2007), it was not shown whether it functions in the same way during bone development *in vivo*. There are a few factors to be considered here. *Atp2b1a* is neither expressed in bone primordia, nor is EGFP in SqET4 expressed in a manner suggesting a direct role of this Ca^{2+} pump in osteoblasts during bone formation. *Atp2b1a* is expressed in somites, suggesting an early role of Atp2b1a in providing Ca^{2+} where it could be required for bone matrix mineralization by osteoblasts differentiated from sclerotome-derived progenitor cells (Inohaya et al., 2007). In the present study, our analysis was restricted to more anterior regions, where somites are not present. Here Atp2b1a seems to be involved in bone formation indirectly by exporting Ca^{2+} from UB, which

expresses this Ca^{2+} pump, and, in addition, via production of calcitonin. The latter is known to regulate Ca^{2+} levels having strong hypocalcaemic effect in blood. This could be achieved, for example, by stimulation of recruitment of Ca^{2+} from blood and other body fluids into bones and other Ca^{2+} deposits, including otoliths that are deficient in *atp2b1a* morphants (Cruz et al., 2009; Go et al., 2010).

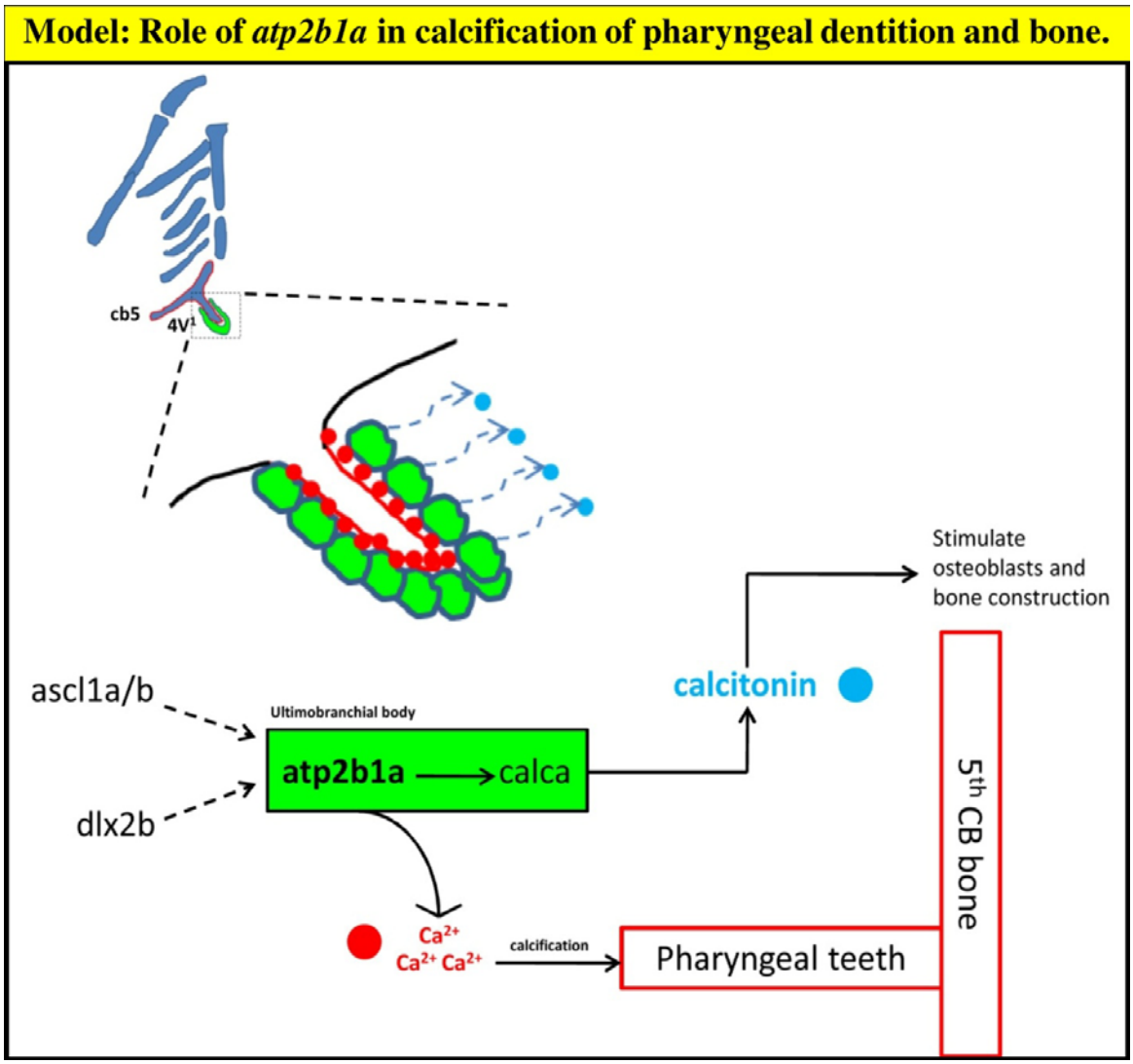

Figure 39: A model for *atp2b1a*'s role in facilitating calcification of pharyngeal dentition and other bones.

CHAPTER 5

Conclusions

"Remember the person who, when he was asked why he was working so hard on something that would come to the attention of scarcely anyone: I will be satisfied with a few, he answered, I will be satisfied with one, I will be satisfied with no one."

Michel de Montaigne, Essais, Livre I, Chap. XXXVIII

CONCLUSIONS

In zebrafish, the mechanosensory cells and the ultimobranchial bodies (UB) are two cell lineages where outwardly extrusion of Ca^{2+} ions mediated by the plasma membrane Ca^{2+} pump, Atp2b1a was found to be required for their respective development and functioning. A "see-saw" relationship between intracellular and extracellular Ca^{2+} mediated by this ATP-driven Ca^{2+} exporter was observed in both situations; where too much inside and too little outside can created their own class of problems.

In mechanosensory cells, Atp2b1a was found to be an important regulator of intracellular Ca^{2+} level. Atp2b1a actively maintains a purposefully low intracellular Ca^{2+} level to ensure that it remains sensitive to its sensory triggers. Disruption to its Ca^{2+} homeostatic state first halted a progression of mechanosensory cells differentiation from its transient precursor state to a terminally differentiated state. This eventually left the inner ear and neuromasts with subnormal numbers of mechanosensory cell. And the phenotype subsequently propagated to a level where severe consequence in auditory and vestibular development resulted.

Atp2b1a's parallel function is to pump Ca^{2+} ions outwards and Ca^{2+} ions could then travels to its target tissues by diffusion. We have determined that this function of Atp2b1a is necessary to facilitate calcification of several developing bones, where a constant supply of raw materials for bone matrix development is essential. We have identified *atp2b1a* to be expressed in UB, and elucidated a role of Atp2b1a in mediating direct calcification of pharyngeal dentitions (PDs). And in hindsight, we may be the first to provide evidence to show that calcification of PDs could be regulated by UB in zebrafish. We have also realized Atp2b1a could in parallel mediate other long-range calcification events of distantly located bones by regulating the levels

of two bone-promoting endocrine hormones, calcitonin and related CGRP peptide. This study is of interest both for demonstrating a role for at least one PMCA in biomineralization and characterizing ultimobranchial body anatomy and function. We are at a beginning of understanding the regulatory network that maintains Ca^{2+} homeostasis of a developing vertebrate. Zebrafish does not develop oral dentitions but nevertheless retained its ability to form pharyngeal dentitions like many cypriniforms. This work validates efforts of several laboratories aiming to establish zebrafish as a model to study biomineralization of dentitions, etc. (Borday-Birraux et al., 2006; Jackman and Stock, 2006; Stock et al., 2006; Stock, 2007Pasco-Viel et al., 2010).

In this work I have extensively employed antisense morpholino technology to knockdown genes of interest due to the absence of mutants. Unlike the situation in mice, being able to analyze the gene's phenotype from a non-lethal morphant clearly is an advantage. In the case of a classical developmental mutant where a gene's function is completely abrogated, and the observed phenotype is usually attributed to the knockout of the gene, such genetic analysis can provide straightforward answers. With the recent availability of targeted mutagenesis technologies mediated by "Zinc Finger Nuclease (ZFN)" or plant pathogens derived "Transciption Activator-like Effector Nucleases (TALEN)", could be used to generate "null mutants" of Atp2b1a, so as to generate more understanding on the gene's function. And that could be a valid future direction. But in retrospect, I would still have made use of morpholino knockdown technology even if a mutant for Atp2b1a will become available at some point in future, since morpholino-mediated knockdown provides additional levels of analysis by being able to restrict morpholino's presence in both spatial and temporal terms.

Another possibility is to verify a co-regulation pathway for the models presented in this thesis, i.e. otoconial and bone development. Both developmental processes have been shown to involve similar sets of processes (reviewed by Hughes et al., 2006) and shown here in this thesis to require the same Ca^{2+} pump. Like bones, otoconia are complex calcium carbonate ($CaCO_3$) biominerals in the utricle and saccule of the vertebrate inner ear that requires local increase of Ca^{2+} to facilitate mineralization. These "ear stones" are required for normal balance and the sensation of linear acceleration (gravity). In mammals, the majority of otoconia is generated only in the embryonic ear and must be maintained throughout life. Ectopic otoconia found in semicircular canal of the ear may cause abnormal sensations of dizziness and loss of balance, a condition referred to as Benign Positional Vertigo (BPV). And like mammals, teleost have otoconial-like structures more commonly known as otoliths and they continue to grow throughout the life of the fish, with daily accretion of layers of extracellular matrix proteins and deposited $CaCO_3$. Yaoi and colleagues (2003) have proposed a regulatory relationship between calcitonin and otoconin 22; a major core protein of otoconia. To support this idea, we have identified *calca* (the gene encoding for calcitonin peptide) to have expression in the same set of mechanosensory cells within the inner ear (data not shown). Since *atp2b1a* is also required to regulate *calca* level in UB for bone development, the same relation may perhaps hold true in otolith formation.

REFERENCES

Ablooglu A.J., Kang J., Handin R.I., Traver D., Shattil S.J.. The zebrafish vitronectin receptor: characterization of integrin aV and B3 expression patterns in early vertebrate development. *Dev. Dyn*. **236** (2007):2268-2276.

Abramowitz J., Gonzalez J.M., Rouse D., Suki W.N., Differential expression of plasma membrane calcium pump mRNA isoforms in rat-osteoblast-like cells. *Miner. Electrolyte Metab.* **21** (1995):367-374.

Abramowitz J., Suki W.N., Ca^{2+}-ATPase and bone cell mineralization. *Miner. Electrolyte Metab.* **22** (1996):336-344.

Alt B., Reibe S., Feitosa N.M., Elsalini O.A., Wendl T., Rohr K.B., Analysis of origin and growth of the thyroid gland in zebrafish. *Dev. Dyn.* **235** (2006):1872-1883.

Amoyel M., Cheng Y.C., Jiang Y.J., Wilkinson D.G., Wnt1 regulates neurogenesis and mediates lateral inhibition of boundary cell specification in the zebrafish hindbrain. *Development* **132** (2004):775-785.

Balak K.J., Corwin J.T., Jones J.E., Regenerated hair cells can originate from supporting cell progeny: evidence from phototoxicity and laser ablation experiments in the lateral line system, *J. Neurosci.* **10** (1990)**:**2502–2512.

Barbiero G., Munaron L., Antoniotti S., Baccino F.M., Bonelli G., Lovisolo D., Role of mitogen-induced calcium influx in the control of the cell cycle in Balb-c 3T3 fibroblasts, *Cell Calcium* **18** (1995):542-56.

Berridge M., OFF Mechanisms. In: Cell Signaling Biology (2009). Portland Press Limited.

Behra M., Bradsher J., Sougrat R., Gallardo V., Allende M. L., Burgess S. M., Phoenix is required for hair cell regeneration, *PLoS Genetics* **5** (2009):1-14.

Bejarano G., Phesant M., Makunin I., Stephen S., Kent W.J., Mattick J.S., Haussler D., Ultraconserved elements in the human genome, *Science* **304** (2004):1321-1325.

Bermingham-McDonogh O., Rubel E.W., Hair cell regeneration: winging our way towards a sound future, *Curr. Opin. Neurobiol.* **13** (2003):119–126.

Bermingham N.A., Hassan B.A., Price S.D. et al., Math1: an essential gene for the generation of inner ear hair cells, *Science* **284** (1999):1837-41.

Bertrand N., Castro D.S., Guillemot F., Proneural genes and the specification of neural cell types, *Nat. Rev. Neurosci*. **3** (2002):517-30.

Bourque C. and Honvras Y., Hooked on zebrafish: Insights into development and cancer of endocrine tissues. Endocr. Relat. Cancer **18** (2011): R149-R164.

Borday-Birraux V., Van der Heyden C., Debias-Thibaud M., Verreijdt L., Stock D.W., et al., Expression of Dlx genes during the development of the zebrafish pharyngeal dentitions: evolutionary implications. Evol. Dev. **8** (2006):130-141.

Borke J.L., Zaki A. el-M., Eisenmann D.R., Mednieks M.I., Localization of plasma membrane Ca^{2+} pump mRNA and protein in human ameloblasts by in situ hybridization and immunohistochemistry. *Connect Tissue Res.* **33** (1995):139-144.

Borke J.L., Zaki A.E., Eisenmann D.R., Ashrafi S.H., Ashrafi S.S. Penniston J.T., Expression of plasma membrane Ca^{2+} pump epitopes parallels the progression of enamel and dentin mineralization in rat incisor. *J. Histochem. Cytochem*. **41** (1993):175.

Bossing T., Udolph G., Doe C.Q., Technau G.M. The embryonic central nervous system lineages of *Drosophila melanogaster*. I. Neuroblast lineages derived from the ventral half of the neuroectoderm, *Dev. Biol.* **179** (1996):41-64.

Brini M., Plasma membrane Ca^{2+}-ATPase: from a housekeeping function to a versatile signaling role, *Pflugers Arch - Eur. J. Physiol.* **457** (2009):657-664.

Brini M., Leva F.D., Domi T., Fedrizzi L., Lim D., Carafoli E., Plasma-membrane calcium pumps and hereditary deafness, *Biochem. Soc. Trans.* **35** (2007)**:**913–918.

Carafoli E., The calcium pumping ATPase of the plasma membrane. *Annu. Rev. Physiol*. **53** (1991):531-547.

Choo B.G.H., Kondrichin I., Parinov S. et al.**,** Zebrafish transgenic Enhancer TRAP line database (ZETRAP), *BMC Dev. Biol.* **6** (2006):5.

Clark M.S., Bendell L., Power D.M., Warner S., Elgar G., Ingleton P.M., Calcitonin: characterisation and expression in a teleost fish, Fugu rubripes. *J. Mol. Endocrinol*. **28** (2002):111–123.

Coffin A.B., Owens K.N., Raible D.W., and Rubel E.W., Extracellular divalent cations modulate aminoglycoside-induced hair cell death in the zebrafish lateral line, *Hear. Res.* **253** (2009):42-51.

Cotanche D.A., Regeneration of the tectorial membrane in the chick cochlea following severe acoustic trauma, *Hear. Res.* **30** (1987):197–206.

Cotanche D.A., Henson M.M., Henson O.W. Jr., Contractile proteins in the hyaline cells of the chicken cochlea, *J. Comp. Neurol.* **324** (1992):353–364.

Cruz S., Shiao J.C., Liao B.K., Huang C.J., Hwang P.P., Plasma membrane calcium ATPase required for semicircular canal formation and otolith growth in the zebrafish inner ear, *J. Exp. Biol.* **212** (2009):639-47.

Cudennec B., Rousseau M., Lopez E., Fouchereau-Peron M., CGRP stimulates gill carbonic anhydrase activity in molluscs via a common CT/CGRP receptor. *Peptides* **27** (2006):2678-2682.

David S., Gerhard H., Walter G., The fates of the blastomeres of the 16-cell zebrafish embryo, *Development* **120** (1994):1791-1798.

De Felice M. and Di Lauro R., Thyroid development and its disorders: genetics and molecular mechanisms. *Endo. Rev.* **25** (2004):722-746.

Epstein J.E. and Cotanche D.A., Secretion of a new basal layer of tectorial membrane following gentamicin-induced hair cell loss, *Hear. Res.* **90** (1995):31–43.

Faucherre A., Pujol-Martı J., Kawakami K., Lopez-Schier H., Afferent Neurons of the Zebrafish Lateral Line Are Strict Selectors of Hair-Cell Orientation, *PLoS ONE* **4** (2009):e4477.

Feijóo C.G., Saldias M.P., De la Paz J.F., Gómez-Skarmeta J.L., Allende, M.L., Formation of posterior cranial placode derivatives requires the Iroquois transcription factor irx4a, *Mol. Cell. Neurosci.* **40** (2009):328-337.

Fettiplace R., Hackney C.M., The sensory and motor roles of auditory hair cells, *Nat. Rev. Neurosci.* **7** (2006):19–29.

Ficarella R., Di Leva F., Bortolozzi M., Ortolano S., Donaudy F., Petrillo M., Melchionda S., Lelli A., Domi T., Fedrizzi L., Lim D., Shull G.E., Gasparini P., Brini M., Mammano F., Carafoli E., A functional study of plasma-membrane calcium-pump isoform 2 mutants causing digenic deafness. *Proc. Natl. Acad. Sci. USA.***104** (2007):1516–1521.

Florea A-M., Busselberg D., Anti-cancer drugs interfere with intracellular calcium signaling, *Neurotoxicology.* **30** (2009):803-10.

Fong S.H., Emelyanov A., Teh C., Korzh V., Wnt signalling mediated by Tbx2b regulates cell migration during formation of the neural plate, *Development* **132** (2005):3587-3596.

Froehlicher M., Liedtke A., Groh K. et al., Estrogen receptor subtype beta2 is involved in neuromast development in zebrafish (Danio rerio) larvae, *Dev. Biol.* **330** (2009) 32-43.

Gilbert S.F., Developmental biology. Sunderland, MA: Sinauer Associates, Inc. (2003):749 p.

Ghysen A., and Dambly-Chaudière C., The lateral line microcosmos, *Genes Dev.* **21** (2007):2118-2130.

Gleason M.R., Nagiel A., Jamet S., Vologodskaia M., López-Schier H., Hudspeth A.J., The transmembrane inner ear (Tmie) protein is essential for normal hearing and balance in the zebrafish, *Proc. Natl. Acad. Sci. USA.* **106** (2009):21347-21352.

Glenney J.R. Jr, Kaulfus P., Matsudaira P., Weber K., F-actin binding and bundling properties of fimbrin, a major cytoskeletal protein of microvillus core filaments, *J. Biol. Chem.* **256** (1981):9283–9288.

Go W., Bessarab D., Korzh V., Atp2b1a regulates Ca^{2+} export during differentiation and regeneration of mechanosensory hair cells of zebrafish. *Cell Calcium* **48** (2010):302-313.

Grati M., Schneider M. E., Lipkow K., Strehler E. E., Wenthold R. J., Kachar B., Rapid turnover of stereocilia membrane proteins: evidence from the trafficking and mobility of plasma membrane Ca^{2+}-ATPase 2, *J Neurosci.* **26** (2006):6386–6395.

Grunditz T, Ekman R, Håkanson R, Rerup C, Sundler F, Uddman R., Calcitonin gene-related peptide in thyroid nerve fibers and C cells: effects on thyroid hormone secretion and response to hypercalcemia. *Endocrinol*.**119** (1986):2313-2324.

Harris J.A., Cheng A.G., Cunningham L.L., MacDonald G., Raible D.W., Rubel E.W., Neomycin-induced hair cell death and rapid regeneration in the lateral line of zebrafish (Danio rerio), *J. Assoc. Res. Otolaryngol.* **4** (2003):219–234.

Hernandez P.P., Moreno V., Olivari F.A., Allende M.L., Sub-lethal concentrations of waterborne copper are toxic to lateral line neuromasts in zebrafish (Danio rerio), *Hear. Res.* **213** (2006):1-10.

Hernandez P.P., Olivari F.A., Sarrazin A.F., Sandoval P.C., Allende M.L., Regeneration in zebrafish lateral line neuromasts: Expression of the neural progenitor cell marker sox2 and proliferation-dependent and-independent mechanisms of hair cell renewal, *Dev. Neurobiol.* **67** (2007):637-654.

Hughes I., Thalmann I., Thalmann R., Ornitz D.M., Mixing model systems: using zebrafish and mouse inner ear mutants and other organ systems to unravel the mystery of otoconial development. *Brain Res.* **109** (2006):58-74.

Husain M., Jiang L., See V., et al., Regulation of vascular smooth muscle cell proliferation by plasma membrane Ca^{2+}-ATPase. *Am. J. Physiol.* **272** (1997):C1947-59.

Inoue D. and Wittbrodt J.. One for all – A highly efficient and versatile method for fluorescent immunostaining in fish embryos, *PLoS ONE* **6** (2011):e19713.

Inoue Y., Uchino S., Asano T., Hasegawa S., Fujioka Y., The mineralization pattern of developing fish tooth enameloid using X-ray probe microanalyzer, historadiography and radioactive tracer (45Ca). *J. Nihon Univ. Sch. Dent.* **15** (1973):52–57.

Isogai S., Horiguchi M., Weinstein B.M., The vascular anatomy of the developing zebrafish: an atlas of embryonic and early larval development. *Dev. Biol.* **230** (2001):278-301.

Isokawa S., Tsuboushi M., Aoki K., Imai M., Kawai A., Tsuchida S., Studies on the developing enameloid of a fish (*Hoplognathus fasciatus*). I. Mineralization pattern of enameloid matrix. *J. Nihon Univ. Sch. Dent.* **12** (1970):43–49.

Itoh M. and Chitnis A.B., Expression of proneural and neurogenic genes in the zebrafish lateral line primordium correlates with selection of hair cell fate in neuromasts, *Mech. Dev.* **102** (2001):263-266.

Jackman W.R, Stock D.W., Transgenic analysis of Dlx regulation in fish tooth development reveals evolutionary retention of enhancer function despite organ loss. *Proc. Natl. Acad. Sci. U.S.A.* **103** (2006):19390-19395.

Kameda Y., Nishimaki T., Miura M., Jiang S.X., Guillemot F., *Mash1* regulates the development of C Cells in mouse thyroid glands. *Dev. Dyn.* **236** (2007):262-270.

Kawano S., Otsu K., Kuruma A. et al., ATP autocrine/paracrine signaling induces calcium oscillations and NFAT activation in human mesenchymal stem cells. *Cell Calcium.* **39** (2006):313-24.

Keeton T.P., Burk S.E., Shull G.E., Alternative splicing of exons encoding the calmodulin-binding domains and C termini of plasma membrane Ca^{2+}-ATPase isoforms 1, 2, 3, and 4. *J. Biol. Chem.* **268** (1993):2740-2748.

Kimmel C.B., Ballard W.W., Kimmel S.R., Ullmann B., Schilling T.F., Stages of embryonic development of the zebrafish, *Dev. Dynam.* **203** (1995):253–310.

Kimmel C.B., DeLaurier A., Ullmann B., Dowd J., McFadden M., Modes of developmental outgrowth and shaping of a craniofacial bone in zebrafish. *PLoS One* **5** (2010):e9475.

Kondrychyn I., Garcia-Lecea M., Emelyanov A., Parinov S., Korzh V., Genome-wide analysis of *Tol2* transposon reintegration in zebrafish, *BMC Genomics.* **10** (2009):418.

Korzh V., Transposons as tools for enhancer-trap screens in vertebrates, *Genome Biol.* **8** (2007): Suppl. 1:S8.

Korzh V., Sleptsova-Friedrich I Liao J, He J, Gong Z, Expression of zebrafish bHLH genes ngn1 and nrD define distinct stages of neural differentiation, *Dev. Dynam.* **213** (1998):92-104.

Kozel P.J., Friedman R.A., Erway L.C., Yamoah E.N., Liu L.H., Riddle T., Duffy J.J., Doetschman T., Miller M.L., Cardell E.L., Shull G.E., Balance and hearing deficits in mice with a null mutation in the gene encoding plasma membrane Ca^{2+}-ATPase isoform 2. *J. Biol. Chem.* **273** (1998):18693–18696.

Kriegstein A., Alvarez-Buylla A.,The glial nature of embryonic and adult neural stem cells, *Annu. Rev. Neurosci.* **32** (2009):149-84.

Kurnellas M.P., Nicot A., Shull G.E., Elkabes S., Plasma membrane calcium ATPase deficiency causes neuronal pathology in the spinal cord: a potential mechanism for neurodegeneration in multiple sclerosis and spinal cord injury, *The FASEB J.* **19** (2005):298-300.

Lafont A.G., Wang Y.F., Chen G.D., Liao B.K., Tseng Y.C., Huang C.J. and Hwang P.P., Involvement of calcitonin and its receptor in the control of calcium regulating-genes and calcium homeostasis in zebrafish (*Danio rerio*). *J. Bone Miner. Res*. **26** (2010):1072-1083.

Lafont A.G., Dufour S., Fouchereau-Peron M., Evolution of the CT/CGRP familia comparative study with new data from models of teleosts, the eel, and cephalopod molluscs, the cuttlefish and the nautilus. *Gen. Comp. Endocrinol*. **153** (2007):155-169.

Lecaudey V., Cakan-Akdogan G., Norton W.H.J., Gilmour D., Dynamic Fgf signaling couples morphogenesis and migration in the zebrafish lateral line primordium, *Development.* **135** (2008): 2695-2705.

Le Douarin N., Fontaine J., Le Lievre C., New studies on the neural crest origin of the avian ultimobranchial glandular cells—interspecific combinations and cytochemical characterization of C cells based on the uptake of biogenic amine precursors. *Histochem.* **38** (1974):297–305.

Le Lievre C.S., Le Douarin N.M., Mesenchymal derivatives of the neural crest: analysis of chimaeric quail and chick embryos. *J. Embryol. Exp. Morphol.* **34** (1975):125–154.

Liao B.K., Deng A.N., Chen S.C., Chou M.Y., Hwang P.P., Expression and water calcium dependence of calcium transporter isoforms in zebrafish gill mitochondrion-rich cells, *BMC Genomics.* **8** (2007):354.

Lipskaia L. and Lompré A.M., Alteration in temporal kinetics of Ca^{2+} signaling and control of growth and proliferation, *Biol Cell.* **96** (2004):55-68.

López-Schier H., Starr C.J., Kappler J.A., Kollmar R., Hudspeth A.J., Directional cell migration establishes the axes of planar polarity in the posterior lateral-line organ of the zebrafish, *Dev. Cell.* **7** (2005):401-412.

López-Schier H. and Hudspeth A. J., A two-step mechanism underlies the planar polarization of regenerating sensory hair cells, *Proc. Natl. Acad. Sci. USA.* **103** (2006):18615-20.

Ma E.Y. and Raible D.W., Signaling pathways regulating zebrafish lateral line development, *Curr. Biol.* **12** (2009):R381-386.

Manor U. and Kachar B., Dynamic length regulation of sensory stereocilia, *Semin. Cell. Dev. Biol.* **19** (2008):502-510.

Martin B., Mathematical model for the mineralization of bone. *J. Ortho. Res.* **12** (1994):375-383.

McDermott B.M. Jr, Baucom J.M., Hudspeth A.J., Analysis and functional evaluation of the hair-cell transcriptome, *Proc. Natl. Acad. Sci. USA.* **10** (2007):11820-5.

Meszaros J.G., Karin N.J., Osteoblasts express the PMCA1b isoform of the plasma membrane Ca^{2+}-ATPase. *J. Bone Miner. Res.* **10** (1993):1235-1240.

Millimaki B.B., Sweet E.M., Dhason M.S., Riley B.B., Zebrafish atoh1 genes: classic proneural activity in the inner ear and regulation by Fgf and Notch, *Development* **134** (2007):295-305.

Moorman S.J., Development of sensory systems in zebrafish (Danio rerio), *ILAR J.* **42** (2001):292-298.

Najib L. and Fouchereau-Peron M., Calcitonin gene-related peptide stimulates carbonic anhydrase activity in trout gill membranes. *Gen. Comp. Endocrinol.* **94** (1994):166-170.

Nagiel A., Andor-Ardo D., Hudspeth A.J., Specificity of Afferent Synapses onto Plane-Polarized Hair Cells in the posterior Lateral Line of the Zebrafish, *J. Neurosci*. **28** (2008):8442-8453.

Nakano Y., Addison W.N. and Kaartinen M.T., ATP-mediated mineralization of MC3T3-E1 osteoblast cultures. *Bone* **41** (2007):549-561.

Navratilova P., Fredman D., Hawkins T.A., Turner K., Lenhard B., Becker T.S., Systematic human/zebrafish comparative identification of *cis*-regulatory activity around vertebrate developmental transcription factor genes. Dev. Biol. **327**(2009):526-540.

Nechiporuk A. and Raible D.W., FGF-Dependent Mechanosensory Organ Patterning in Zebrafish, *Science* **320** (2008):1774-1777.

Nicolson T. The Genetics of Hearing and Balance in Zebrafish, *Annu. Rev. Genet.* (2005): **39**:9-22.

Ntambi J.M. and Takova T., Role of Ca^{2+} in the early stages of murine adipocyte differentiation as evidenced by calcium mobilizing agents, *Differentiation.* **60** (1996):151-8.

Oertner T.G. and Matus A., Calcium regulation of actin dynamics in dendritic spines, *Cell Calcium.* **37** (2005):477–482.

Okunade, G. W., Miller, M. L., Pyne, G. J., Sutliff, R. L., O'Connor, K. T., Neumann, J. C., Andringa, A., Miller, D. A., Prasad, V., Doetschman, T., Paul, R. J., and Shull, G. E., Targeted ablation of plasma membrane Ca^{2+}-ATPase (PMCA) 1 and 4 indicates a major housekeeping function for PMCA1 and a critical role in hyperactivated sperm motility and male fertility for PMCA4. *J. Biol. Chem.* **279** (2004):33742–33750

Olson S., Wang M.G., Carafoli E., Strehler E.E., McBride O.W., Localization of two genes encoding plasma membrane Ca(2+)-transporting ATPases to human chromosomes 1q25-32 and 12q21-23, *Genomics.* **9** (1991):629-641.

Owens K.N., Cunningham D.E., Macdonald G., Ultrastructural analysis of aminoglycoside-induced hair cell death in the zebrafish lateral line reveals an early mitochondrial response, *J. Comp. Neurol.* **502** (2007):522-543.

Owens K.N., Santos F., Roberts B. et al., Identification of genetic and chemical modulators of zebrafish mechanosensory hair cell death, *PLoS Genet.* **4** (2008):e1000020.

Oughterson S.M., Munoz-Chapuli R., De Andres V., Lawson R., Heath S., Davies D.H., The effects of calcitonin on serum calcium levels in immature brown trout, *Salmo trutta*. *Gen Comp Endocrinol.* **97** (1995):42-48.

Parinov S., Kondrichin I., Korzh V. Emelyanov A., Tol2 transposon-mediated enhancer trap to identify developmentally regulated zebrafish genes in vivo, *Dev. Dynam*. **231** (2004):449-459.

Pasco-Viel E., Charles C., Chevret P., Semon M., Tafforeau P., et al., Evolutionary trends of the pharyngeal dentition in cypriniforms (Actinopterygii: Ostariophysi). *PLoS ONE* **5** (2010):e11293.

Poon K.L., Liebling M., Kondrychyn I., Garcia-Lecea M., Korzh V., Zebrafish Cardiac Enhancer Trap Lines: New Tools for *in vivo* Studies of Cardiovascular Development and Disease, *Dev. Dynam.* **239** (2010):914-926.

Raphael Y., Evidence for supporting cells mitosis in the chick cochlea, *J. Neurocytol.* **31** (1992):663–671.

Rauch G.J., Lyons D.A., Middendorf I., Friedlander B., Arana N., Reyes T., Talbot W.S., Submission and Curation of Gene Expression Data. ZFIN Direct Data Submission (2003) (http://zfin.org).

Renn J., Winkler C., Schartl M., Fischer R., Goerlich R., Zebrafish and medaka as models for bone research including implications regarding space-related issues. *Protoplasma* **229** (2005):209-214.

Riley B.B. and Moorman S.J., Development of utricular otoliths, but not saccular otoliths, is necessary for vestibular function and survival in zebrafish, *J. Neurobiol.* **43** (2000):329-337.

Sandelin A., Bailey P., Bruce S., Engstrom P.G., Klos J.M., Wasserman W.W., Ericson J., Lenhard B., Arrays of ultraconserved non-coding regions span the loci of key developmental genes in vertebrate genome, *BMC Gen.* **5** (2004): 99.

Sarrazin A.F., Villablanca E.J., Nunez V.A., Sandoval P.C., Ghysen A., Allende M.L., Proneural gene requirement for hair cell differentiation in the zebrafish lateral line, Dev. Biol. **295** (2006) 534-545.

Schmid A., Chiba A., Doe C.Q., Clonal analysis of Drosophila embryonic neuroblasts: neural cell types, axon projections and muscle targets, *Development.* **126** (1999):4653-89.

Setsuko L.M., Lisa L.C., Lynne A.W. et al., Developmental differences in susceptibility to neomycin-induced hair cell death in the lateral line neuromasts of zebrafish (Danio rerio), *Hear. Res.* **186** (2003):47-56.

Shepard J.L., Stern H.M., Pfaff K.L., Amatruda J.F., Analysis of the cell cycle in zebrafish embryos. The Zebrafish: Cellular and Developmental Biology, 2nd Ed. *Methods Cell Biol.* **76** (2004):109-125.

Slusarski D.C. and Pelegri F., Calcium signaling in vertebrate embryonic patterning and morphogenesis, *Dev. Biol.* **307** (2007):1-13.

Spoorendonk K.M., Peterson-Maduro J., Renn J., Trowe T., Kranenbarg S., Winkler C., Schulte-Merker S., Retinoic acid and Cyp26b1 are critical regulators of osteogenesis in the axial skeleton, Dev. **135** (2008) 3765-3774.

Stains J.P., Weber J.A., Gay C.V., Expression of Na^{+}/Ca^{2+} exchanger isoforms (NCX1 and NCX3) and plasma membrane Ca^{2+} ATPase during osteoblast differentiation. *J. Cell Biochem.***84** (2002):625-635.

Stock D.W., Zebrafish dentition in comparative context. *J. Exp. Zool. B Mol. Dev. Evol.* **308B** (2007):523-549.

Stock D.W., Jackman W.R., Trapani J., Developmental genetic mechanisms of evolutionary tooth loss in cypriniform fishes. *Development* **133** (2006):3127-3137.

Stone J.S. and Cotanche D.A., Identification of the timing of S phase and the patterns of cell proliferation during hair cell regeneration in the chick cochlea, *J. Comp. Neurol.* **341** (1994):50–67.

Street V.A., McKee-Johnson J.W., Fonseca R.C., Tempel B.L., Noben-Trauth K., Mutations in a plasma membrane Ca^{2+}-ATPase gene cause deafness in deafwaddler mice, *Nat. Genet.* **19** (1998):390–394.

Suzuki N, Suzuki D, Sasayama Y, Srivastav AK, Kambegawa A, Asahina K., Plasma calcium and calcitonin levels in eels fed a high calcium solution or transferred to seawater. *Gen Comp Endocrinol.* **114** (1999):324-329.

Takahashi K. and Kitamura K., A point mutation in a plasma membrane Ca^{2+}-ATPase gene causes deafness in Wriggle Mouse Sagami. *Biochem. Biophys. Res. Commun.* **261** (1999):773–778.

Tempel B.L. and Shilling D.J., The plasma membrane calcium ATPase and disease, *Subcell. Biochem.* **45** (2007):365-83.

Thisse, B., Pflumio, S., Fürthauer, M. et al., Expression of the zebrafish genome during embryogenesis (NIH R01 RR15402), ZFIN Direct Data Submission (2001): (http://zfin.org).

Thisse B. and Thisse C., Fast Release Clones: A High Throughput Expression Analysis, ZFIN Direct Data Submission (2004): (http://zfin.org).

Tomita M., Reinhold M.I., Molkentin J.D. Naski M.C., Calcineurin and NFAT4 induce chondrogenesis. *J. Biol. Chem*. **272** (2002):42214-42218.

Ton C. and Parng C.,The use of zebrafish for assessing ototoxic and otoprotective agents, *Hear. Res.* **208** (2005):79-88.

Van der Heyden C., Huysseune A., Sire J.-Y., Development and fine structure of pharyngeal replacement teeth in juvenile zebrafish (*Danio rerio*) (Teleostei, Cyprinidae). *Cell Tiss. Res.* **302** (2000):205-219.

Villablanca E.J., Renucc A., Sapède D. et al., Control of cell migration in the zebrafish lateral line: implication of the gene "tumour-associated calcium signal transducer," tacstd, *Dev. Dynam.* **235** (2006):1578-88.

Wagner G.F., Jaworski E.M., Radman D.P., Salmon calcitonin inhibits whole body Ca2+ uptake in young rainbow trout. *J. Endocrinol*. **155** (1997):459-465.

Walker M.B. and Kimmel C.B., A two color acid-free cartilage and bone stain for zebrafish larvae. *Biotechnic and Histochem.* **82** (2006):23-28.

Wanaverbecq N., Marsh S.J., Al-Qatari M., Brown D.A., The plasma membrane calcium-ATPase as a major mechanism for intracellular calcium regulation in neurones from the rat superior cervical ganglion, *J. Physiol.* **550** (2003):83-101.

Warchol M.E., Characterization of supporting cell phenotype in the avian inner ear: implications for sensory regeneration, *Hear. Res.* **227** (2007):11–18.

Webb S.E., and Miller A.L., Ca(2+) Signalling and early embryonic patterning during zebrafish development, *Clin. Exp. Pharmacol. Physiol.* **34** (2007):897-904.

Westerfield M., The Zebrafish Book: a Guide for the Laboratory Use of Zebrafish, *The University of Oregon Press* (2000).

Whitfield T.T., Riley B.B., Chiang M.Y., Phillips B., Development of the zebrafish inner ear, *Dev. Dynam.* **223** (2002):427-458.

Woolfe A., Goodson M., Goode D.K., Snell P., McEwen G.K., Vavouri T., Smith S.F., North P., Callaway H., Kelly K., Walter K., Abnizova I., Gilks W., Edwards Y.J., Cooke J.E., Elgar G., Highly conserved non-coding sequences are associated with vertebrate development, *PLoS Biol*. **3** (2005): e7.

Yamoah E.N., Lumpkin E.A., Dumont R.A., Smith P.J., Hudspeth A.J., Gillespie P.G., Plasma membrane Ca^{2+}-ATPase extrudes Ca2+ from hair cell stereocilia, *J. Neurosci.* **18** (1998) 610-24.

Yaoi Y, Suzuki M, Tomura H, Sasayama Y, Kikuyama S, Tanaka S. Molecular cloning of *otoconin-22* complementary deoxyribonucleic acid in the bullfrog endolymphatic Sac: effect of calcitonin on *otoconin-22* messenger ribonucleic acid levels. *Endocrinol.***144** (2003): 3287–3296.